3-11-2022

Kinetics, Characterization, and Applications in the Development of Next-Generation Cure-on-Demand Polymeric Materials through Frontal Polymerization

Daniel Paul Gary

KINETICS, CHARACTERIZATION, AND APPLICATIONS IN THE DEVELOPMENT OF NEXT-GENERATION CURE-ON-DEMAND POLYMERIC MATERIALS THROUGH FRONTAL POLYMERIZATION

A Dissertation

Submitted to the Graduate Faculty of the
Louisiana State University and
Agricultural and Mechanical College
in partial fulfillment of the
requirements for the degree of
Doctor of Philosophy

in

The Department of Chemistry

by
Daniel Paul Gary
B.S. McNeese State University, 2017
May 2022

I dedicate this dissertation to:

My late father, Jimmy Gary (1952-1995)

My late Grandparents Rene Gary (1927-2009) and Mary Gary (1932-2015)

Jessica Ancelet (1993-2020)

To the parents of children with disabilities

To those on the autism spectrum – “ different not less” – Dr. Temple Grandin

ACKNOWLEDGMENTS

I would like to thank my family for their support, love, and patience throughout my education. Mom you never gave up on me despite the multiple setbacks throughout my life and for that, I am deeply grateful. I want to also thank my late grandparents for the love and support they gave me throughout my childhood and adolescence. Mahmuod, thank you for being a great stepfather. I would also like to extend my gratitude to my siblings and extended family. To my dear friends, without you, I would not be here today. You gave me the support and strength that I needed to get through university.

To my teachers in primary and secondary school, I thank all of you who gave their time and energy to help me succeed. I would like to especially thank Mrs. Mary Trahan Tervort for her constant support throughout my time in high school and Mrs. Edith Miller who opened the door for me to learn more than I could ever imagine.

To my university professors and mentors, I thank you for challenging me and enabling me to succeed. I especially want to thank my Ph.D. advisor Dr. John Pojman, who took me in when no one else believed in me. You challenged me, showed me kindness, and remained patient throughout the entire process. I will greatly miss working for you. I also want to thank Dr. Charles White for the opportunity to develop a nonskid coating. working on this project was challenging but incredibly rewarding. I would like to thank Dr. David Spivak and Dr. Matthew Chambers for being excellent professors and committee members.

Lastly, I would like to thank all the members of the Pojman Lab. To my colleagues Anowar, Anthony, Baylen, Brecklyn, Dennel, Fahima, Maria, and Sam, I enjoyed working with

each of you and I will forever cherish the memories. To my undergraduate colleagues, Imogen, Douglas, and Amer, I appreciate all your help, and I enjoyed being your mentor.

The non-skid coating work presented in Chapters 3 and 4 was funded by SERPD (GR-000081630). We would like to thank personnel from the Naval Surface Warfare Center, Carderock Division including Charles White, Kylee Fazende, and Jay Ong. Personnel from Vison Point Systems including Tamara Lubysheva, Matthew Frichtl, and Wayne McGaulley were responsible for the coefficient of friction testing. The work on charge transfer complexes presented in Chapter 5 was partially supported by the NSF EPSCoR-Louisiana Materials Design Alliance (LAMDA) program (Grant No. OIA-1946231).

TABLE OF CONTENTS

LIST OF TABLES

LIST OF FIGURES

LIST OF ABBREVIATIONS

Charge transfer complexes	**CTCs**
N,N-dimethyl-p-toluidine	**DMPT**
Bis(4-fluorophenyl)iodonium triflate	**IOC-FT**
Bis(4-tert-butylphenyl)iodonium hexafluorophosphate	**IOC-P**
Bis(4-tert-butylphenyl)iodonium triflate	**IOC-T**
Bis[4-(tert-butyl)phenyl]iodonium tetra(nonafluoro-tert-butoxy)aluminate	**IOC-A**
Coefficient of friction	**COF**
Frontal polymerization	**FP**
Montmorillonite K10	**MMT K10**
N,N-dimethylaniline	**DMA**
N-phenylglycine	**NPG**
P-(octyloxyphenyl)phenyliodonium hexafluoroantimonate	**IOC-8**
Parts per hundred resin	**Phr**
Pentaerythritol triacrylate	**PETIA**
Trimethylolpropane triacrylate	**TMPTA**
Volatile organic compounds	**VOCs**

ABSTRACT

Frontal polymerization (FP) is a process in which a front propagates in a localized reaction zone converting monomer into polymer. This work explored the kinetics and applications of FP for the development of cure-on-demand materials.

The kinetic effects of fillers on frontal polymerization have not been thoroughly explored. In Chapter 2, various fillers were used, and their effects on front velocity and front temperature were determined. Clay minerals are primarily used, but the thermal conductive effects of milled carbon fiber were also explored. It was found that some fillers inhibit frontal polymerization through radical scavenging, while others increased the front velocity through thermal effects.

Non-skid coatings are applied to the decks of marine vessels to provide both an anti-slip surface and corrosion protection. In Chapter 3, a base formulation for a one-component cure-on-demand coatings based on frontal polymerization was developed and studied. The coating is based on free-radical polymerization of acrylates and cures within minutes with the use of an infrared heater. In Chapter 4, the base formulation was applied as a non-skid coating engineered for a cure-to-service within minutes after cure initiation. The extended pot life and ability to selectively cure the coating will reduce waste, prevent error due to short working times, and improve operational availability by reducing the downtime from long cure-to-service times. The performance of the coating showed high value and potential application to marine vessels. Potential ways to improve the current non-skid coating are also discussed.

Charge Transfer Complexes (CTCs) based on electron donor and acceptor interactions have been shown to act as dual thermal and photoinitiators. The first study done using charge transfer complexes as thermal initiators in frontal polymerization is presented in Chapter 5.

Various iodonium salts and amines were explored as electron acceptors and donors, respectively. The mole ratio of the iodonium salt to the amine, steric effects, and electronic effects were explored. It was found that the front velocity reached a maximum at a certain mole ratio of amine to iodonium salt. The relationship between the type of iodonium salt and front velocity was also explored. Chapter 6 concludes the work.

CHAPTER 1. FRONTAL POLYMERIZATION

1.1. Fundamentals of Frontal Polymerization

Cure-on-demand synthesis of materials is an efficient and convenient way of making materials rapidly.[1] Polymeric materials are traditionally cured through bulk thermal polymerization or photopolymerization. In the case of thermal curing, the materials often take several minutes or longer to cure. Photocuring can be done within seconds but suffers drawbacks of its own. The inner filler effect limits the depth of cure for photocuring of materials. In addition to depth, light has difficulty curing highly pigmented or highly filled systems.[2, 3]

Frontal polymerization is a process that can combine the in-depth cure and curing of highly filled systems offered by bulk polymerization with the high speed of photopolymerization. Frontal polymerization is a polymerization process in which a front propagates in a localized reaction zone; the monomer is converted into polymer as the front passes through an unstirred medium.[4] The process can be rapid, does not require constant energy input (with the exception of photofrontal polymerization) and can be done using a one-pot formulation. FP was originally discovered by Chechilo and Enikolopyan in the 1970s[5-8] and then independently discovered by Pojman in the early 1990s.[4, 9-15]

Frontal polymerization can be classified as photo frontal, isothermal, or thermal.[16] Photofrontal polymerization occurs through continuous input of light. Isothermal polymerization is used to describe fronts driven by the Norrish-Trommsdorff effect where monomer and initiator diffuse into a polymer seed. As demonstrated in Figure 1.1, thermal frontal polymerization (FP) is started by an external energy source such as heat or light and is the most studied type of frontal

polymerization. Propagation in FP depends on thermal diffusion and the Arrhenius dependence of the reaction rate of an exothermic polymerization.[1]

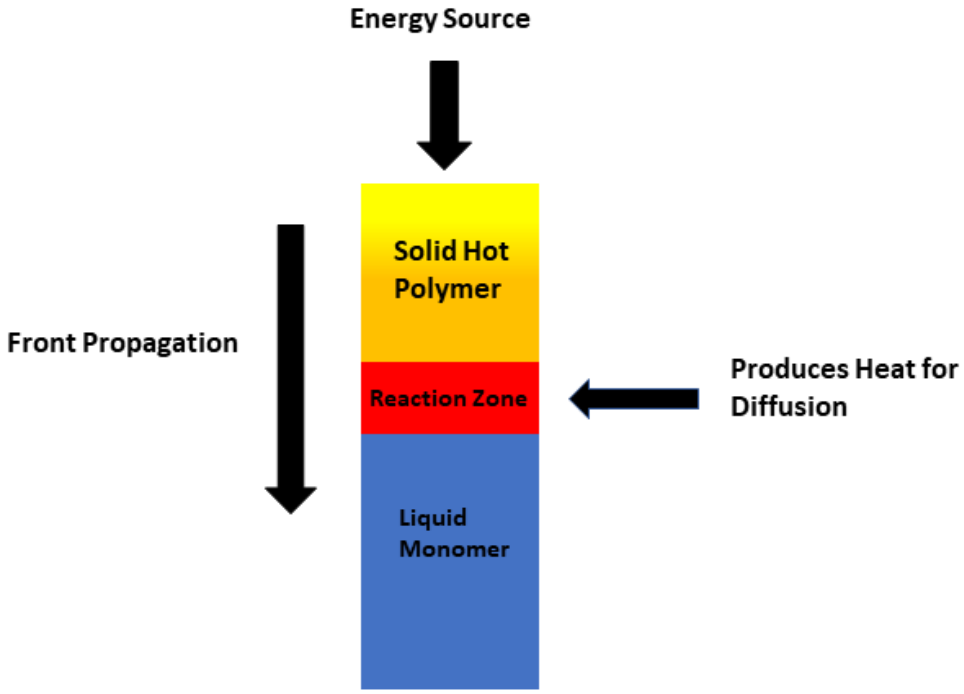

Figure 1.1. Schematic showing the process of frontal polymerization.

There are certain requirements for FP to occur. The activation energy must be high so that the system does not react at the ambient temperature but have a high reaction rate at the front temperature. This is necessary as the front will quench if the rate of heat loss exceeds the rate of heat production. Free-radical polymerization meets these requirements and is the most applicable polymerization mechanism in systems that support FP.[16]

When referring to the activation energy, each step in the polymerization (initiation, propagation, and termination) must be accounted for. Shown in equation [1.1] the steady-state theory of polymerization shows an approximate relationship between the overall activation energy and the activation energy for each step in the mechanism.[17]

$$E_{eff} = E_p + \left(\frac{E_i}{2}\right) - \left(\frac{E_t}{2}\right) \quad [1.1]$$

Equation 1.1. The total activation energy for free radical polymerization.

The activation energy for initiator decomposition is the largest term and therefore the most important factor in determining the overall activation energy. This means the choice of initiator is crucial to both the existence and propagation of a front; factors such as the front temperature and velocity are ultimately related to the initiator type and concentration.

1.2. Challenges of Frontal Polymerization

Frontal Polymerization, like all processes, has its limitations. One such limitation is the formation of voids, which results in the formation of pores in the material. These voids are due to gases generated from initiator decomposition, the presence of O_2, N_2, in the monomer, and the presence of water in the monomer. Initiator decomposition can give rise to byproducts such as carbon dioxide, nitrogen, and acetone gases that result in the formation of bubbles.[26] These voids can limit certain applications in material synthesis. One way to suppress bubbles is to increase the pressure, Pojman and coworkers discovered that bubbles can be suppressed at low pressures (less than 30 atm), but there is a decrease in the front velocity. Bubbles increase the front velocity due to expansion, which causes unreacted monomer to be forced around the contracting polymer.[9] Masere et al.[18] demonstrated that initiators that do not give off gases such as ammonium persulfate can be utilized; however, polymer degradation is an issue. Mariani[19] and coworkers synthesized organic soluble persulfate phosphonium ionic liquids thermal initiators that could give a front velocity similar to that of traditional thermal initiators (BPO, AIBN, APO).

Bomze[20, 21] and coworkers utilized benzopinacol (1,1,2,2-tetraphenylethanediol) as a non-peroxide gas-free initiator. Despite being a gas-free initiator, benzopinacol has the

drawbacks of low relativity and poor solubility. More research will need to be done to explore safer and novel initiating systems for frontal polymerization.

One of the biggest challenges of FP is buoyancy-driven convection. In the case of FP, the front forms the high-density fluid (polymer) as it propagates through the resin, which has a lower density. This instability lowers the front velocity and can quench the front.[22] This instability can be eliminated via high pressure,[2-5] the addition of a viscosity-enhancing additive, or in the case of vertical thermoset forming systems (in test tubes), initiating the front at the top so that it propagates downward in thermoset forming systems.[4] Pojman[7], Bowden[23], and McCaughey[24] showed that fumed silica can be added to enhance the viscosity of the resin. The enhanced viscosity eliminates buoyancy-driven convection, which sustains the front and increases velocity.[7,30-31] Experiments by Pojman showed that the addition of fumed silica has no effect on the molecular weight of the polymer formed and is, therefore, a good inert additive that can be used to control the viscosity.[25]

1.3. Applications of Frontal Polymerization

Since its discovery, FP research has been extended to other areas such as Deep Eutectic Solvents,[26-29] hydrogels,[30] ROMP,[31] gradient materials,[32] and cationic-initiated polymerization.[21, 33-36] Cure on-demand synthesis of materials is perhaps the most applicable area of research, which includes the development of materials such as composites,[37-40] functional gradient materials[32], and adhesives.[41] These applications of frontal polymerization are well documented but applications in the synthesis of thin films have only recently been explored. Bansal et al.[42] studied the kinetics of film formation on wood through frontal polymerization. The study showed that it is possible to form films as thin as 15 mils while maintaining a front. It was found that the front velocity and front temperature increased as the film thickness increased. This increase in

velocity can be attributed to less heat loss. As the film thickness increases, there is less heat loss due to a decrease in the ratio of surface area to volume. The films were porous, and porosity was found to be spatially dependent. Porosity decreased from the bottom layer near the substrate to the surface layer of the film. The large heat loss associated with thin layers along with porosity issues currently limits the applications of FP as a method to make cure-on-demand coatings.

CHAPTER 2. CHEMICAL AND THERMAL EFFECTS OF FILLERS ON FRONTAL POLYMERIZATION

2.1. Introduction to Fillers and Frontal Polymerization

Fillers are incorporated into polymeric materials to change various properties while maintaining cost efficiency. The addition of fillers can change properties such as hardness, chemical resistance, and scratch resistance. In the case of FP, fillers are typically added to reduce buoyancy-driven convection.[43, 44]

Pojman showed that kaolin clay can be added to give the resin a putty-like viscosity, which is useful as the resin could be molded into different shapes; This putty-like consistency eliminates buoyancy-driven convection.[43] Viner et al. studied the effects of fumed silica and Polygloss®90 (ultrafine kaolin clay) on the front velocity of a binary frontal system. In comparison to kaolin, Viner found that less fumed silica was needed to achieve a more viscous formulation. Fumed silica has a higher surface area, lower bulk density, and smaller particle size than Polygloss®90, as a result, it absorbs more media than the same mass of Polylgoss®90. In addition, more kaolin was needed to form a putty, which resulted in the absorption of heat and a decrease in front velocity.[44] In addition to being used as viscosity enhancers, fillers have also been used for other applications in fronts.

This chapter was previously published as D. P. Gary, S. Bynum, B. D. Thompson, B. R. Groce, A. Sagona, I. M. Hoffman, C. Morejon-Garcia, C. Weber, J. A. Pojman, Thermal transport and chemical effects of fillers on free-radical frontal polymerization. *J. Polym. Sci.* 2020, *58*, 2267. Reprinted by permission of Wiley.

Nason and coworkers studied the effects of trithiol, kaolin, and calcium carbonate as additives in photo-induced thermal frontal polymerization. This work showed fillers can be used in conjunction with trithiol to make composites using photo-induced frontal polymerization.[45] Montmorillonite was used as a filler to make various materials, including nanocomposites[37] and hydrogels.[38]

The Novozhilov equation is useful in understanding how fillers might influence fronts. Derived in the 1960s, this equation describes the dependence of the propagating velocity of a thermal front for a one-step reaction on front temperature, the activation energy of the reaction, and the thermal diffusivity of the system.[46] As shown in Equation [2.1], E is the activation energy of the reaction, T_f is the front temperature, and α is the thermal diffusivity.

$$vel \propto \sqrt{\alpha}\, T_f e^{-2E/RT_f} \quad [2.1]$$

Equation 2.1. Relationship between front velocity and the thermal properties of a system.

The equation shows that the velocity of a propagating thermal front is proportional to the square root of thermal diffusivity. From this, it can be hypothesized that systems that incorporate fillers with higher thermal diffusivities will give higher front velocities in comparison to fillers with lower thermal diffusivities.

In addition to thermal effects, it is also important to consider the chemical effects of fillers on frontal polymerization. Studies have shown that phyllosilicate clay minerals can affect cationic, anionic, and free-radical polymerization.[47-49] As shown in Figure 2.1, phyllosilicate clays consist of octahedral and tetrahedral sheets along with an interlayer space. Classification is based on the ratio of the tetrahedral to octahedral sheets. The interlayer space containing water and cations separates these sheets.[50] Clays such as bentonite (2:1 ratio) and kaolin (1:1 ratio) are well known to contain both Lewis and Brønsted acid sites.[50] The presence of such sites has

allowed clay minerals to be applied in the catalysis of organic transformations including polymerization.[50]

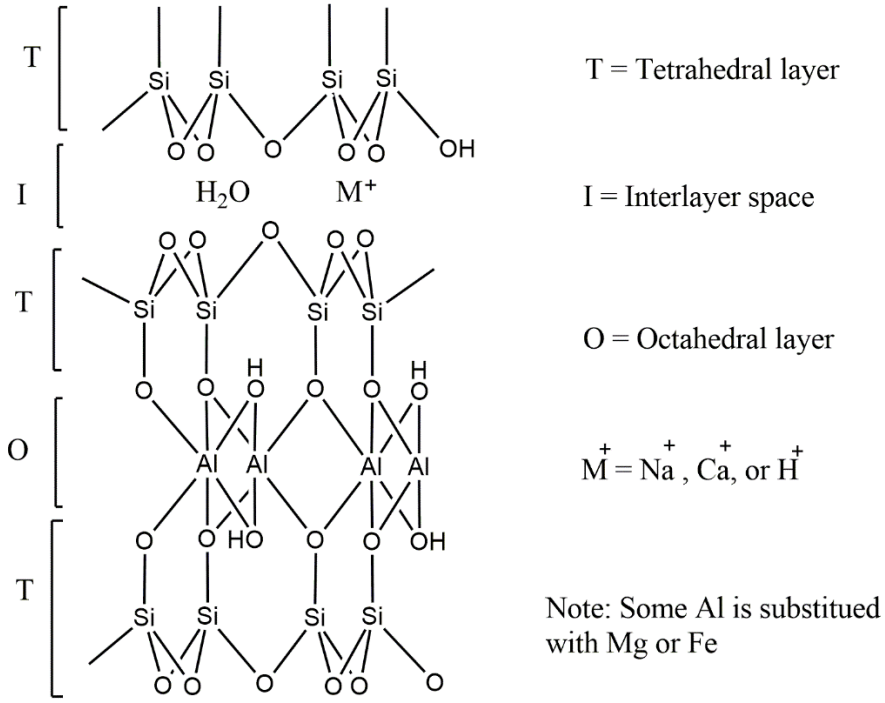

Figure 2.1. General Structure of clay crystal lattice for bentonite.

Solomon and coworkers demonstrated that clay minerals can catalyze the cationic polymerization of polystyrene. The work by Solomon and coworkers suggests the mechanism involves a one-electron transfer that results in the formation of a styrene radical cation.[47]

In addition to acting as catalysts, research suggests that clay minerals can act as inhibitors in free-radical polymerization. Solomon and Swift discovered that the polymerization of methyl methacrylate was inhibited in the presence of magnesium and aluminum phyllosilicates.[48] Solomon proposed that a non-propagating carbonium ion is formed from electron transfer of the radical on methyl methacrylate to clay.[51] Such a species does not undergo cationic polymerization due to the electron-withdrawing tendency of acrylates. More recent research by Wang et al. has shown that polymerization of ethylene intercalated into montmorillonite resulted

in a decrease in the initiation, propagation, and termination rates along with the formation of a higher molecular weight polymer.[52]

In addition to inherent acidity, clay minerals can be acid-activated. Acid activation is typically accomplished by treating the mineral with an inorganic acid. In acid activation, cation exchange takes place between the interlayer cations in the clay and protons from the acid. Also, there is an increase in the surface area of the clay. The result is an increase in the Brønsted and Lewis acidity. [53] It has been proposed that the Lewis acid catalysis/inhibition from these minerals is due to electron transfer to metals such as aluminum exposed at the edge of the crystal lattice.[49]

The effects of different fillers on front temperature and velocity were investigated. Several fillers including milled carbon fiber, kaolin, montmorillonite (bentonite), and calcium carbonate are studied. milled carbon fiber as a high thermal diffusivity was compared to kaolin clay. Milled carbon fiber has a slightly lower heat capacity than kaolin clay, but its thermal diffusivity is approximately seven times larger. It is hypothesized that the increase in thermal diffusivity will lead to an increase in the front velocity without significantly affecting the front temperature as predicted by the Novozhilov equation [2.1].

2.2. Materials and Methods

Technical grade trimethylolpropane triacrylate (TMPTA) was obtained from Allnex (Alpharetta, GA). 1,1-bis(tert-butylperoxy)-3,3,5-tricyclohexane (Luperox ® 231) and Montmorillonite K10 (acid-activated bentonite, MMT K10, 250 m^2/g surface area) were obtained from Sigma-Aldrich. Polygloss®90 (referred to simply as kaolin for the remainder of the paper) a kaolinite clay (0.4 microns) was obtained from KaMin performance minerals (Macon, GA). Fumed silica (Aerosil®200, 175-225m^2/g BET surface area) was obtained from Evonik Industries (Parsippany,

NJ). Zoltek®PX35 (milled carbon fiber, 150 x 7.2 squared microns) was provided by Zoltek Companies, Inc. (St. Louis, MO). Bentolite®L10 (calcium bentonite, 95% < 44 microns, 56 m^2/g BET surface area), Laponite®RD (a synthetic hectorite, 370 m^2/g surface area), and Fulcat®435 (acid-activated bentonite, 270 m^2/g surface area) were all purchased from BYK Additives & Instruments (Wallingford, CT). Volclay®325 (sodium bentonite, 95% < 44 microns, 23 m^2/g BET surface area) was purchased from The American Colloid Company (Hoffman Estates, IL). Hubercarb®Q3 (calcium carbonate, 3.2 microns median particle size) and talc (98 % < 74 microns) were purchased from Huber Materials (Quincy, IL) and Natural Minerals (Van Horn, TX), respectively. All materials were used as received. The BET surface areas of Volaclay®325 and Bentolite®L10 were experimentally determined by a Micromeritics ASAP 2020. Table 2.1 shows the physical/thermal properties of interest for the various fillers. Figure 2.2 shows the chemical structures of the monomer and initiators.

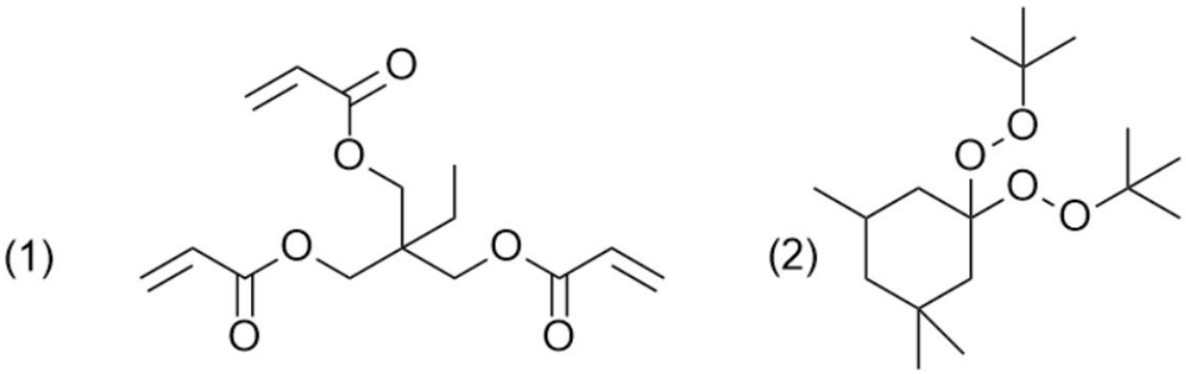

Figure 2.2. Chemical structures for reagents. (1) trimethylolpropane triacrylate (TMPTA) (2) 1,1-bis(tert-butylperoxy)-3,3,5-tricyclohexane (Luperox®231)

Table 2.1. Thermal properties of fillers

Filler	**ρ (g cm^{-3})**	**C_p (J g^{-1}K^{-1})**	**□ (Wcm^{-1}K^{-1})**	**α (cm^{2}s^{-1})**
Milled Carbon Fiber[a]	1.8	0.60	6.4 x 10^{-2}	5.9 x 10^{-2}
Calcium Carbonate[a,54]	2.7	0.87	2.5 x 10^{-2}	1.1 x 10^{-2}
Talc[a,54]	2.8	0.87	2.1 x 10^{-2}	8.6 x 10^{-3}
Kaolin[a,54]	2.6	0.92	2.0 x 10^{-2}	8.2 x 10^{-3}
Bentonite[a,55, 56]	2.6	1.3	1.0 x 10^{-2}-1.3 x 10^{-2}	3.0 x 10^{-3} - 3.9 x 10^{-3}
Fumed Silica[a,54]	2.2	0.79	1.5 x 10^{-4}	8.6 x 10^{-5}

Note: (a) provided by the manufacturer.

For the milled carbon fiber experiments, TMPTA and 1 part per hundred resin (phr) of initiator were mixed with fillers to form a putty. (The abbreviation "phr" refers to the amount of material (in grams) that was added per one hundred grams of resin, i.e., monomer.) The putty was loaded into a wooden mold with dimensions of 2.0 cm wide x 0.6 cm high x 10 cm long. To measure front temperature, a type K thermocouple connected to a laptop with Logger Lite® software was inserted into the middle of the strip of putty at approximately half depth. To initiate the fronts, a handheld butane soldering iron was used to heat a small portion of the strip at one end. Front propagation was monitored through an overhead video camera. The front velocity was calculated by taking the slope of a position vs. time plot. All experiments were performed in triplicate.

The total filler loading was chosen to be 49% by weight. This loading eliminates convection and allows the formulator to form a moldable putty. The amount of milled carbon fiber used in a sample is reported as a fraction of the total filler amount. Figure 2.3 shows an example of a formulation containing milled carbon fiber and kaolin both before and after undergoing frontal polymerization. Initially, only kaolin was mixed with milled carbon fiber, but later fumed silica (4.9 % w/w) was incorporated to form a cohesive formulation with the consistency of putty.

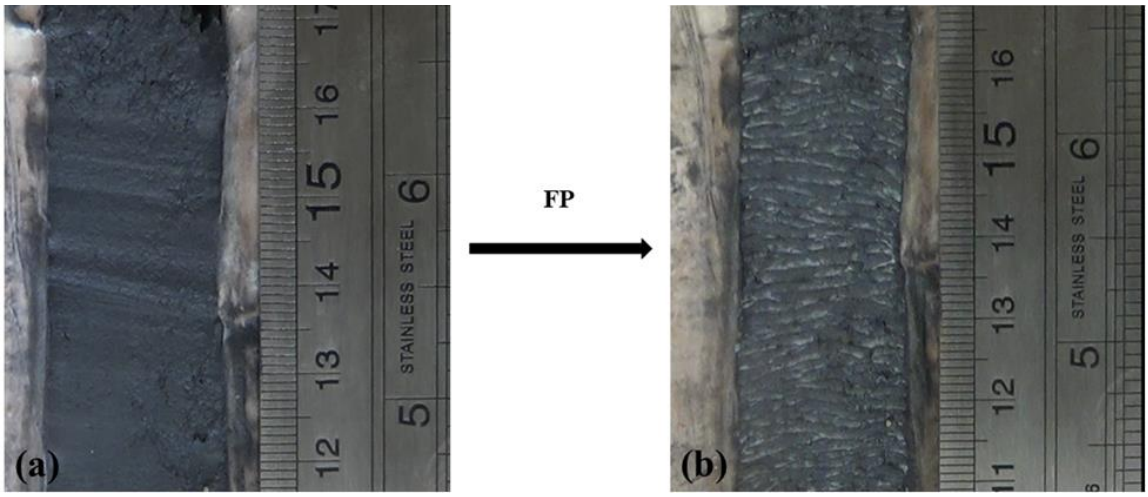

Figure 2.3. Milled carbon fiber formulation before (a) and after (b) undergoing frontal polymerization.

For frontal polymerization of systems containing clay minerals as additives, TMPTA, 1 phr of Luperox®231, and various clay fillers were mixed to form a viscous formulation. Filler loading was measured in terms of phr. Some formulations contained $CaCO_3$ along with an acid-activated clay (multiple filler systems), but the total loading of the two fillers was kept constant at 60 phr. 8 phr of fumed silica was added to all formulations so that a moldable putty was formed. The formulations were loaded into a horizontal wooden mold with dimensions of 2.0 cm wide x 0.6 cm high x 10 cm long. Fronts were then initiated and analyzed as previously mentioned.

For certain experiments, the filler was dried in an oven at 200 ˚C for three hours to a constant weight. The water content was determined by the mass loss. Dried Laponite® RD and bentonites were studied as fillers.

To acid-activate the kaolin, Polygloss®90 (50 g) was treated with a 1 M solution of $AlCl_3$ (500 mL). The system was then stirred for 24 hours. The clay was washed with deionized water until the filtrate reached a neutral pH.

An initiator study was done to see if a relationship between the fillers, initiators, and front velocity could be found. Three separate formulations were prepared; one containing calcium

carbonate (60 phr) as the standard along with two mixed systems composed of calcium carbonate and MMT K10 as the acid-activated clay. One of the mixed formulations had calcium carbonate (45 phr) and MMT K10 (15 phr), and the other formulation consisted of calcium carbonate (30 phr) and MMT K10 (30 phr). All formulations contained TMPTA as the monomer along with fumed silica (8 phr) as a viscosity additive. The amount of Luperox®231 was varied (1phr to 8 phr) in each formulation.

2.3. Effects of Milled Carbon Fiber as a Thermally Conductive Additive for Frontal Polymerization

As shown in Figure 2.4, the initial substitution of kaolin with milled carbon fiber increased the front velocity, but the velocity remained constant after more milled carbon fiber was substituted. There was an increase in resin expansion as more milled carbon fiber was added and this was accounted for in determining the front velocities.

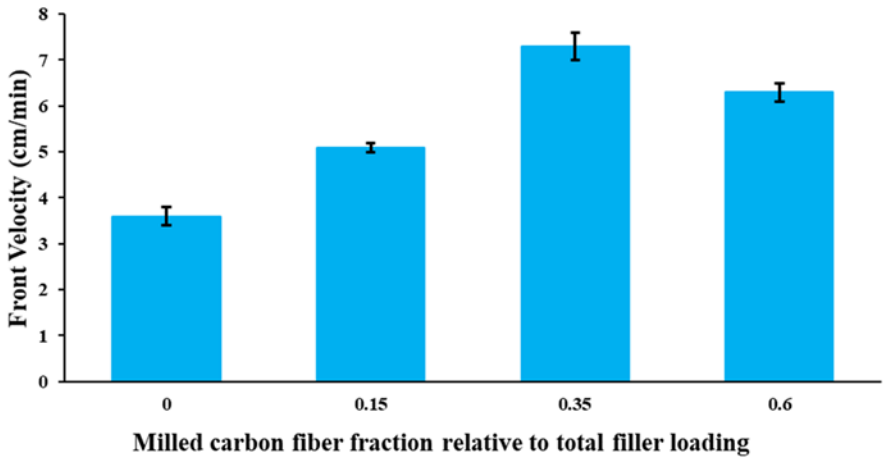

Figure 2.4. The formulation contains 51% w/w 1 phr Luperox®231 in TMTPA and 49% w/w total filler loading.

As shown in Figure 2.5 it appears that the monomer was forced out as the front passed through the resin. This was attributed to the poor wetting between the milled carbon fiber and the resin; hydrophilic fumed silica was added to alleviate this problem.

Figure 2.5. Resin being forced out as front propagates in a system consisting of kaolin (0.85 mass fraction) and milled carbon fiber (0.15 mass fraction)

The fumed silica increased wetting between the resin and the filler via hydrogen bonding. TMPTA acts as a hydrogen bond acceptor to the -OH groups on fumed silica. The hydrogen bonding forms a network that increases viscosity and keeps other fillers suspended.[57] The enhanced cohesiveness of the resulting putty minimized expansion. In addition, the monomer was no longer be forced out as the front propagated. The net result as shown in Figure 2.6, is a constant increase in front velocity as more kaolin is substituted with milled carbon fiber. The front velocity was tripled at the highest loading and while the front temperature remained relatively constant. This demonstrates the ability of milled carbon fiber to act as an additive that can increase front velocity without altering the front temperature.

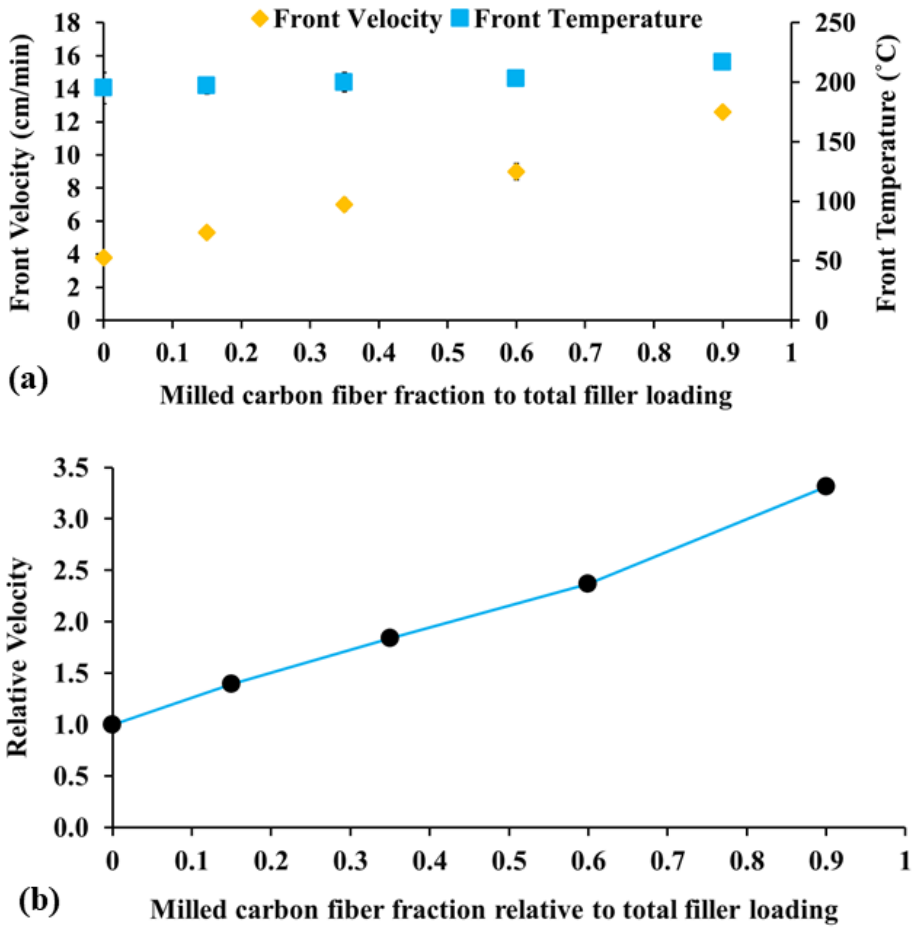

Figure 2.6. The formulation contains 51% w/w 1 phr Luperox®231 in TMTPA and 49% w/w total filler loading. 4.9% w/w fumed silica is included in the total filler loading. (a) raw front velocity and temperature data (b) relative velocity as a function of filler loading.

2.4. Clay Minerals as Fillers

To study the chemical effects of clay minerals on FP, $CaCO_3$ was used as an inert standard. As shown in Figure 2.7, the systems containing calcium carbonate, kaolin, and talc had similar front velocities and temperatures. This is expected because these three fillers have similar thermal properties. Based on these findings, it appears that kaolin and talc are acting as chemically inert fillers in these systems. Both the bentonites gave a lower front velocity and temperature. The reduced front velocities of the formulations with the bentonites were expected because of their smaller thermal diffusivities. An average front velocity could not be obtained from the system with the Laponite® RD as the front quenched before the formulation was entirely cured. The

front velocities of the bentonite formulations were about three times slower than the front velocity of the formulation with calcium carbonate.

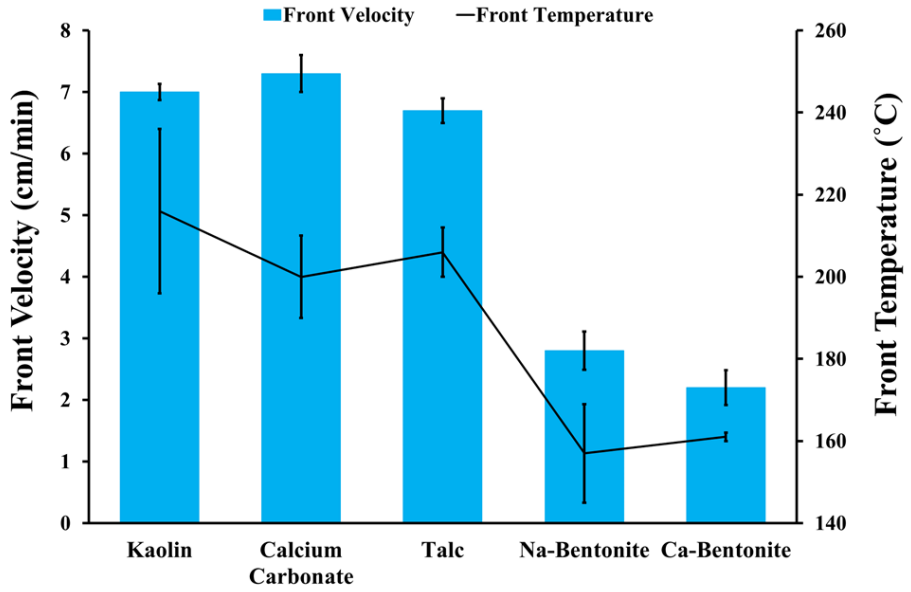

Figure 2.7. Effect of filler choice on front velocity.

Since the front velocity is proportional to the square root of the thermal diffusivity, and the fillers only make up a minority of the formulation in terms of mass, it is plausible that the differences in thermal diffusivity alone may not account for the dramatic differences in the front velocity.

It is important to note that the surface area of the fillers may affect FP, but that was not in the scope of the study. With increasing surface area, there is more interaction between the filler and the reactive species. This means that there is more potential for more side reactions with the filler as the surface area increases.[53] However, we did not investigate the dependence of the front velocity on the surface areas of the fillers in this work.

Certain clay minerals are known to absorb moisture; the water in these "swelling clays" is largely contained in the interlayer space. Swelling clays, such as bentonite, contain a significant amount of water compared to other fillers. Bynum et al. showed that water present in the monomer will decrease the front velocity and temperature, which arises from the absorption of

heat through water evaporation.[58] The absorption of heat lowers the front temperature and velocity. Water content also plays a role in the type of acidic sites present in silicate clays. Upon drying unbound water as well as possible water bound to Lewis acid sites such as Al^{3+} is removed, and this increases Lewis acidity.[58] Bound water reduces Lewis acidity by acting as a Lewis base and coordinating to Al.[49] This suggests that removing water from a clay mineral filler could decrease the front velocity due to the enhanced Lewis acidity or increase the velocity as the removal of water leads to less heat loss from vaporization. Table 2.2 shows that the Laponite® RD and bentonites contained a significant amount of water in comparison to the other fillers. Figure 2.8 shows the effect of using dried bentonites and dried Laponite®RD. There was an increase in the front velocity and temperature after drying the fillers.

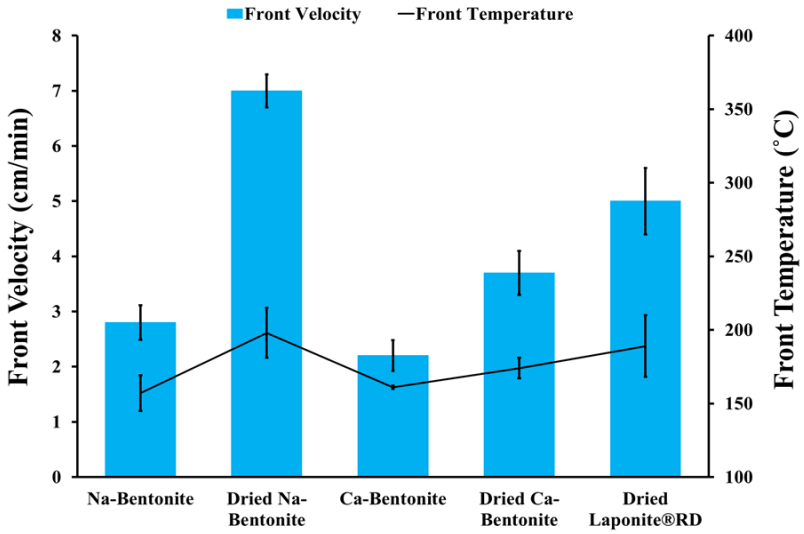

Figure 2.8. Effect of drying clay mineral fillers on frontal polymerization

Table 2.2. water loss (wt%) after drying fillers

Filler	**Wt. % Water**
Calcium Carbonate	0.8
Polygloss 90D	1.9
Talc	2.6
Bentonite	12.4
Bentolite-L 10	15
Laponite	8.8
MMT K10	10.7
Fulcat 435	7.0
AA Polygloss 90D	1.0

Notably, the increases in velocity and temperature were significantly greater for sodium bentonite and Laponite-RD than for calcium bentonite. Despite both being bentonites, the front velocity for sodium bentonite was nearly double that of calcium bentonite. This result suggests that there is more radical scavenging from Lewis acid sites in the dried calcium bentonite relative to that of the dried sodium bentonite. This might also be explained by the higher surface area of the calcium bentonite (56 m^2/g) versus the sodium bentonite (23 m^2/g), which would result in more interactions between acidic sites and free radicals.

The images in Figure 2.9 demonstrate that the formulations with 60 phr of acid-activated clay were not able to undergo frontal polymerization. In all three cases, the filled resin was burnt by the soldering iron, but a front was not generated. The inability of the system containing the acid-activated kaolin to undergo FP shows that the inhibitory behavior from acid activation is not limited to bentonites. Before acid-activation, kaolin was able to sustain a front, which shows that acid-activation inhibits FP. These results show that acidic sites in clay minerals inhibit free-radical polymerization to such a degree that a front could not be sustained.

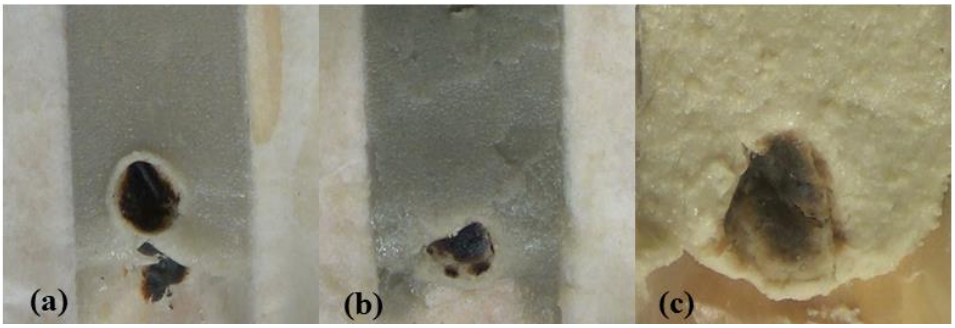

Figure 2.9. Images showing systems with acid-activated clays after FP was attempted (a) Fulcat® 435, (b) MMT K10, (C) acid-activated kaolin.

Since no front could be initiated with 60 phr of acid-activated clay, the filler loading of the commercially available acid-activated clays were reduced by mixing the Fulcat®435 and MMT K10 with calcium carbonate at various ratios (mixed filler systems). The total filler loading was held constant at 60 phr. As shown in Figure 2.10, there was a decrease in the front velocity as the fraction of acid-activated clay increased. Figure 2.10 also demonstrates that a front could not be sustained with 15 phr of Fulcat®435. In the case of MMT K10, a front could be sustained with higher filler loadings. These results show that Fulcat®435 is more inhibitory towards frontal polymerization than MMT K10, which suggests that Fulcat®435 may be more Lewis acidic than MMT K10. When comparing the acidity of clay minerals, water content plays a role. The differences in the front velocity may be due to enhanced Lewis acidity of Fulcat®435, arising from the lower water content, shown in Table 2.2. The lower water content may result in a lower number of Lewis acid sites bound by water.

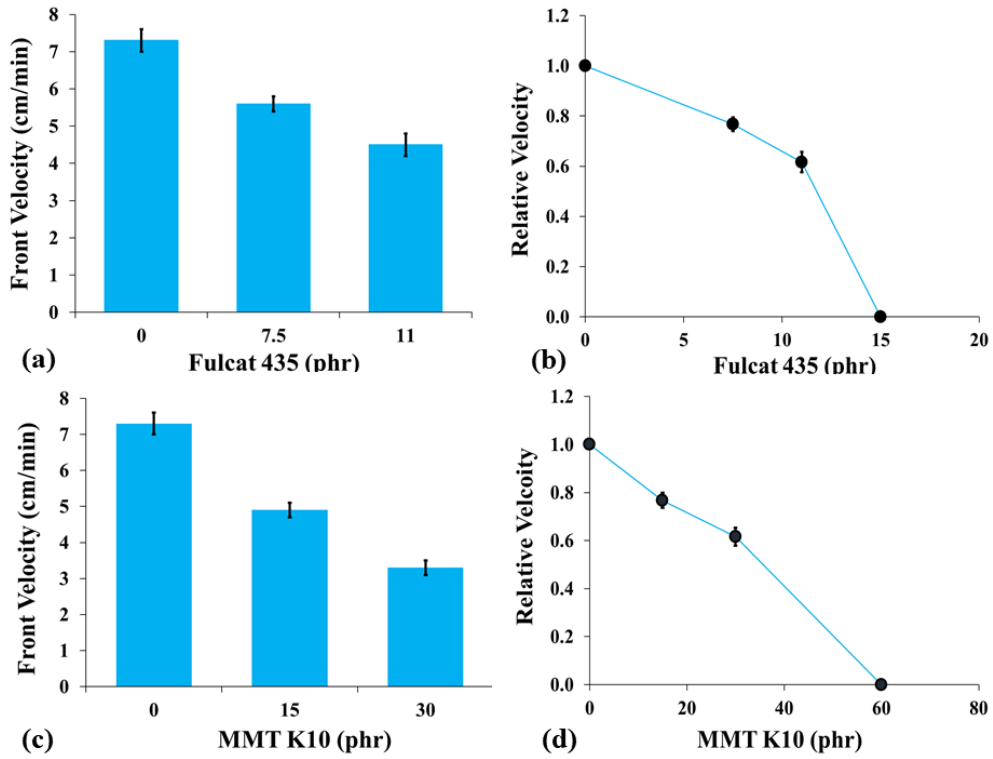

Figure 2.10. Effect of acid-activated filler in mixed filler systems: (a) raw front velocity and (b) relative front velocity of Fulcat® 435 systems (c) front velocity of MMT K10 systems (d) relative front velocity of MMT K10 systems

MMT K10 and Fulcat®435 were dried and then used in the mixed filler systems. Figure 2.11a shows the effect of drying the acid-activated clays on the frontal polymerization of the multiple filler systems. The front velocity did not change in the system with Fulcat®435; however, only a small amount of Fulcat®435 was in the formulation. A front could not be initiated in the multiple filler formulation containing the dried MMT K10; the attempt of FP with this system is demonstrated in Figure 2.11b. Figures 2.11c and 2.11d demonstrate that FP could not be initiated in systems with 60 phr of dried Fulcat®435 or dried MMT K10. These results show that the heat absorbed by water in the clays is not solely responsible for the lower front velocities in these systems. In the case of the mixed MMT K10 system, removing water increased the inhibitory behavior of the clay towards FP. This strongly suggests that the increase in Lewis acidity from drying inhibited FP.

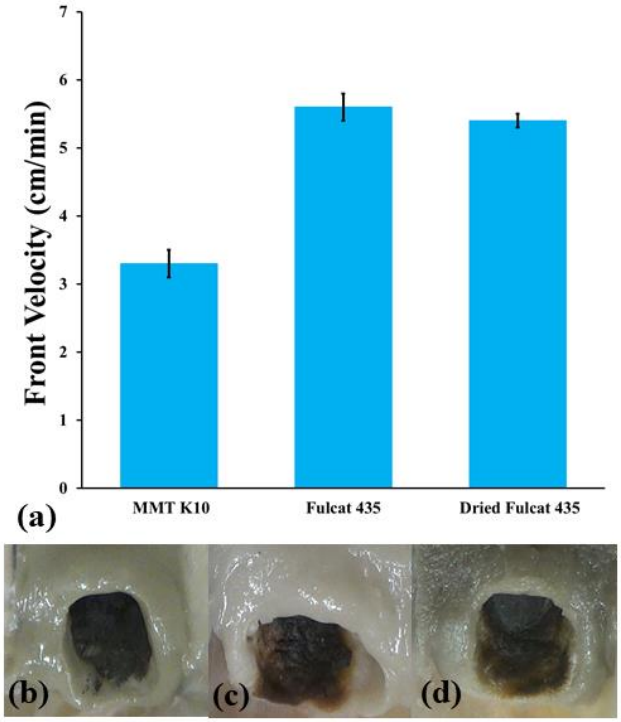

Figure 2.11. (a) Effect of drying the acid-activated clays on the front velocity of the multiple filler systems; the MMT K10 mixed formulations contained 30 phr of MMT K10 and the Fulcat® 435 mixed formulations contained 7.5 phr Fulcat 435. (b)the mixed system containing 30 phr dried MMT K10 and 30 phr $CaCO_3$. (c). the system with 60 phr dried MMT K10, (d) the system with 60 phr dried Fulcat®435

The effect of initiator concentration on the front velocity with both calcium carbonate and two multiple filler formulations was explored. Shown in Figure 2.12, the front velocity increases as the concentration of Luperox® 231 increases. Previous work[12, 59] indicates that the increase in the front velocity with initiator concentration is expected; however, the addition of the acid-activated fillers still lowered the front velocity. The exponent of the power functional fit revealed that there was no trend between the front velocity dependence on initiator concentration and the amount of acid-activated clay (MMT K10) in the system.

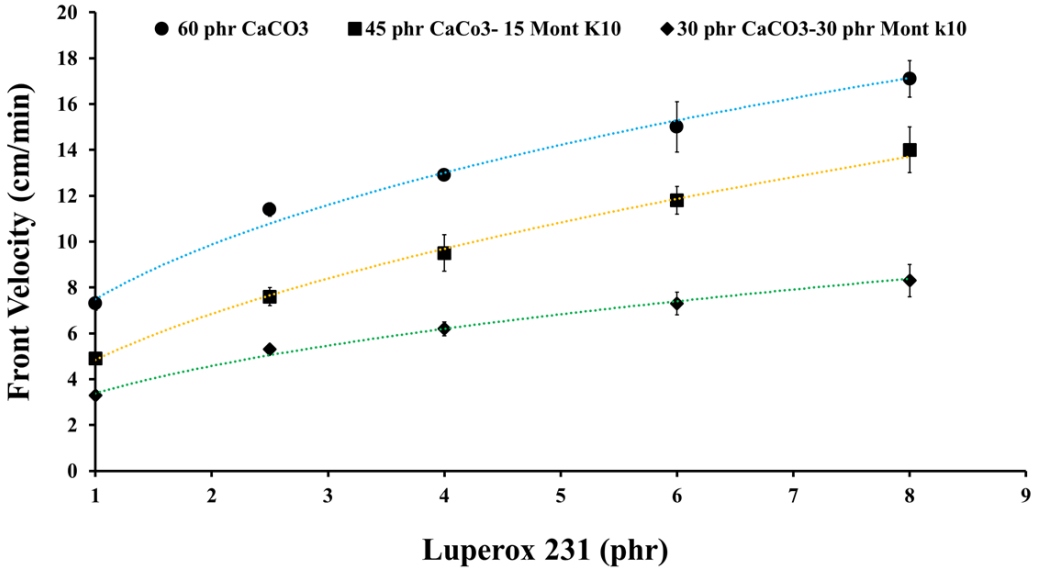

Figure 2.12. Effect of initiator concentration on front velocity for the $CaCO_3$ formulation and formulations containing both $CaCO_3$ and MMT K10. The power function fit exponent revealed the velocity dependence on initiator concentration to be 0.40 for the 60 phr $CaCO_3$ formulation, 0.50 for the 45 phr $CaCO_3$-15 phr MMT K10 formulation, and 0.44 for the 30 phr $CaCO_3$-30 phr MMT K10 formulation.

2.5. Conclusions

The thermal and chemical effects of various fillers on the frontal polymerization of a multifunctional acrylate was studied. Fillers act as heat sinks, lowering the front temperature and thus the front velocity. To overcome this issue, milled carbon fiber, a thermally conductive material was mixed into the clay system to allow for greater thermal transport and thus faster-moving fronts. The front velocity tripled in systems filled with milled carbon fiber, a cheaper filler. Despite the increase in velocity from milled carbon fiber, the front temperature did not change significantly.

In addition to milled carbon fiber, clay minerals were also studied. The addition of bentonite fillers decreased the front velocity in comparison to other fillers. Experiments in which fillers were dried, before being added to the formulation, increased the front velocity. The increase in velocity showed that water present within clay minerals can have a detrimental effect

on the front velocity. Acid-activated clays such as MMT K10 and acid-activated kaolin inhibited frontal polymerization, which suggests that Lewis acid sites in the clays are inhibiting free-radical polymerization. Increasing the initiator concentration increased the front velocity in formulations consisting of calcium carbonate and MMT K10. No trend between the amount of acid-activated clay and the front velocity dependence on the initiator concentration could be found.

CHAPTER 3. FORMULATION OF CURE-ON-DEMAND COATING

3.1. Introduction to Cure-on-Demand Coatings

Cure-on-demand technology can be used to combat challenges in the development and application of coatings. Current coatings often require two-part mixing for application, long cure times, and release volatile organic compounds (VOCs). Cure-on demand technology includes photocuring of traditional systems such as acrylate and epoxy-based formulations.[1, 60-63] Photocuring can be used to cure coatings rapidly but the inner filter effect limits through-cure of thick samples. In addition to thickness, the presence of fillers and or pigments impedes light penetration thereby reducing the cure of the material.[2] Such challenges can make photocuring a difficult process in the curing of highly filled and or thick coatings.

A post-thermal cure is a potential way to overcome this issue, but it requires additional time and resources.[64] Redox initiated polymerization can be used to rapidly prepare materials such as coatings and composites without the drawback of the inner filter effect.[65-68] However, their pot life is limited, and two-part mixing is required.[68]

Frontal Polymerization (FP) is a potential method that can be used to rapidly cure a highly filled and or thick coating without the drawbacks of photocuring and redox polymerization. Recently, Bansal *et al.* demonstrated the first use of FP to make thin films on wooden substrates.[42] However, there is no reference of the use of FP to manufacture thin films on steel substrates. One of the drawbacks of FP is heat loss to the substrate, which can be exacerbated more on substrates such as steel because of their high thermal conductivity. Additionally, the presence of fillers also results in further heat loss.[45] Because of this, it is difficult to maintain a front without continuous input of energy. In addition, buoyancy-driven convection from the density difference between the

formed polymer and resin creates an instability that can quench the front.[16] Adding fillers to form a moldable putty is one way to eliminate buoyancy-driven convection.[69]

Herein, we utilize the process of frontal polymerization to rapidly cure a base formulation for cure-on-demand coating applications on steel substrates. Unlike traditional FP, where the front self-propagates after initiation, here the coating is continuously irradiated with an infrared heated to sustain the FP. A base formulation consisting of Ebecryl®605 (73 wt% bisphenol A epoxy acrylate diluted with 27 wt% tripropylene glycol diacrylate) and pentaerythritol triacrylate (PETIA) was used as the resin. Ebecryl®605 was chosen as the oligomer to impart adhesion to the epoxy primer and provide barrier properties. PETIA, a 1:1 mixture of tri- and tetra-acrylate, was used as a reactive diluent to reduce cure time, increase crosslink density, and maintain adhesion. Fumed silica was added to suppress buoyancy-driven connection. Zoltek®PX35 is a high aspect ratio milled carbon fiber filler used to reduce cracking from thermal stresses. Figure 3.1 shows the chemical structures of the initiator and resins.

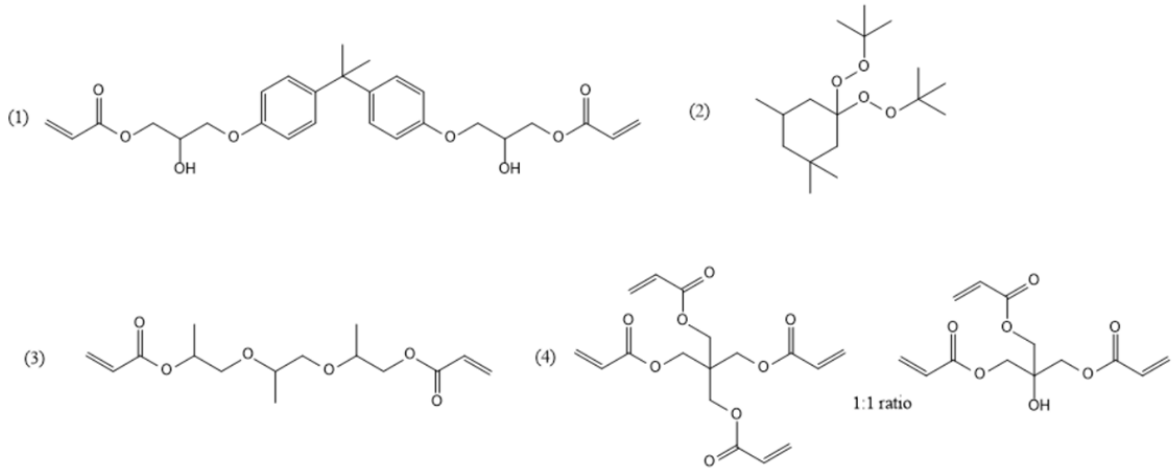

Figure 3.1. Structures of (1) bisphenol-A epoxy acrylate, (2) 1,1-bis(tert-butylperoxy)-3,3,5-tricyclohexane, (3) tripropylene glycol diacrylate, and (4) pentaerythritol triacrylate.

3.2. Materials and Methods

Ebecryl®605 and pentaerythritol triacrylate (PETIA) were purchased from Allnex (Alpharetta, GA). 1,1-*bis*(*tert*-butylperoxy)-3,3,5-tricyclohexane (Luperox®231) was obtained from Sigma

Aldrich. Fumed silica (Aerosil®200, 175 – 225 m^2/g BET surface area) was obtained from Evonik Industries (Parsippany, NJ). Zoltek®PX35 (referred to as Zoltek or milled carbon fiber, 150 x 7.2 squared microns) was provided by Zoltek Companies, Inc. (St. Louis, MO). Microglass®6608 (referred to as milled glass fiber, 470 x 16 squared microns) was obtained from Fibertec, inc (Bridgewater, MA). Polygloss®90 (a kaolinite clay referred to simply as kaolin for the remainder of the paper, 0.4 microns) was obtained from KaMin performance minerals (Macon, GA). Hubercarb®Q3 (calcium carbonate, 3.2 microns median particle size) was purchased from Huber Materials (Quincy, IL). Ethanol (200 proof) was purchased from Koptek (King of Prussia, PA).

To study the effect of fumed silica on the formulation , a standard resin blend (10 g) consisting of Ebecryl®605 (60 wt%) and PETIA (40 wt%) was prepared and one parts per hundred resin (phr) of Luperox®231 was added to it. Phr refers to the amount of material added (in grams) for every 100 grams of resin. Various amounts of fumed silica were then added (0 to 5 phr). The formulations were mixed after the addition of each component. 6″ x 4″x 1/8″ steel panels coated with an epoxy primer (Interbond®998, from International Paint) were used as the substrates. The panels were previously primed, and all coatings in this work were applied after the overcoat window. The panels were sanded down using 60 grit sandpaper and then cleaned with ethanol before coating application. All surface preparation for the work described in this chapter and Chapter 4 was done as just described. A drawdown bar (10 cm x 2 cm) was used to apply the coatings at a wet film thickness of 1000 μm (40 mils). Coating cure was initiated using an infrared Solary®1R1 heater (1,00 W, 15″ x 2.75″) hanging from approximately 10 cm (4″) above the coating. Figure 3.2 shows the general experimental setup. Temperatures were recorded using an infrared thermometer, NUB®8500H, with the laser pointed towards the center of the coating surface from approximately 45 cm. A stopwatch was used to record time

parameters. There is an apparent color change when the coating is done curing; each coating was probed to ensure a complete cure.

Figure 3.2. General set-up for experiments.

After adding fumed silica, cracking remained a challenge so other fillers were added. The resin and initiator were added as previously mentioned. A filler (milled carbon fiber, kaolin, or calcium carbonate) was added, and the formulation was then applied and cured as previously mentioned. For the milled carbon fiber formulations, the fillers were added in increments of 5 phr. 20 phr of filler was added for the kaolin and calcium carbonate-containing formulations. Fumed silica (5 phr) was then added. The formulations were mixed by hand after the addition of each component.

To study the effect of wet film thickness on cure time, first the resin and initiator were added as described earlier. Fumed silica (5 phr) was then added, and the formulation was mixed. The wet film thickness was controlled using a drawdown bar and varied from 250 μm to 1000 μm (10 to 40 mils).

The composition of the resin mixture was varied from 0 wt% to 100 wt% PETIA or Ebecryl®605, fumed silica (5 phr) was added, and the formulation was mixed. The coatings were then applied (40 mils) and cured as previously mentioned.

Varying the Distance of Heat Source:

The distance between the infrared heater and panel was varied from 2″ (5 cm) to 8″ (20 cm). For these experiments, a resin blend of Ebecryl®605 (60 wt%) and PETIA (40 wt%) was prepared and 1 part per hundred resin (phr) of Luperox®231 was added to it. 5 phr of fumed silica was added last, and the formulations were mixed. Each coating was applied to the panel at a wet film thickness of 40 mils through the drawdown bar.

3.3. Base Formulation Parameters

The initial formulation consisted of the initiator and resin. As shown in Figure 3.3, convection and spread of the resin occurred during curing. The spread of the resin formed thinner coatings at the edges. These edges along with other areas required additional time to cure. This formulation could not support a front and overall cure time was in the 10-minute range. 5 phr of fumed silica was required to eliminate convection and sustain a front. The coating adheres to the substrate; however, cracking is apparent. These cracks were formed during the cure process and after as the coating cooled to ambient temperature.

Figure 3.4 shows the cure time as a function of fumed silica loading. The results demonstrate that the cure time decreases with increasing amounts of fumed silica. As shown in Table 3.1, the average front start time was approximately two minutes with a temperature of 105 ˚C on the coating surface. The fronts could not be sustained without constant IR irradiation. Despite this, the generation of fronts significantly reduced cure time. Fumed silica (5 phr) was added to each formulation from this point forward.

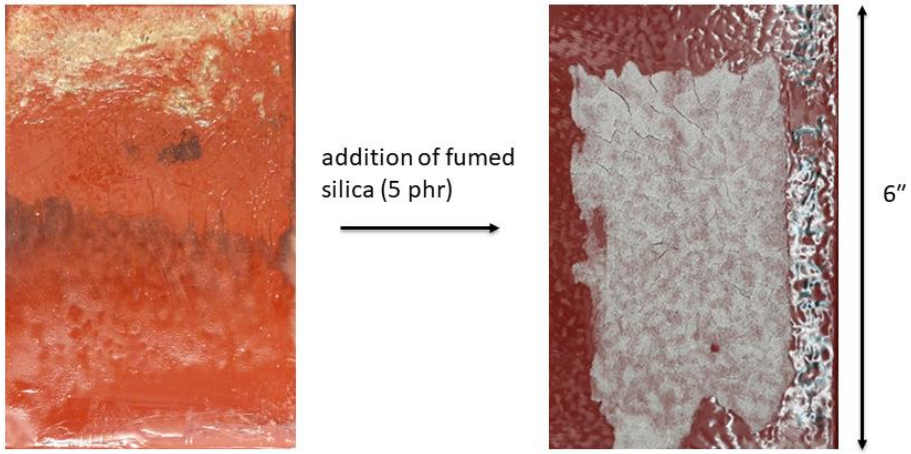

Figure 3.3. Unfilled coating after curing (right) and coating filled with fumed silica (left). Both coatings were cured when the substrate was 10 cm below the heater. The wet coating thickness was kept constant (40 mils) through a drawdown bar. Cracking was present in both coatings.

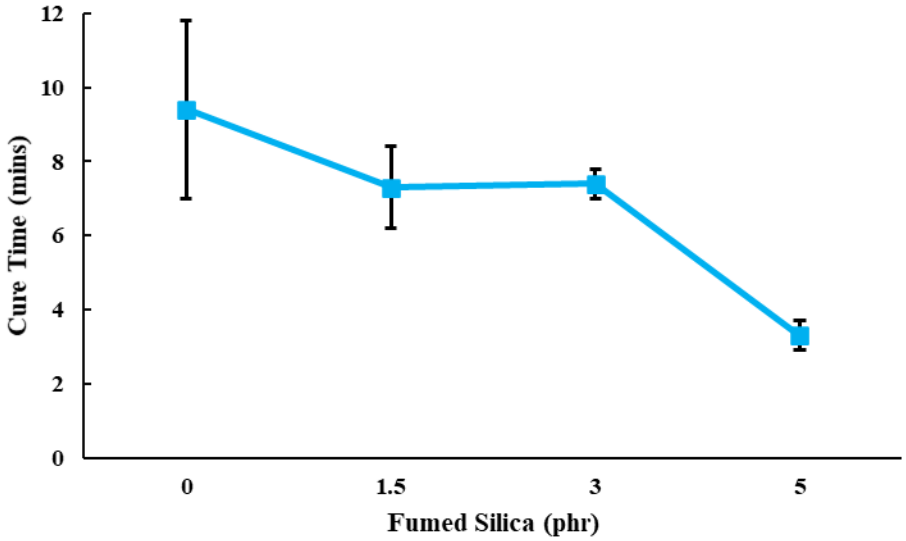

Figure 3.4. Effect of fumed silica loading on cure time of coatings.

Table 3.1. Fumed silica loading vs. front start time and surface temperature

Fumed Silica Loading (phr)	Front Start Time (mins)	Temp of Coating Surface at Start of FP (˚C)
0	2.3 +/- 0.4	111 +/- 13
1.5	2.2 +/- 0.1	110 +/- 9
3	2.0 +/- 0.2	108 +/- 11
5	1.9 +/- 0.1	105 +/- 2

Parameters such as wet film thickness, resin concentration, and the distance between the substrate and the infrared heater were studied. The results in Figure 3.5a show that the cure time was lower for the thicker layers (30 and 40 mils). Thinner layers lose more heat due to a higher surface area to volume ratio. In addition, surface tension-driven convection can also arise. The work by Bansal *et al.* also demonstrates that thinner layers result in lower front velocities.[42] Figure 3.5b shows that the cure time reached a minimum when the heater was 10 cm above the substrate. Figure 3.6 shows that charred and cracked coatings were formed when the heater was 5 cm above the substrate. As shown in Figure 3.7, cracking still occurred in the coatings cured 20 cm below the IR heater.

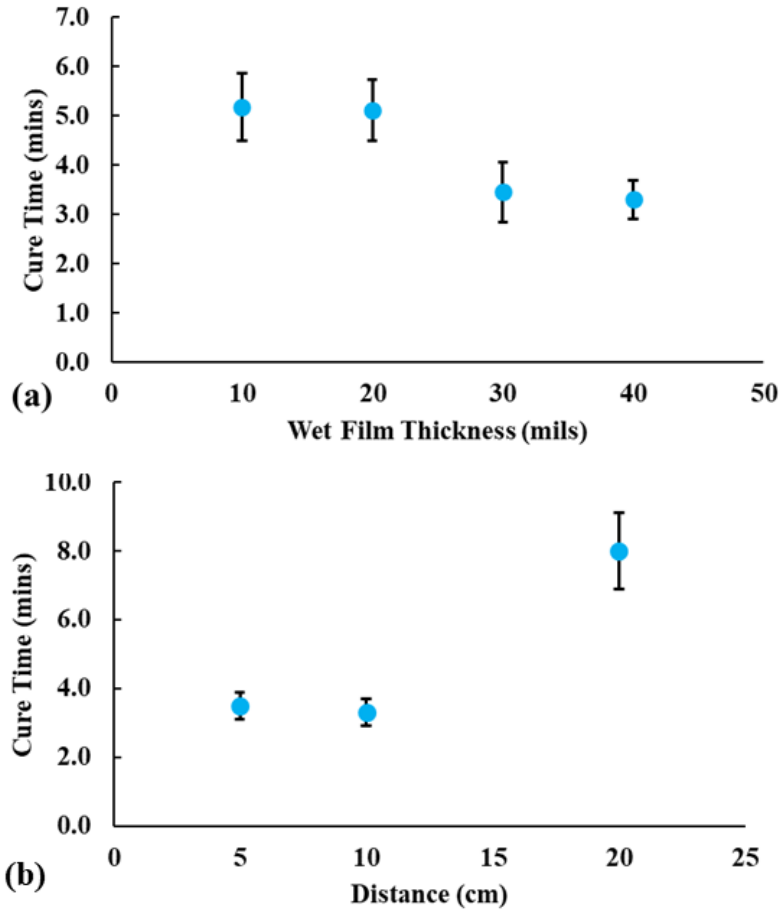

Figure 3.5. Effects of different parameters on the base formulation: (a) effect of wet film thickness on cure time, (b) effect of resin composition on cure time. The wet film thickness of all coatings is maintained through a drawdown bar (40 mils, unless specified). Each coating is cured while the substrate is 10 cm below the heater except for those in the distance study

Figure 3.6. Image showing the charred and cracked coatings formed after curing 5 cm beneath the IR heater.

Figure 3.7. Image showing cracked coatings formed 20 cm beneath IR heater.

Figure 3.8a shows that the cure time decreases as the weight percentage of PETIA was increased relative to that of Ebecryl®605. This result can be explained by the higher density of double bonds per molecular weight in PETIA compared to Ebecryl®605. These results align with the findings of Bynum and coworkers that that front velocity generally increased as the number of double bonds per molecular weight of an acrylate increased.[70] Figure 3.8b shows that the non-skid formulations containing more PETIA formed more brittle coatings while those with more Ebecryl®605 had more cracking. A resin composition consisting of Ebecryl®605 (60 wt%) and PETIA (40 wt%) was used to optimize cure time while maintaining desirable physical properties.

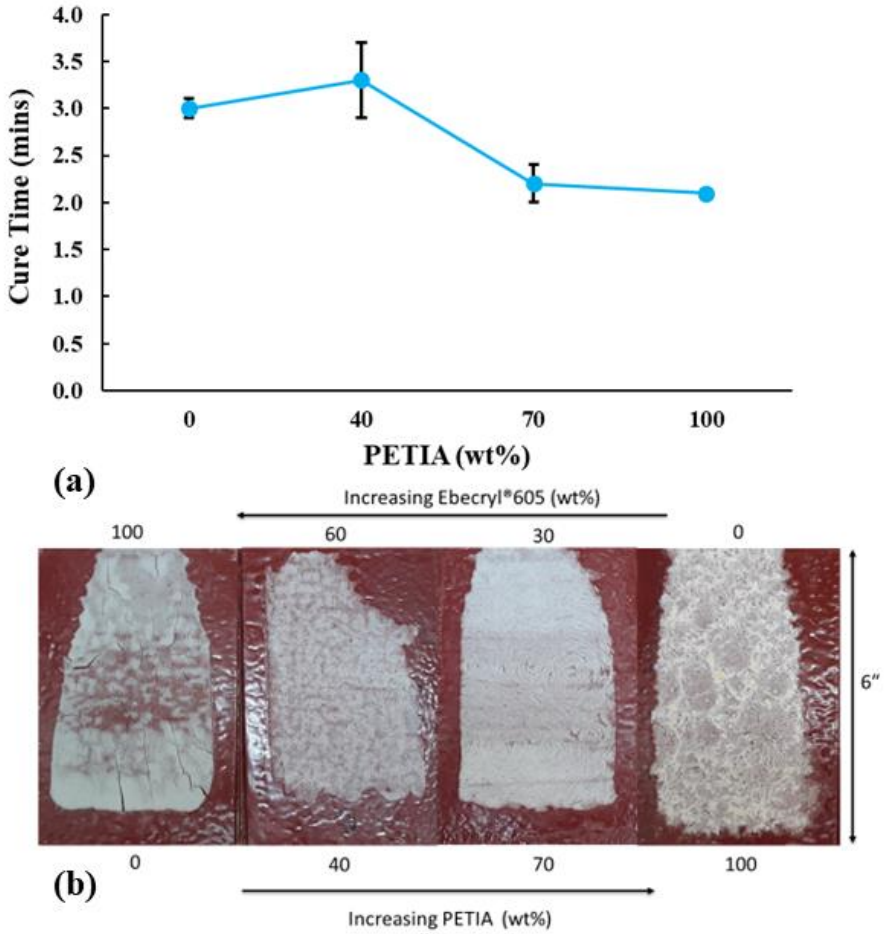

Figure 3.8. The effect of the resin composition on (a) cure time (b) coating appearance. The wet film thickness of all coatings is maintained through a drawdown bar (40 mils). Each coating is cured while the substrate is 10 cm below the heater.

3.4. Effect of Milled Fibers on Cracking

Parameters such as thickness, fumed silica loading, the distance between the substrate and heater, and resin composition were optimized. However, cracking remained a challenge. As shown in Figure 3.9, the current base formulation showed significant cracking. According to the Zoltek corporation, Zoltek®PX35 is a high aspect ratio milled carbon fiber filler with a negative coefficient of thermal expansion (CTE, -0.75 x 10^{-6}/K). One of the causes of cracking is due to internal stresses arising from the CTE mismatch between the coating and the steel substrate. Steel has a lower CTE compared to polymer-based coatings; milled carbon fiber is added to reduce the CTE mismatch.[71] As shown in Figure 3.9, the addition of milled carbon fiber (20 phr) to the

formulation reduces cracking. Figure 3.10b demonstrates that as little as 10 phr of milled carbon fiber is needed to prevent cracking, but the surface of the coating gains a more non-skid texture as more milled carbon fiber is added. As shown in Figure 3.11, there is a slight increase in cure time as milled carbon fiber is added. The overall average cure time for each loading was relatively similar, in the 3 – 5-minute range. Table 3.2 shows that the average front started after approximately 1.5 to 2 minutes of heat irradiation and when the surface of the coating reached around 100 ˚C.

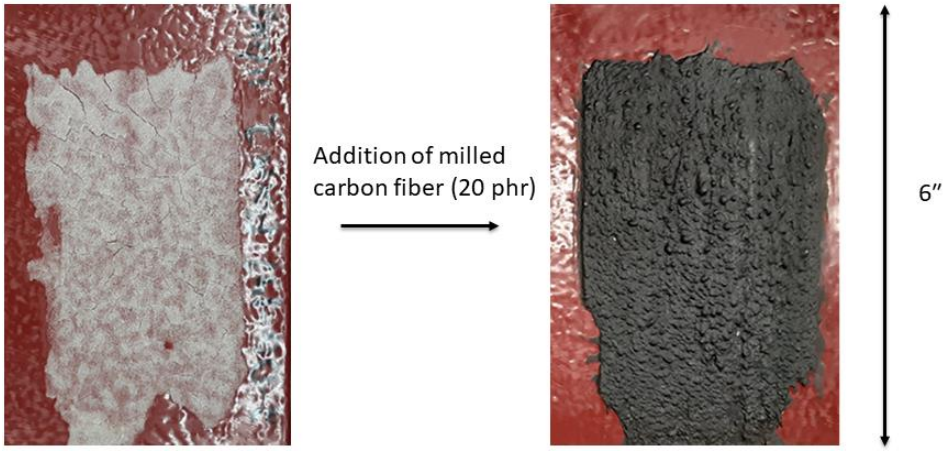

Figure 3.9. The image shows that the addition of milled carbon fiber (20 phr) reduces cracking and forms a non-skid texture.

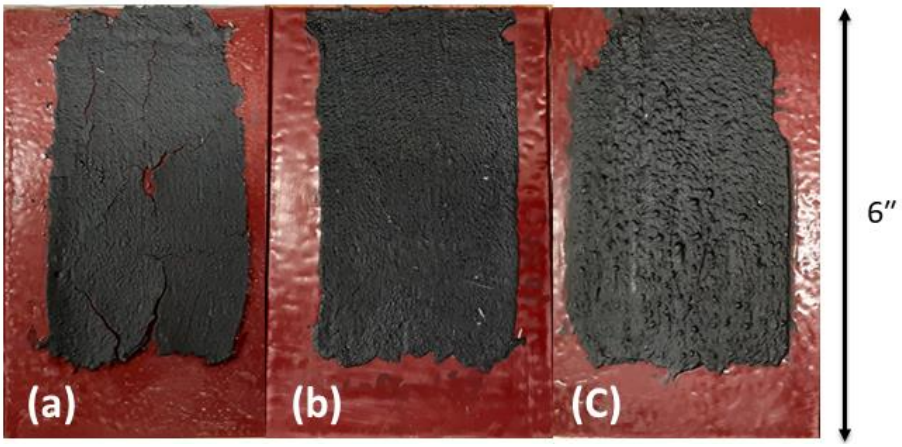

Figure 3.10. Image showing the coatings formed using milled carbon fiber with loadings of (a) 5 phr (b) 10 phr and (c) 20 phr.

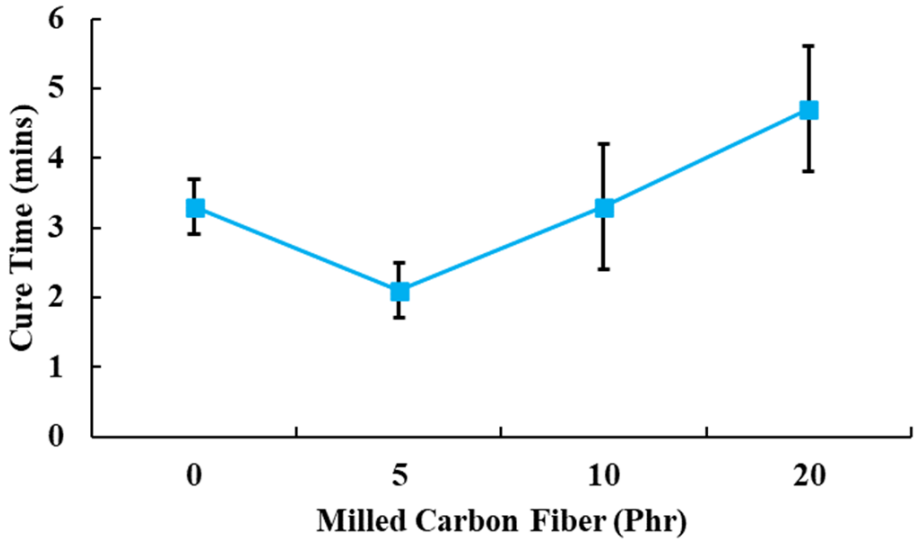

Figure 3.11. Effect of milled carbon fiber loading on cure time. The wet film thickness (40 mils) and distance between heater and substrate (10 cm) were kept constant.

Table 3.2. Effect of milled carbon fiber loading on front start time and surface temperature

Milled Carbon Fiber Loading (phr)	Front Start Time (mins)	Temp of Coating Surface at Start of FP (˚C)
0	1.9 +/- 0.1	105+/- 2
5	1.4+/- 0.1	99 +/- 6
10	1.4 +/- 0.2	106+/- 2
20	1.5 +/- 0.2	106+/- 8

Zoltek®PX35 is an elongated filler with an aspect ratio of 21:1. By comparison microglass® 6608(a milled glass fiber made from E-glass filaments) has an aspect ratio of 27:1 and can be added to thermosets to decrease distortion at high temperatures. Zoltek®PX35 has a CTE of -0.75 $X10^{-6}$ /K and E-glass has a CTE of 5.4 x 10^{-6} /K. The milled glass fiber will be added to determine if adding fibers with high aspect ratios reduces cracking. As shown in Figure 3.12a, Figure 3.12b, and Figure 3.12c Initially no visible cracks can be seen in cured coatings formed from the formulations containing 5 phr, 10 phr and 20 phr of the microglass milled fiber. a closer inspection, shown in Figure 3.13, reveals very minor cracking on a coating sample loaded with 5 phr milled glass fiber. The formulation containing 5 phr of milled glass fiber had

more apparent cracking, the cracks were still (small) minor but larger in number in comparison to the cracks in the samples containing more milled glass fiber. As shown in Figures 3.12b and 3.12c, Cracking is largely eliminated with higher loadings of milled glass fiber. Despite the reduction in cracking, the coatings have a non-uniform color that may be a result of poor wetting between the milled glass fiber and the resin.

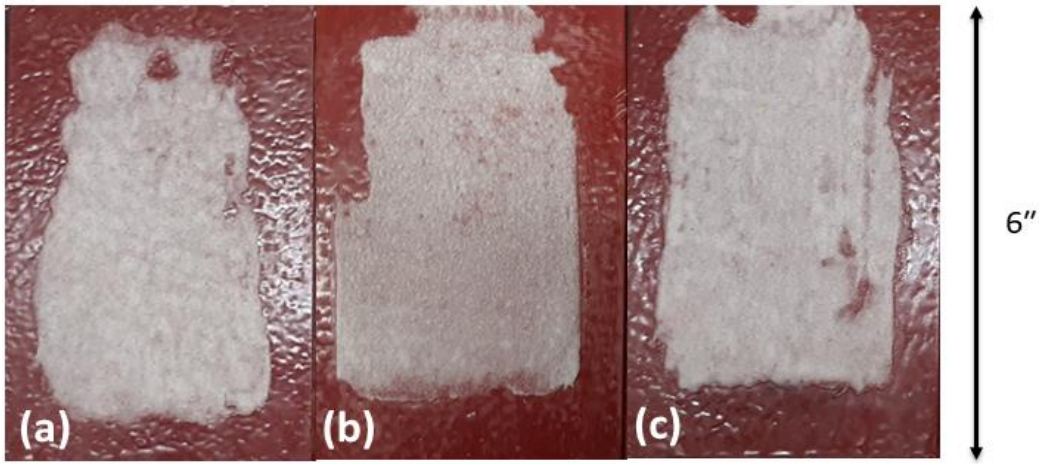

Figure 3.12. Image showing the coatings formed using milled glass carbon fiber with loadings of (a) 5 phr (b) 10 phr and (c) 20 phr.

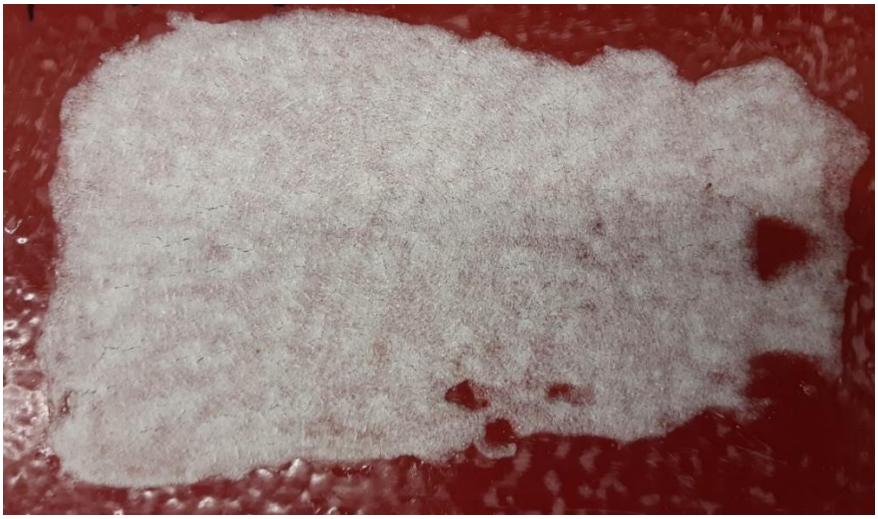
Figure 3.13. Close up of a film containing 5 phr of microglass milled fiber. The cracks are small but can be seen up close.

As shown in Figure 3.14, the cure time remains in the 3-minute range at various loadings (0 to 20 phr) of milled glass fiber. Table 3.3, reveals an average front start time of around 2 minutes and a coating surface temperature of around 100 C. This is comparable to the front start

time and coating surface temperatures for the formulations containing milled carbon fiber (Zoltek®PX35).

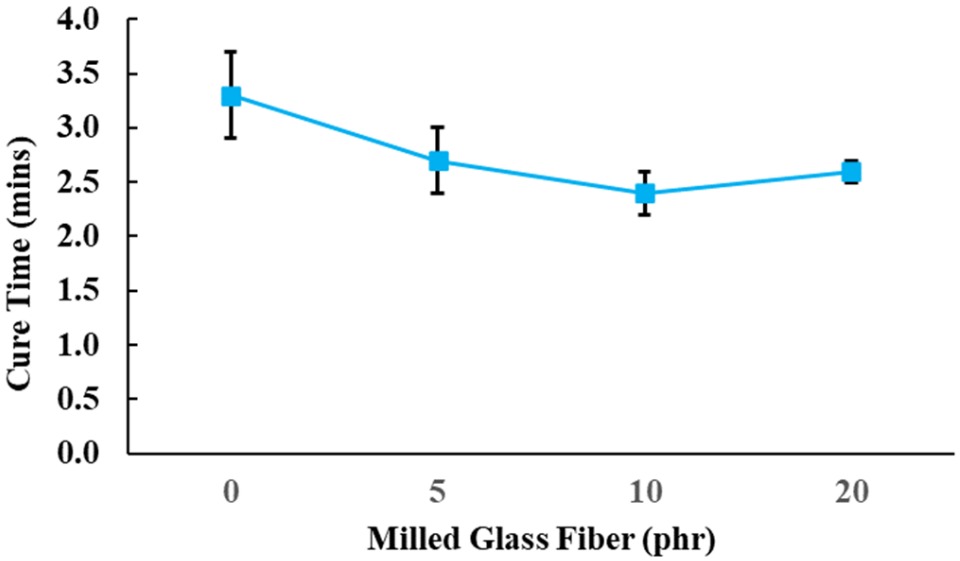

Figure 3.14. Effect of microglass milled fiber loading on cure-time of coatings.

Table 3.3. Effect of milled glass fiber loading on front start time and surface temperature

Milled Fiber Loading (phr)	Front Start Time (mins)	Temp of Coating Surface at Start of FP (˚C)
0	1.9 +/- 0.1	105+/- 2
5	2.0 +/- 0.1	104 +/-4
10	1.9 +/- 0.1	82+/- 7
20	2.0 +/- 0/1	108 +/- 2

3.5. Effects of Adding Calcium Carbonate and Kaolin Clay

To determine if the high aspect ratio of milled carbon fiber and milled glass fiber is responsible for the reduction in cracking, kaolin, and calcium carbonate, which have irregular shapes are added as fillers. Figures 3.15a and 3.15b show that fillers with irregular shapes such as calcium carbonate and kaolin were not able to prevent cracking at the same loading (20 phr) as milled carbon fiber and milled glass fiber. These results demonstrate that the high aspect ratios of the

milled glass fiber and milled carbon fiber significantly reduced the cracking of the cured coatings.

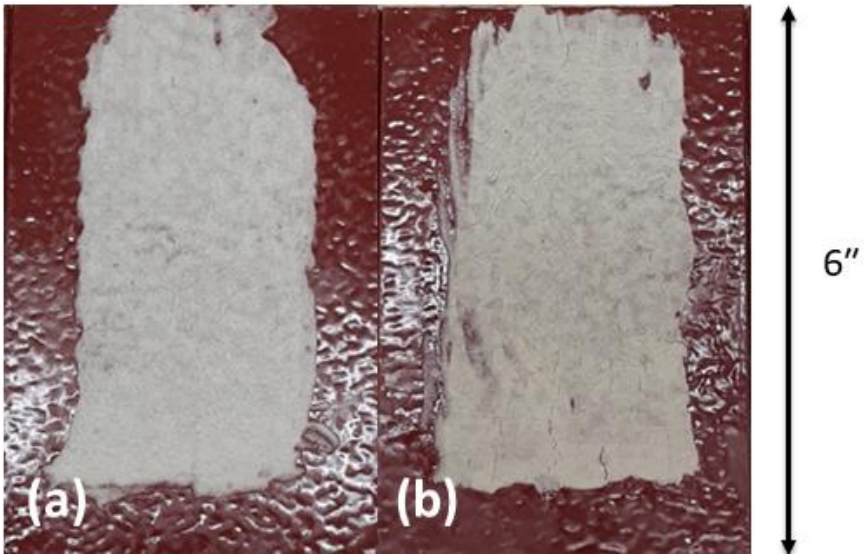

Figure 3.15. Images of cracked coatings formed with 20 phr of (a) calcium carbonate (b) kaolin

As shown in Table 3.4, The front start time for the coatings containing the zoltek is around 30 seconds shorter compared to the other films. Like the previous coatings, the average coating surface temperature for the kaolin and calcium carbonate formulations is around 100 ˚C when FP starts. As shown in Figure 3.16, the overall cure time for the milled fiber containing coatings is higher (approx. 5 mins vs. ~ 3 mins for the other samples) than those containing calcium carbonate, kaolin, milled glass fiber, or only fumed silica. During the curing process, the edges of the coating took longer to cure in the milled carbon fiber coatings. This might be attributed to the relatively nonskid surface being formed during the curing process. The non-skid surface would lead to the formation of thinner areas.

Table 3.4. Effect of various fillers on front start time and surface temperature

Filler	Front Start Time (mins)	Temp of Coating Surface at Start of FP (˚C)
Fumed Silica only (5 phr)	2.0 +/- 0.1	105 +/- 2
Calcium Carbonate (20 phr)	2.1 +/- 0.1	104 +/- 1
Kaolin (20 phr)	2.2 +/- 0.1	110 +/- 1
Milled Fiber (20 phr)	2.0 +/- 0.1	108 +/- 2
Milled Carbon Fiber (20 phr)	1.5 +/- 0.2	106 +/- 8

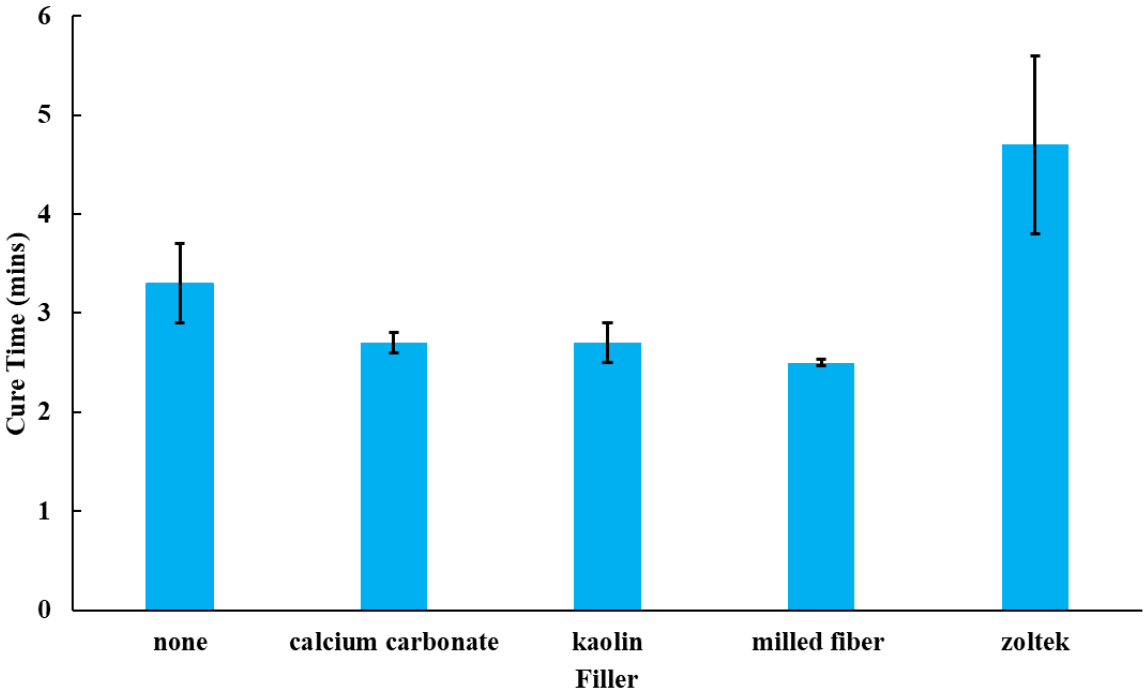

Figure 3.16. Cure time for 20 phr of various fillers. Note* the sample labeled with none is the base formulations containing 5 phr of fumed silica**.**

3.6. Conclusions

A base formulation consisting of a bisphenol-A epoxy acrylate mixture and PETIA was optimized as a coating for cure-on-demand applications on primed steel substrates. Fumed silica (5 phr) was added to eliminate convection thereby allowing frontal polymerization. Curing of the coating was done by constantly applying to heat to generate frontal polymerization.

Other parameters such as wet film thickness, resin composition, and distance between the heater and substrate were tested for optimization of the coating. It was found that cure time is reduced for thicker layers. Regarding the resin composition, increasing the amount of PETIA in the formulation reduces cure time but also increases porosity, therefore a mixture of Ebecryl®605 (60 wt% of resin mass) and PETIA (40 wt% of resin mass)is optimal. It was determined that a 10 cm distance between the coated substrate and infrared heater gives the shortest cure time without charring the coating and causing additional cracking. Milled carbon fiber was added to eliminate cracking and provide a non-skid appearance. The resulting base formulation had a cure time in the 5-minute range and when applied as a 40 mils thick coating. Milled glass fiber was also effective at reducing cracking; however, the coatings were less non-skid and uniform in appearance. Kaolin and calcium carbonate, which have an irregular shpe, were used as analogs to show that high aspect ratio fillers such as Zoltek®PX35 and Microglass®6608 reduce cracking.

CHAPTER 4. APPLICATION OF CURE-ON-DEMAND COATING AS MARITIME NON-SKID COATINGS

4.1. Introduction to Corrosion

Corrosion is a process in which a metal is converted into its combined state in compounds that are similar to or identical to the original form, such as Iron oxide. Corrosion of a metal occurs through electrochemical reactions with its environment. For corrosion to occur, an electrolyte, electronic pathway, anode, and a cathode must all be present. Corrosion occurs due to the differences in potential between the cathodic and anodic sites; this difference in potential is what drives corrosion. As shown in Equation [4.1], the difference is equal to sum of the reduction potentials of the oxidation and reduction reactions which occur at the anode and cathode sites, respectively.[72]

$$E^{\circ}_{cell} = E^{\circ}_{OX} + E^{\circ}_{RED} \quad [4.1]$$

The spontaneity of corrosion can be determined by relating the potential of a cell to Gibbs free energy (ΔG) through Equation [4.2], where n is the number of electrons transferred in the reaction and F is Faraday's constant. [72]

$$\Delta G = -nFE_{Cell} \quad [4.2]$$

$$\Delta G = \Delta G^{\circ} + RT \ln Q \quad [4.3]$$

Equation [4.2] demonstrates that the larger the potential difference (the more positive $E_{cell}$is) is between the two half cells, the more thermodynamically favorable the reaction will be. As shown in Equation [4.3], when taking concentration into account, the change in free energy in the nonstandard state can be related to the standard state change in free energy. R is the gas constant, T is temperature, and Q is the reaction quotient. The Nernst, Equation [4.4], equation is found by substituting Equation [4.2] and $\Delta G^{\circ} = -nFE^{\circ}_{Cell}$ into Equation [4.3].[72]

$$E_{Cell} = E^{\circ}_{Cell} - \frac{RT}{nF}\ln Q \quad [4.4]$$

The Nernst equation and relates the electrode potential or electromotive force (emf) to the standard electrode potential of the cell and the concentrations of reductants and oxidants. The potential increases as the concentration of the oxidizer increases. Oxidizers such as oxygen and H^+ increase the favorability of corrosion.[72]

The rusting of iron in steel is a classic example of the corrosion process, which occurs through the reduction of oxygen at the cathode (1) and oxidation of Iron at the anode (2).

(1) $2H_2O(l) + O_2(aq) + 4e^- \rightarrow 4OH^-(aq)$

(2) $Fe(s) \rightarrow 2e^- + Fe^{2+}(aq)$

Next Iron hydroxide will undergo oxidation and decomposition reactions to form rust ($Fe_2O_3H_2O$).[73]

There are different types of corrosion such as general corrosion, galvanic corrosion, crevice corrosion, and pitting corrosion. In general, or uniform corrosion, a relatively uniform area of the steel surface is corroded. Galvanic corrosion occurs when two different alloys or metals are coupled to each other. One alloy (the more active one) will preferentially corrode to the more noble metal. Crevice corrosion occurs where steel is connected to a different alloy or nonmetallic material. Pitting corrosion is a result of localized corrosion that leads to formation of pits in the steel; these pits can be deep or shallow. Galvanic corrosion is due to the the differences in electrode potential between the coupled metals. The galvanic series, shown in Table 4.1, lists metals based on their electrode potential from most active to least active (more noble). Corrosion will occur in the anode which is the metal with more potential. Metals such as Al, Mg, and Zn tend to corrode preferentially to metals such as gold and platinum. [72]

Table 4.1. The galvanic series in seawater.

Anodic (active)
Magnesium
Zinc
Aluminum
Mild Steel
Cast Iron
Copper
Graphite
Gold
Platinum
Cathodic (noble)

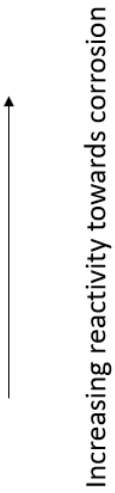

4.2. Introduction to Corrosion Protection

Three methods of corrosion protection include galvanic (sacrificial) protection, inhibitor coatings, and barrier coatings. Galvanic protection is based on galvanic corrosion, where one metal corrodes preferentially to the other one. In this case, a metal or alloy that has a higher electrochemical potential than the substrate that is to be protected. After the more active material corrodes, the corroded products will then act as a barrier against further corrosion. Galvanic protection is limited to primers as they must be in direct contact with the substrate. Powder coatings formulated with zinc dust are examples of galvanic protective coatings. Inhibitive coatings rely on the formation of a protective layer on the substrate resulting from a reaction between the substrate and the dissolved components of inorganic pigments. When moisture permeates these coatings, the inorganic pigments dissolve and are then carried to the substrate.[73]

Barrier coatings form a protective film on the substrate that impede the diffusion of water, salt, and oxygen. The choice of raw materials such as resins and fillers have a dramatic

impact on the ability to create a good barrier against corrosion. Factors such as crosslink density and filler shape impact the permeability of the coating. A higher crosslink density decreases diffusion of molecules into the coating, and this improves resistance to corrosion and chemicals. Lamellar shaped fillers create a tortuous path that impedes the movement of molecules through the coating, by comparison, molecules such as water can move more easily around spherical shaped fillers and pigments. [73, 74]

Corrosion of maritime vessels is a significant economic and environmental issue. The annual cost of corrosion is estimated to constitute a significant percentage of the gross national product of the western world.[73] In addition, more drag on ships leads to higher fuel costs and more burning of fossil fuels. In addition to economics, corrosion failures have led to loss of life, such examples include collapse of bridges, airline accidents, and ruptures in pipes. Due these large economic and safety concerns, significant research and product development is done to protect against corrosion. As shown in Figure 4.1, Current nonskid coating technology often takes days to cure to service and requires two-part mixing of separate formulations.[75] In addition to curing time and mixing, there is an increasing desire to reduce VOCs.[76]

The formulation developed in Chapter 3 will be applied as a non-skid coating. Aluminum oxide was added to provide a non-skid texture. The high crosslink density of the coating provided good chemical and corrosion resistance as well as hardness. Epoxy acrylates such as Ebecryl®605 are known to provide good barrier properties while PETIA provided a high crosslink density and reduced cure time. Characterization such as impact testing, flexibility, and corrosion & chemical resistance is done to show potential application.

MIL-PRF-24667C: Type; Composition [Service Lifetime]	VOC Content (lbs/gal)	Touch Dry; Full Service Cure	Pot Life	Volumetric Mix Ratio (Volumetric)
Type V Comp G [3 years]	0.77	4 Hours 10 Days	1 Hour @ 73°F	4:1
	0.95	7 Days	2 Hours @ 70°F	4.6:1
Type II Comp G [3 years]	1.4	5 hours; Not provided	2 Hours @ 70°F	5:1
	1.21	5 Hours; 10 Days	1 Hour @ 73°F	4:1
	0.77	4 Hours 10 Days	1 Hour @ 73°F	3:1
	3.9	24 Hours	8 Hours @ 70°F	9:1
	4	12 Hours; 7 Days	2 Hours @ 70°F	5.7:1
	1	12 Hours; 7 Days	2 Hours @ 70°F	6.7:1
	1.6	12 Hours; 7 Days	4 Hours @ 70°F	7.9:1
Type VI Comp G [1 year]	0.9	9 Hours 3 Days	2 Hours @ 70°F	3.4:1
Type VIII Comp G [1 year]	0.75	3 Hours 2 Days	25 mins @ 77°F	4:1
	0.3	12 Hours 4 Days	45 mins @ 70°F	3:1
Type VII Comp G OR L [30 days]	0.75	8 Hours 1 Day	30 mins @ 73°F	5:1
	0.3	16 Hours 6 Days	45 mins @ 70°F	2.9:1

Figure 4.1. Chart showing cure times, pot lives, mix ratios, and VOC content of current nonskid coatings. [75]

4.3. Materials and Methods

Ebecryl®605 and pentaerythritol triacrylate (PETIA) were purchased from Allnex (Alpharetta, GA). 1,1-*bis*(*tert*-butylperoxy)-3,3,5-tricyclohexane (Luperox®231) was obtained from Sigma Aldrich. Fumed silica (Aerosil®200, 175 – 225 m^2/g BET surface area) was obtained from Evonik Industries (Parsippany, NJ). Zoltek®PX35 (referred to as Zoltek or milled carbon fiber, 150 x 7.2 squared microns) was provided by Zoltek Companies, Inc. (St. Louis, MO). Microglass®6608 (referred to as milled glass fiber, 470 x 16 squared microns) was obtained from Fibertec, inc (Bridgewater, MA). Aluminum oxide (16 grit, 14 mesh) was obtained from Floorguard Products, Inc. (Aurora, IL). Natural seawater was obtained from the Gulf of Mexico (Gulf Shores, AL). Synthetic seawater (following ASTM D1141) was obtained from Grainger (Arlington, TX). Skilcraft®1064006 (nonionic liquid detergent) was purchased from SkyGeek (LaGrangeville, NY). Ethanol (200 proof) was purchased from Koptek (King of Prussia, PA).

Castrol®GTX High Mileage (synthetic motor oil) was purchased from BP Lubricants USA, Inc. (Wayne, NJ). AVL-TKS anti-icing de-icing fluid was purchased from Aviation Laboratories, Inc. (Houston, TX).

All non-skid coatings were prepared using a resin blend consisting of Ebecryl®605 (60 wt%) and PETIA (40 wt%) was prepared, and 1 phr of Luperox®231 was added to it. The amount of blend prepared depended on the size of the substrate area to be coated. 11 g of resin was used for a 6″ x 3″ area, 15 g of resin was used for a 6″ x 4″ area, 22.5 g for a 6″ x 6″ area, and 90 g for a 12″ x 12″ area. Milled carbon fiber or milled glass fiber (20 phr) was added followed by fumed silica (5 phr). Initially, 100 phr of aluminum oxide was added (the preliminary non-skid), this was later reduced to 25 phr. The formulations were mixed after the addition of each component. Each substrate was primed with Interbond®998 and sanded down as described in Chapter 3. The coating with 25 phr of aluminum oxide was applied on the substrate using a fiberglass aluminum alloy roller (11″ total length). The roller (3″ x 0.75″) had 1 mm deep groves. The preliminary non-skid was applied by a 2″ flat edge paintbrush onto 6″ x 4″x 1/8″ primed panel. In the preparation of the non-skid for impact testing, the temperature of the panel surface not coated with non-skid is measured. The temperature of the non-skid surface is measured for the other formulations. A stopwatch was used to record the time. Coating cure was apparent with a color change. Each coating was probed to ensure a complete cure. To determine the amount of coating loss as vapor, the mass change of the resin between the wet and cured state was determined for the preliminary non-skid.

Impact testing was done following ASTM G14. A 4 Ib weight was dropped onto an indenter punch resting on the coated panel. A total of 25 impact tests were made in a 3″ x 3″ area using the sequence shown in Figure 4.2 A 1″ chisel was then used to remove any loosened

nonskid around the impact zone. The number of connections between adjacent impacts was counted. The score was determined by multiplying the sum of these connections by 2.5 and then subtracting from 100. The total score reflects the percentage of intact coating remaining in between the impact sites. The coating formulation was applied in a 6″ x 6″ area (half of the panel area) on a 12″ x 6″ x 1/8″ primed panel. Two non-skid panels were impacted without treatment and four were impacted after treatment with synthetic salt water for 15 days in accordance with ASTM D1141.

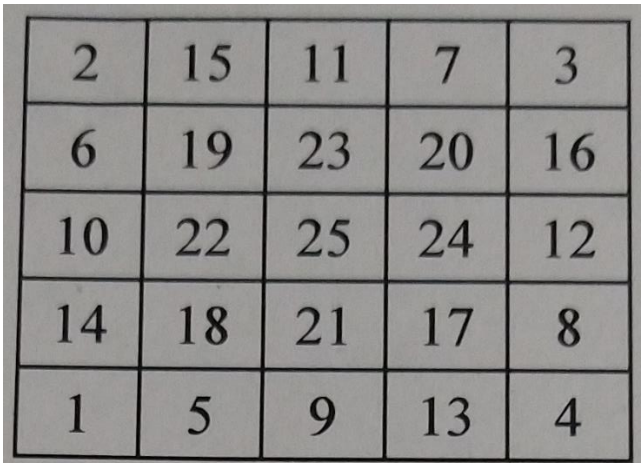

Figure 4.2. The impact sequence for the impact test.

Flexibility was determined by bending over a 5″ mandrel. The non-skid was prepared on 6″ x 3″ x 1/16″ flexible primed aluminum panels. To test for flexibility, the non-skid panels were bent over the mandrel until cracks appeared in the coating. Ridges of the non-skid profile ran parallel to the axis of the bend. Cracking within 1/2″ of the edge was ignored. The degree of bending at which cracking appeared was recorded.

The panels were then bent 20˚ over the mandrel. Cure parameters such as time and temperature were recorded. All the panels were conditioned at room temperature for 24 hours before testing in accordance with ASTM F137.

Qualitative chemical testing was done to determine the relative resistance of the non-skid coating to various chemicals including ethanol, natural saltwater, motor oil, detergent, and deicing-defrosting fluid. For each test, two non-skid coatings were prepared (see the preparation of non-skid for details) on 6″x 4″x 1/8″ primed steel panels. One non-skid sample was impacted twice, with the impacts being four inches apart from each other and one inch from the edges. Each non-skid coating was placed in a beaker (1500 mL) and halfway submerged in each chemical; the beakers were then sealed with foil. The non-skid coatings were submerged for 24 hours in ethanol and deicing-defrosting fluid, and four weeks in the seawater, motor oil, and detergent. After removal, each non-skid panel was probed with a 1″ chisel for loss of adhesion or softening of the coating. The unsubmerged and submerged parts were compared along with the impacted versus non-impacted coating. The coatings submerged in ethanol and deicing-defrosting fluid were given a six-hour recovery period before evaluation.

A salt fog test was done to test corrosion resistance. Two abrasive blasted steel test panels (3-4 mils) were coated with interbond®998 (a qualified MIL-PRF-23236 Type VII coating). The panels were 12 x 12 x 1/8 inches (304.8 x 304.8 x 3.17 millimeters). A 5 ¾- by ¼-inch (145- by 6-millimeter) (nominal) linear scribe in the nonskid system was cut to the bare steel using a drill bit and drill press. The two samples were subjected to accelerated corrosion for 1,000 hours in a salt fog cabinet in accordance with ASTM B1170. Upon completion of the accelerated corrosion exposure, the samples were removed from the salt fog cabinet, rinsed in potable water, and dried with lint-free laboratory wipes. Immediately after the residual rinse water was removed, the scribe area of each panel was prepared and inspected in accordance with ASTM D1654 for separation between layers, loss of adhesion, undercutting, and corrosion. Finally, an area of the non-skid and primer around the scribe was removed with a 2-inch pneumatic die grinder. 16 grit

aluminum oxide abrasive paper was then used to remove any remaining coating on the substrate. The exposed substrate was then visually inspected for discoloration and or corrosion.

A coefficient of friction (COF) test was done to measure the roughness of the coating. The non-skid was prepared on 12″ x 12″ x 1/8″ primed steel panels. The dynamic coefficient of friction was measured using the rotating arm meter for dry and wet substrates (μ-Deck Rotating Arm COF Meter) from Vision Point Systems Inc. The test was conducted on two panels. The COF test panel was tested in the as-applied state and was not subjected to nonskid conditioning or wear cycles before testing. The as-applied test panel was subjected to this test procedure under both dry and wet conditions. After completion of the dry condition test, the panels were uniformly wetted with synthetic seawater per ASTM D1141 from a spray bottle until the synthetic seawater ran off the side of the panel surface. The dynamic COF test was performed on each panel immediately after uniform wetting with synthetic seawater.

The dynamic COF meter was used in accordance with the manufacturer's directions, and the test procedure was performed. A ball was inserted into the ball holder, and the contact ball was locked into the holder. This was done while ensuring that the surface was in contact with the surface to be measured, which had not been previously used for a previous measurement. The Vision Point Systems Inc μ-Deck Rotating Arm COF Meter was placed on the test panel ensuring that the ball remained in contact with the surface of the test panel throughout the full 360-degree rotation of the contact ball. The surface temperature (Ts) of the nonskid panel was recorded in degrees Fahrenheit. The Ts of the panel after each COF reading and the uncorrected COF (COFU) was recorded. The temperature corrected COF (COFC) was calculated using the equation

COFC = COFU – 0.0048 (75 – Ts). To be considered a pass, the COF must meet the

requirements of the MIL-PRF-24667D specification. This calls for minimum dynamic COF values of 1.4 (dry substrate) and 1.1 (wet substrate).

Viscosity was determined by using a TA Discovery HR-2 rheometer. The viscosity (Pa·s) was measured in a flow ramp setting (shear rate from 1 to 100 (1/s)). Initially, the plate height was set to 1550 mm, excess coating removed and then reduced to 1500 mm to ensure total probe coverage. Viscosity was measured for both the non-skid containing aluminum oxide (16 grit, 14 mesh) and base (no aluminum oxide) formulations. Three replicates were tested for each formulation. To determine if the samples were thixotropic, peak hold experiments were performed at low (1 Hz) and high (10 Hz) shear rates. The first step was at 1 Hz for 60 s, followed by an increase to 10 Hz for 60 s, and returned to 1 Hz for 60 s. Recovery percent and thixotropy index (TI) were calculated and compared between replicates and formulations with and without aluminum oxide particles.

4.4. Cure Process of Non-Skid

Figure 4.3 demonstrates the curing process of the non-skid formulation . Irradiation of heat ignites a propagating front which then travels and cures the coating. Through experimentation it was found that keeping the heater on during the process was necessary to sustain the front. The front does not propagate in the thinner areas of the coating and therefore additional heat irradiation is needed to complete the cure.

4.5. Preliminary Non-Skid Formulation

Figure 4.4 shows an image of the cured non-skid coatings while Table 4.2 shows the curing data. No cracking or delamination occurred in any of the coatings formed, and an average cure time of around 7 minutes was achieved. The higher cure time in comparison to the base formulation can be explained by the peaks and valleys of the non-skid. As shown in Figure 3.5a, the cure time

decreased as the thickness of the film decreased, and this was attributed to heat loss. Heat loss from the resin prevents propagation of fronts in the thinner areas of the coating. The overall result is that the thicker areas cure quickly while the thinner areas take longer to cure as no propagating front is generated. This also explains the wider range of cure times in comparison to the base formulation.

To determine the amount of evaporant released during curing, the difference between the mass of the coating resin before and after curing was determined. It was found that the coating lost approximately 5 wt% of its resin mass (approximately 2 wt% of the total coating mass) after curing.

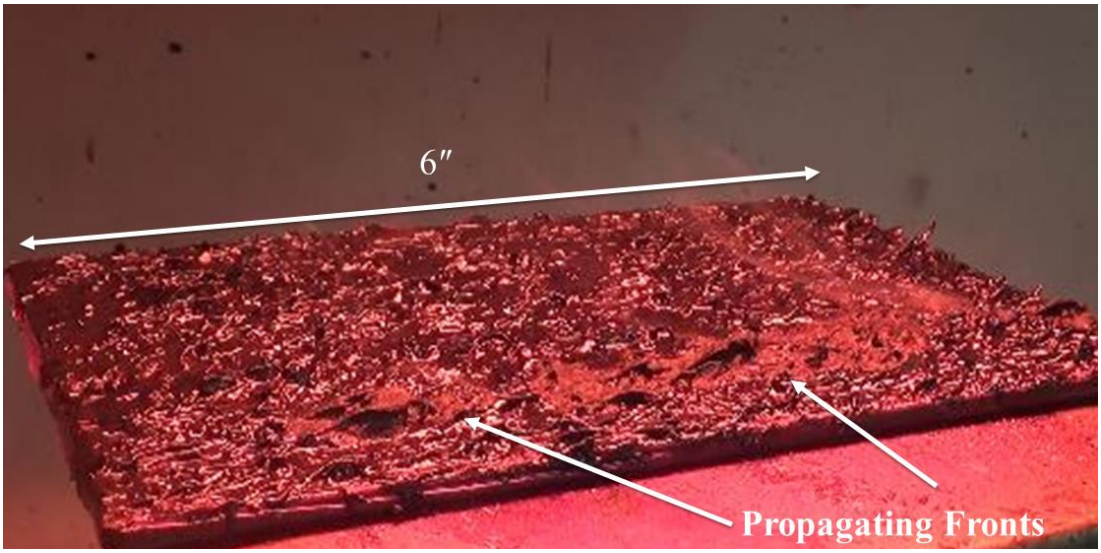

Figure 4.3. Image showing propagating fronts as non-skid is being cured under heat.

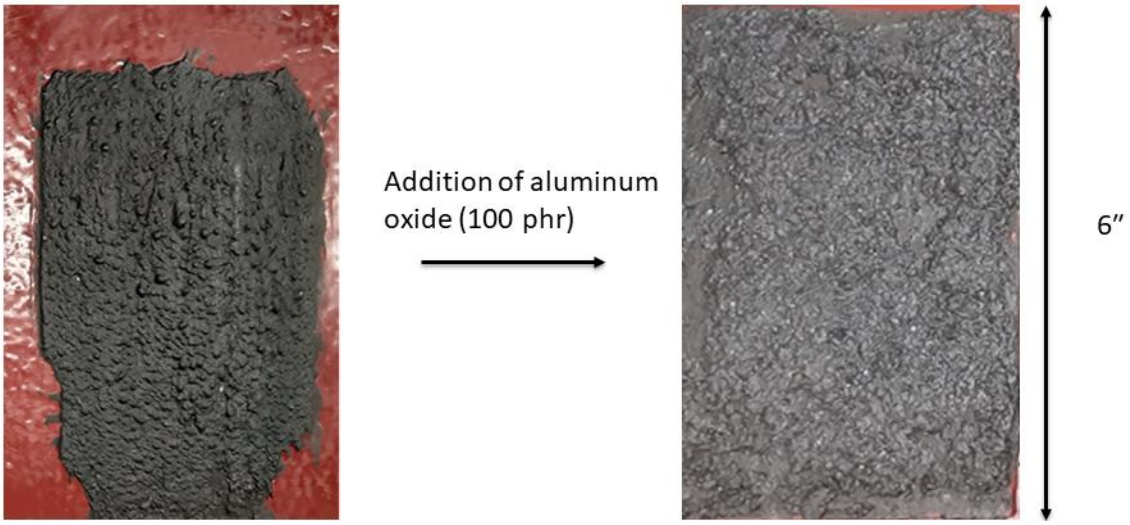

Figure 4.4. Non-skid coating applied via paint brush after the addition of 100 phr of aluminum oxide.

*Note: All other nonskid coatings were applied with a roller (fiberglass aluminum alloy-based roller; roller is 20 mm x 75 mm and contains grooves (10 mm deep).

Table 4.2. Cure parameters for preliminary non-skid coating.

Non-skid Sample	FP Start Time (mins)	Temp of Coating Surface at Start of FP (˚C)	Cure Time (mins)	Mass Loss of Resin after Cure (wt%)
One	1.4	116	8.0	4.8
Two	1.6	115	6.8	4.5
Three	1.5	114	6.8	4.7
Average	1.5 +/- 0.1	115 +/- 1	7.2 +/- 0.7	4.7 +/- 0.2

4.6. Physical Properties of Non-Skid Coating

The results in Figures 4.5a and 4.5b demonstrate impact scores of 52.5% and 15%, respectively (33.8% average). This poor and inconsistent performance was attributed to the high loading of the aluminum oxide. This loading led to increased brittleness of the coating and therefore poor impact resistance. To improve impact resistance, the amount of aluminum oxide

was reduced from 100 to 25 phr. The results in Figures 4.5c and 4.5d demonstrate improved impact scores of 87.5% and 77.5% (82.5% average) for non-skid coatings made from formulations containing 25 phr of aluminum oxide.

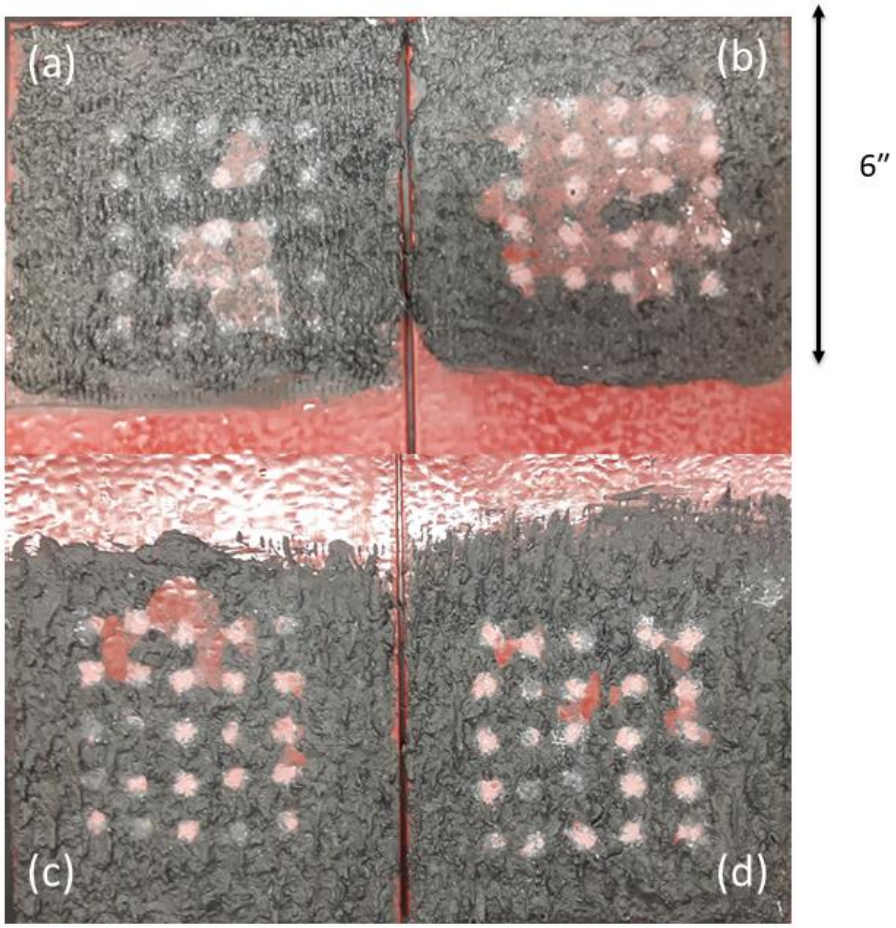

Figure 4.5. Non-skid coatings after impact score with 100 phr of aluminum oxide (top) and 25 phr of aluminum oxide (bottom). The scores were (a) 52.5% (b) 15% (c) 77.5% and (d) 87.5%.

A total of four non-skid coatings with 25 phr of aluminum oxide were treated with synthetic seawater and then subsequently tested for impact resistance. As shown in Figure 4.6, two of the treated non-skid coatings showed a large reduction (scores of 40% and 22.5%) in the impact resistance; however, both coatings had visible discontinuities (holidays). Figure 4.7 shows an example of a discontinuity after the nonskid was treated.

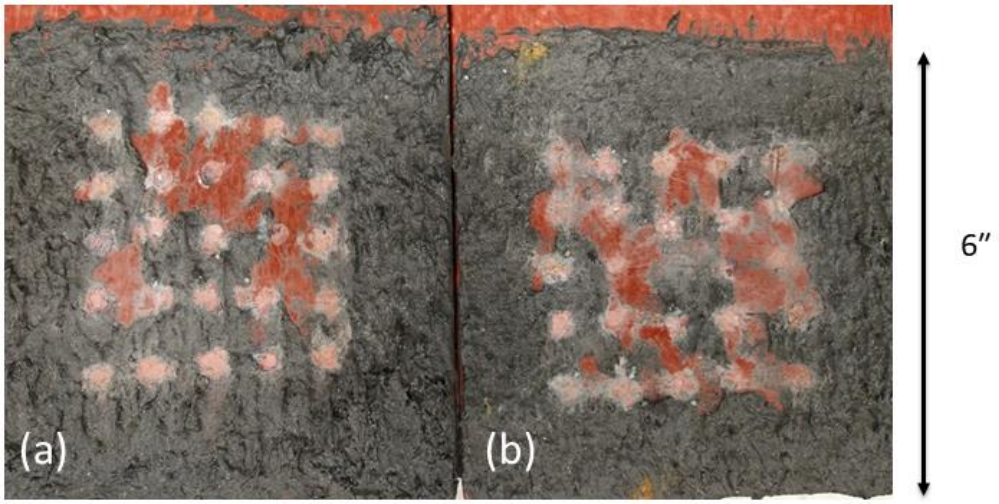

Figure 4.6. Non-skid coatings containing milled carbon fiber after impact testing. the coating on the left scored (a) 40.0% and the coating on the right (b) scored 22.5%. Both coatings were submerged in synthetic saltwater (ASTM D1141) for 15 days before testing.

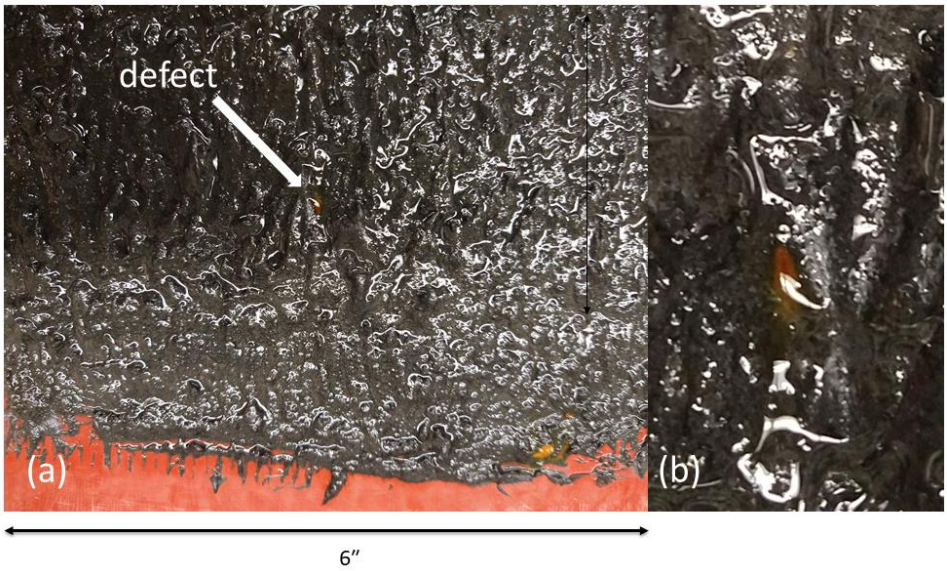

Figure 4.7. Image (a) shows an overview of a non-skid with a holiday after treatment with synthetic seawater for 15 days. (b) A close-up of the discontinuity.

Two more non-skid coatings were treated with synthetic seawater and subsequently tested for impact resistance. These non-skid coatings had no apparent holidays. The non-skid coatings in Figure 4.8b demonstrated comparable impact resistance to the untreated samples. These more carefully applied coatings have consistent impact scores of 87.5% after treatment. This demonstrates the importance of ensuring complete coverage when applying the nonskid to prevent holidays in the coating.

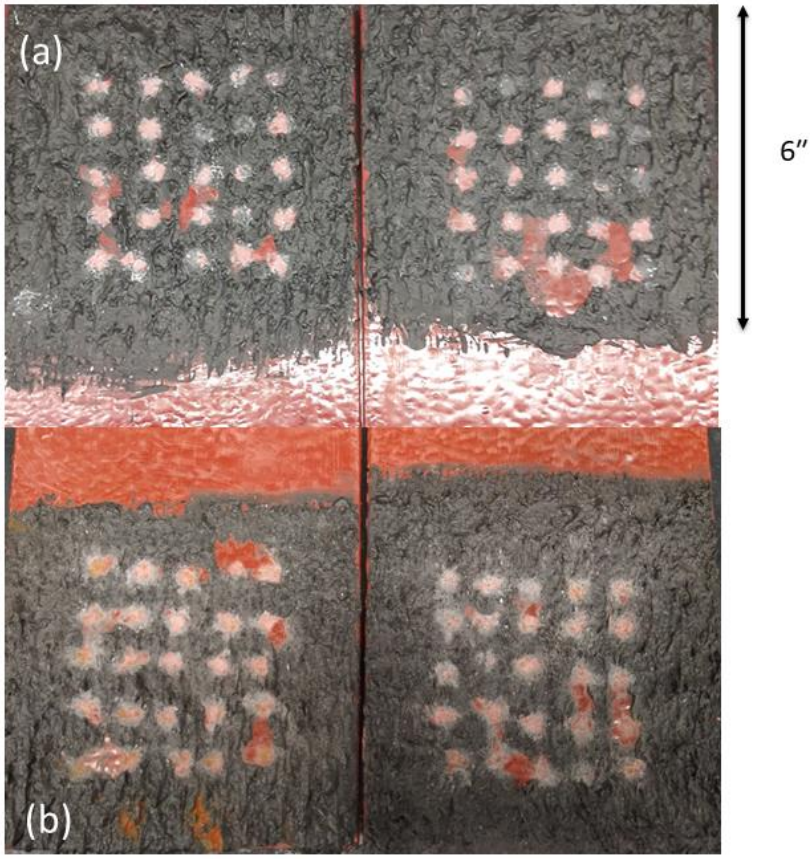

Figure 4.8. The impact score for the reduced aluminum oxide formulations is comparable between the (a) untreated non-skid coatings, and (b) non-skid coatings treated with synthetic seawater (ASTM D1141) for 15 days. The non-skid coatings averaged impact scores of (a) 82.5% and (b) 87.5%.

These results show that the impact performance is improved after reducing the amount of aluminum oxide. In addition, the coating can maintain performance after treatment with synthetic seawater if it is applied carefully to avoid discontinuities. The current non-skid coating does not meet the impact resistance score (95%) requirement by Navy military specifications. However, the current scores are applicable for a non-skid repair product.

Tables 4.3 and 4.4 shows the various cure parameters for the non-skid panels tested for impact. Table 4.3 list data pertaining to the non-skid coatings loaded with 100 phr of aluminum oxide while table 4.4 pertains to the non-skid coatings with aluminum oxide loadings of 25 phr. Both tables include temperature parameters such as the substrate temperature when FP starts along

with the ambient substrate temperature before cure. The time in which FP starts along with the total cure time is also recorded.

Based on the results, the non-skid loaded with 100 phr of aluminum oxide has an average cure time of around 7 minutes and curing begins as the substrate temperature approaches 70˚C. In comparison, the non-skid loaded with 25 phr of aluminum oxide starts undergoing FP as the surface temperature of the substrate approaches the mid-50s (˚C). By the end of the cure, the temperature of the substrate exceeds 160 ˚C. The cure time varies between 5 and 8 minutes with an average of 7.6 minutes. The results indicate that the aluminum oxide loading does not affect the overall cure time.

Table 4.3. Cure data for milled carbon fiber non-skid that underwent impact testing (100 phr aluminum oxide).

Parameter	Non-skid 1	Non-skid 2	Average
Initial Substrate Temp (˚C)	24	23	24
Front Start Temp of substrate (˚C)	75	70	73
Substrate Temp at End of Cure (˚C)	192	183	188
Front Start Time (mins)	1.02	1.33	1.17
Total Cure Time (mins)	6.17	7.67	6.92

Table 4.4. Cure data for non-skid coatings that underwent impact testing (25 phr aluminum oxide).

Initial Substrate Temp (˚C)	Temp of Substrate at Start of FP (˚C)	Substrate Temp at End of Cure (˚C)	FP Start Time (mins)	Total Cure Time (mins)
24	54	167	0.90	5.43
24	58	181	0.97	8.67
22	56	186	0.98	7.08
23	60	165	1.10	7.87
25	61	181	0.93	8.33
22	55	198	0.90	8.42
23 +/- 1	57 +/- 3	180 +/- 12	0.96 +/- 0.08	7.63 +/- 1.21

Figures 4.9a and 4.9 show the milled glass fiber non-skid (100 phr of aluminum oxide) coatings before and after the impact test. The milled glass fiber non-skid formulations scored 35% and 32% (33.5% average) on the impact test. By comparison the impact scores were 52.5% and 15% for the milled carbon fiber (zoltek) non-skid coatings loaded with 100 phr of aluminum oxide. Table 4.5 shows that the cure time for the milled glass fiber nonskid is shorter in comparison to the milled fiber nonskid; this is only considering the non-skid containing 100 phr of aluminum oxide. This may be due to the more nonskid surface of the coating formed in the latter. The valleys of the nonskid take longer to cure and this results in a longer cure time. In addition to having a more nonskid surface, the milled fiber non-skid is less uniform in color. As previously stated, the milled glass fiber also appears to not wet well with the resin. More through mixing may be needed to optimize the formulations with milled glass fiber. For these reasons, milled carbon fiber is the preferred additive for this application.

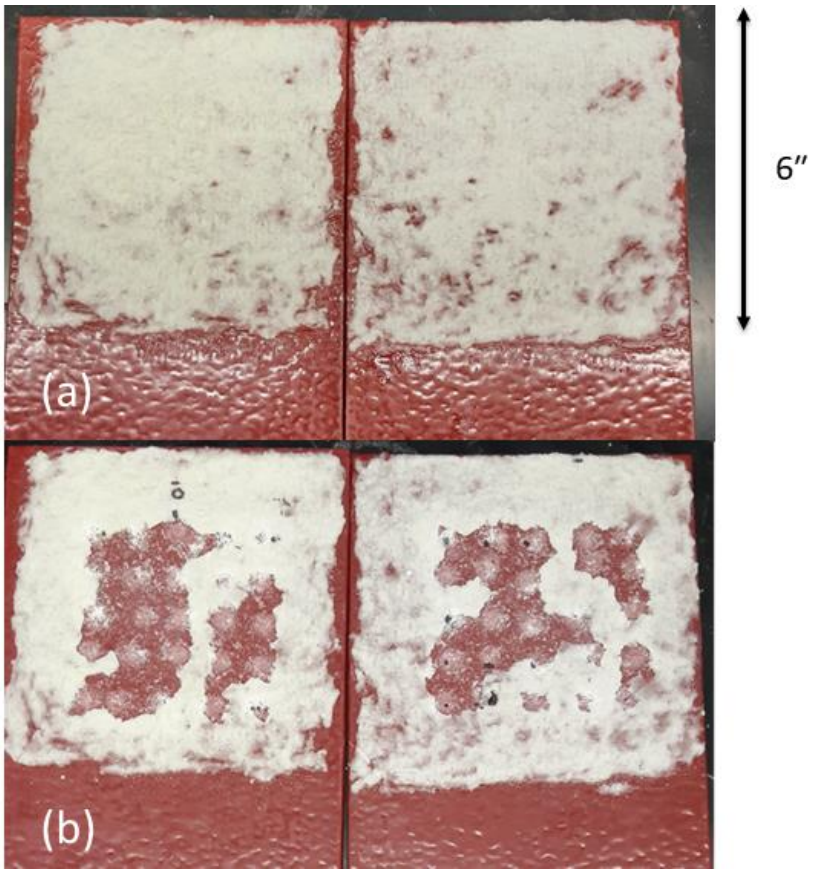

Figure 4.9. Milled glass fiber Non-Skid panels with aluminum oxide (100 phr) before (a) and after (b) the impact test. The panels scored an average of 33.5% on the impact test, with scores of 35% (left panel) and 32% (right panel)

Table 4.5. Data for non-skid (100 phr milled glass fiber).

Parameter	Non-skid 1	Non-skid 2	Average
Initial Substrate Temp (˚C)	24	24	24
Front Start Temp of substrate (˚C)	85	89	87
Substrate Temp at End of Cure (˚C)	139	156	148
Front Start Time (mins)	1.95	1.92	1.94
Total Cure Time (mins)	4.28	5.32	4.8

Reducing the aluminum oxide loading from 100 to 25 phr was also tested using milled glass fiber instead of milled carbon fiber. As shown in figure 4.10b, the nonskid coatings scored 67.5% and 97.5% on the impact test (82.5% average). Like the Zoltek containing nonskid, reducing the aluminum oxide loading resulted in a significant improvement in impact resistance. Despite this improvement, the inconsistency between the two scores along with the previously mentioned wetting issue makes milled glass fiber less desirable than milled carbon fiber for this application. Table 4.6 demonstrates that reducing the aluminum oxide loading (100 phr to 25 phr) increased the total cure times for the milled glass fiber non-skid coatings from approximately 5 minutes to 8 minutes.

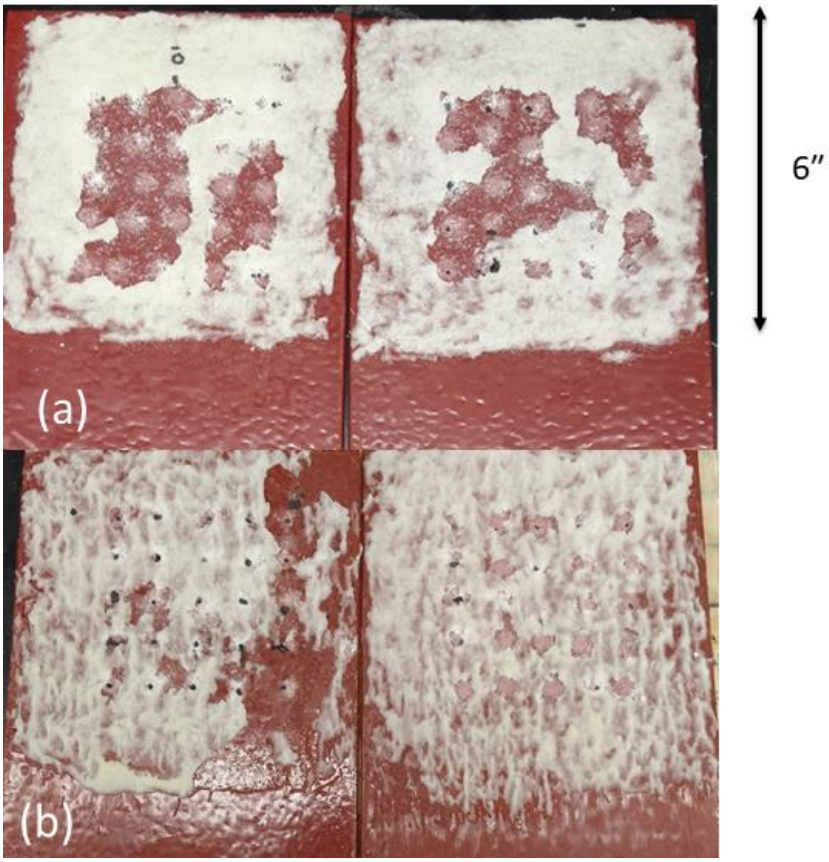

Figure 4.10. Milled glass fiber Non-Skid panels after impact test (a) non-skid contains 100 phr of aluminum oxide and (b) 25 phr of aluminum oxide. The Average impact test scores were (a) 33.5% and (b) 82.5%. The non-skid panels in (b) scored 67.5% (left panel) and 97.5% (right panel).

Table 4.6. Temperature and cure time data for milled fiber nonskid and aluminum oxide (25 phr)

Parameter	Non-skid 1	Non-skid 2	Average
Initial Substrate Temp (˚C)	23	23	23
Front Start Temp of Substrate (˚C)	80	70	75
Substrate Temp at end of Cure (˚C)	187	168	178
Front start time (mins)	1.33	1.73	1.53
Total cure time (mins)	8.15	7.37	7.76

The non-skid on average was able to bend 12˚ before the appearance of cracks. Figure 12a shows the bent nonskid coatings. With this flexibility, the nonskid coatings can tolerate a reasonable amount of bend without failure such as cracking or delamination. As shown in Figure 12b, delamination is not present even if the coatings are bent to the maximum 20˚ over the mandrel. Cracking was minor even at these bends. The data in Table 3 shows that the cure time was dramatically lower (less than 1 minute) in comparison to the non-skid applied on the other panels. This lower cure time can be attributed to a reduction in heat loss to the thinner aluminum panels in comparison to the thicker steel panels. For these experiments, the thinner aluminum panels were used as the substrate as opposed to the thicker steel panels used in the other experiments.

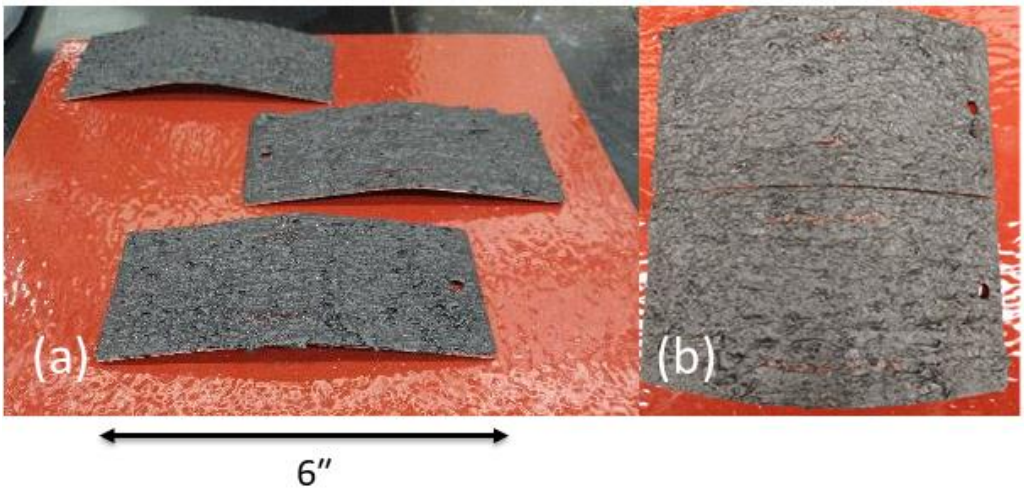

Figure 4.11. Non-skid coatings after mandrel bending test (a) bending until failure (first appearance of cracks), and (b) bending to 20˚.

Table 4.7. Cure Parameters for non-skid prepared on panels for mandrel bending test

Non-skid Sample	FP Start Time (secs)	Temp of Coating Surface at Start of FP (˚C)	Cure Time (sec)
One	25	115	45
Two	28	114	50
Three	32	117	56
Average	28 +/- 4	115 +/- 2	50 +/- 6

The non-skid coatings showed no delamination or softening upon being submerged in the various chemicals. No differences between such properties were present between the submerged and non-submerged areas and the impacted and non-impacted coating. Table 4.8 lists the various chemicals tested. These results demonstrate the good chemical resistance performance of the nonskid. As an example, Figure 4.12 shows the result of the qualitative test after being submerged in natural seawater for four weeks. The corrosion present is not a concern as it only occurred in the impact zone and in areas where the coating was not applied.

Table 4.8. Results of qualitative chemical testing on non-skid

Chemical	Time Submerged	Result
Ethanol	24 hours	Pass
Natural seawater	4 weeks	Pass
Detergent	4 weeks	Pass
Deicing-defrosting	24 hours	Pass
Motor oil	4 weeks	Pass

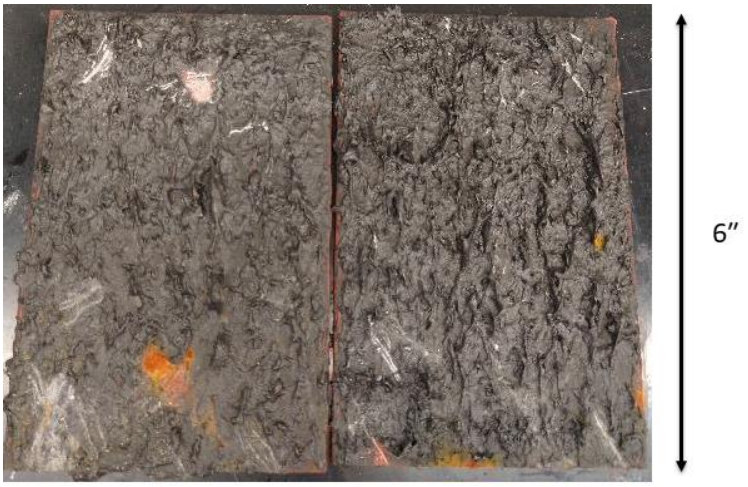

Figure 4.12. Non-skid after being submerged in seawater for a month and undergoing the qualitative chemical resistance test.

Figure 4.13a and 4.13b show the non-skid coatings after undergoing the salt fog test for 1,000 hours. Upon inspection there is no delamination of the non-skid around the scribe, corrosion beyond the scribe, or separation between layers. The results demonstrate the corrosion resistance of this non-skid.

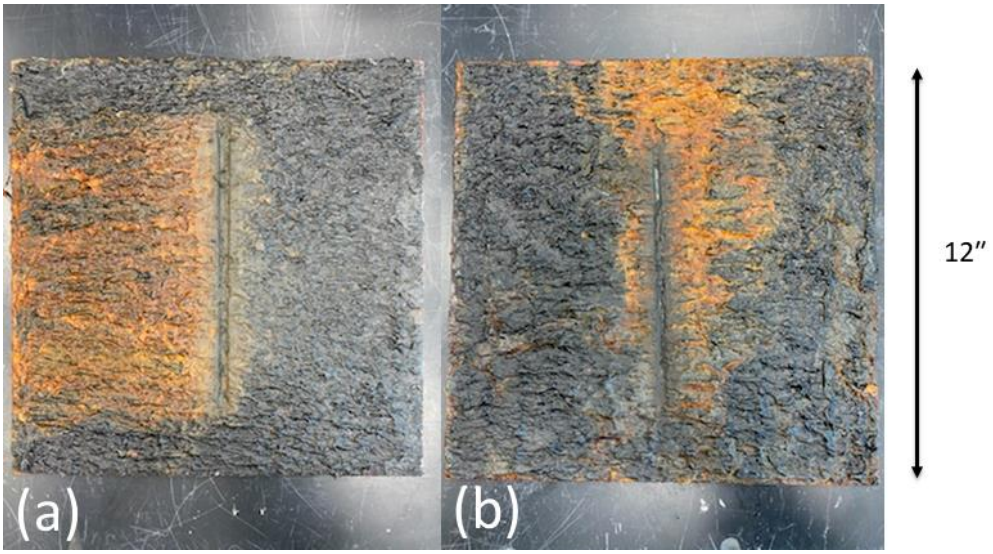

Figure 4.13. Images of non-skid coatings after undergoing the salt fog test for 1000 hours.

The specified COF values required are 1.4 (dry) and 1.1 (wet). The results in Table 4.9 demonstrate that the non-skid coating exceeds these requirements and allow room for further optimizing of the formulation.

Table 4.9. Results for Coefficient of Friction Testing

Summary	Average COF Dry	Average COF
Panel 1	1.81	1.50
Panel 2	1.80	1.45

4.7. Rheology

The results in Figure 4.14a present the viscosity with increasing shear rate for the replicates of non-skid formulations. The fewer number of data points in the non-skid formulation compared to the base formulation can be attributed to the presence of sharp spikes in the raw viscosity data for the non-skid formulation. These spikes are a result of the aluminum oxide particles contacting the probe. This is further confirmed with sharp spikes in the probe axial force at similar time points during the procedure.

To improve the accuracy of the results, the spikes were removed from the data. In the absence of aluminum oxide particles, there are no viscosity spikes in the base formulation, shown in Figure 4.14b. At a low shear rate, 1 (Hz or 1/s), the average viscosities were 302,000 +/- 44,000 cP and 475,000 +/- 40,000 cP for the non-skid and base formulations, respectively. At a higher shear rate, 10 (Hz or 1/s), the average viscosities were 54,000 +/- 11,000 cP and 43,000 +/- 1,000 cP for the non-skid and base formulations, respectively.

Figure 4.15 shows that the formulation is thixotropic. The decrease in viscosity under high shear followed by recovery allows the applicator to easily apply the formulation while also allowing sufficient viscosity recovery for frontal polymerization to occur. Figure 4.16 shows that the non-skid and base formulations have an average viscosity recovery of around 60 percent within 60 seconds of undergoing high shear.

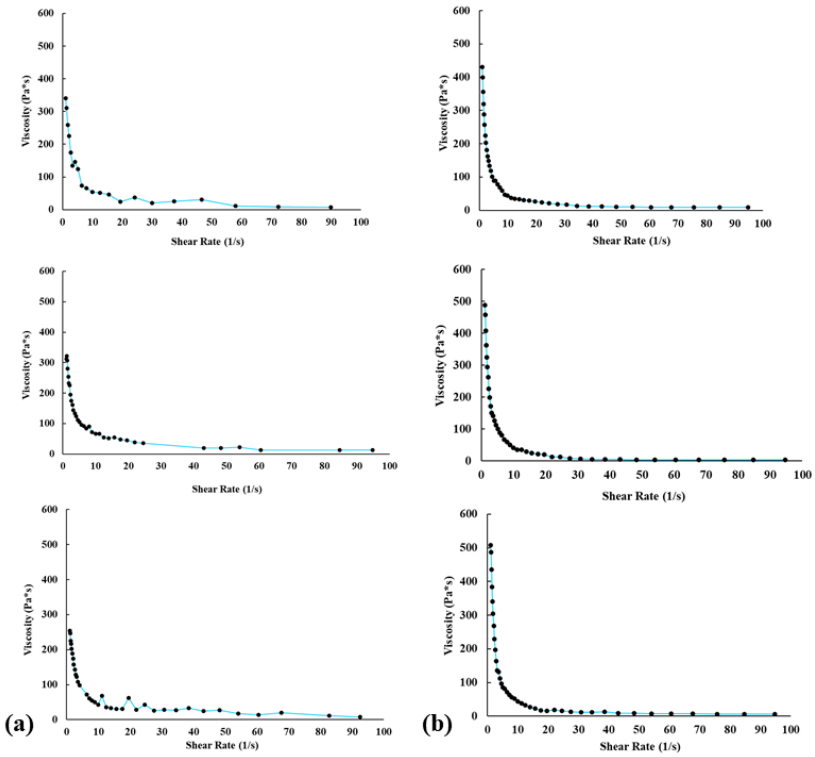

Figure 4.14. The viscosity of coating formulations as a function of shear rate (a) non-skid formulation (b) base formulation.

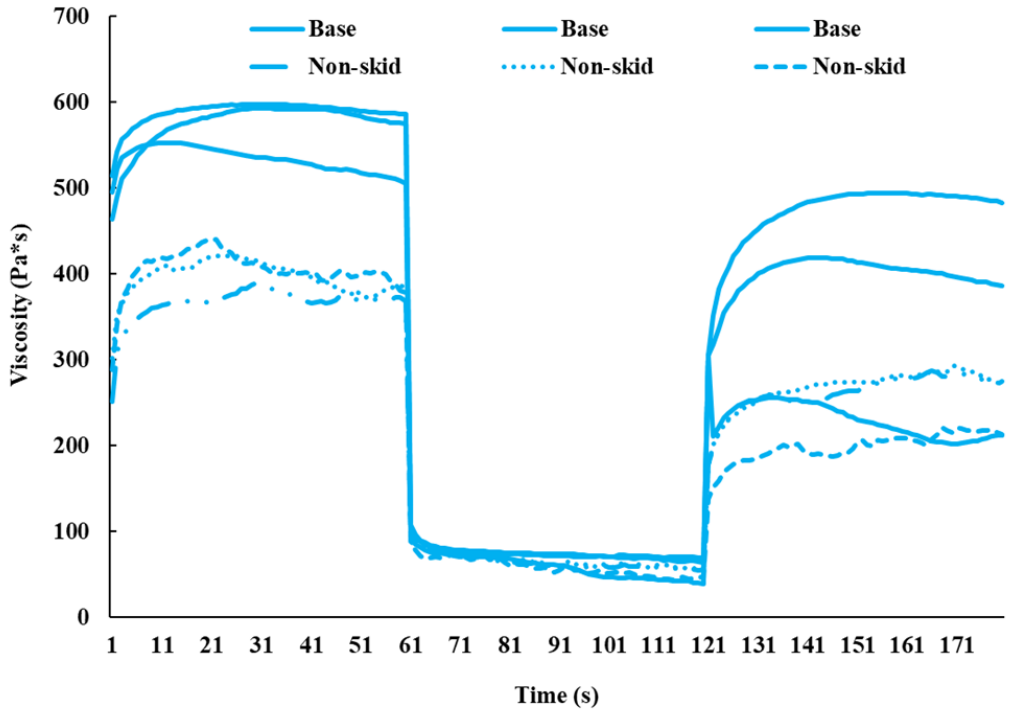

Figure 4.15. Thixotropic behavior of the base and non-skid formulations at low (1 Hz) and high (10 Hz) shear rates.

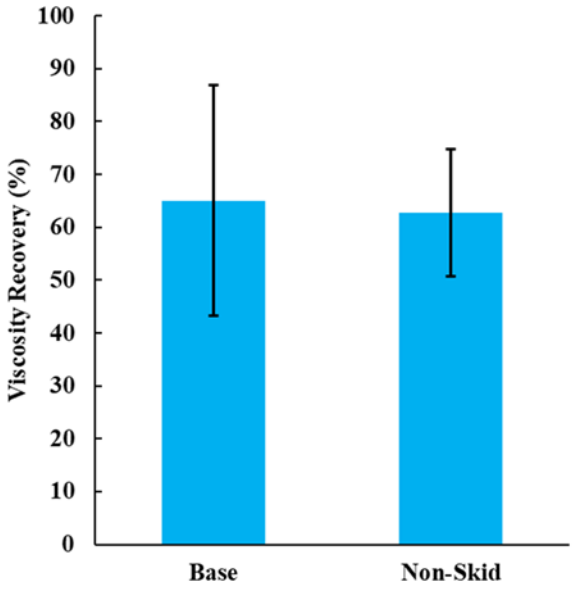

Figure 4.16. The viscosity recovery while undergoing low shear (1 Hz) after undergoing high shear (10 Hz) for 60 seconds (a) and the thixotropic index (b).

4.8. Conclusions

Aluminum oxide was added to the base coating formulated in chapter 3 to provide a desirable non-skid texture. This combination allowed for the development of a zero VOCs cure-on-demand high solids non-skid coating for corrosion protection on marine vessels. The coating has an average cure to service time in the 7-minute range and curing starts when the surface of the steel panel exceeds 54 ˚C. The non-skid coating demonstrated impact resistance with average scores of 82.5% before and 87.5% after treatment in synthetic seawater. Qualified chemical testing demonstrated a wide range of resistance to chemicals such as ethanol and motor oil. Mandrel bend test indicated that the coating will not crack below a bend of 12˚, and delamination does not occur. It was also determined that the non-skid will cure more quickly when applied to thinner steel substrates. The non-skid coating meets military COF specifications and corrosion testing is currently ongoing. Rheology of the non-skid formulation revealed thixotropic behavior and viscosities in the 500,00 mPa·s range under low shear. The current formulation demonstrates promise as a repair coating for non-skid decks on maritime vessels. Further work will be done to improve impact resistance and meet all Navy specifications.

4.9. Future Work

Additional work will be done to explore the effects of the environmental conditions on the cure time of the non-skid coating. All previously reported experiments were done in a laboratory setting at room temperature, future experiments will be conducted outside or in a colder environment to study the effect of lower temperatures on the cure time.

The current non-skid prototype does not meet the Navy's impact testing specification. The specification requires impact scores of 95% both before and after treatment in salt water and the current coating has average scores of 82.5% (untreated) and 87.% (treated). It was found that

reduction in the aluminum oxide loading from 100 to 25 phr increased the average impact score from 33.8% to 82.5%. The current non-skid exceeds coefficient of friction requirements so further reduction in the amount of aluminum oxide to improve impact resistance while maintaining the COF requirements is possible. Reducing the crosslink density and volume shrinkage is another potential way to increase impact resistance. The addition of a sterically hinder monomer with a low functionality can be used to decrease volume shrinkage. Isobornyl acrylate (IBOA) is a high T_g sterically hindered bicyclic monofunctional acrylate that gives low volume shrinkage while also maintaining hardness. The addition of IBOA to the formulation can lower volume shrinkage and therefore increase adhesion and impact resistance while maintaining hardness.[77]

In addition to meeting all military specifications, optimization will include cost reduction. One such way is to optimize mixing of the formulation to improve wetting which may allow the use of milled glass fiber instead of milled carbon fiber as a filler to prevent cracking. Wollastonite is another a high aspect ratio mineral filler that can also be used in this formulation.

CHAPTER 5. CHARGE TRANSFER COMPLEXES AS DUAL THERMAL/PHOTO INITIATORS FOR FREE-RADICAL FRONTAL POLYMERIZATION

5.1. Introduction to Iodonium Salts

Since their discovery in the 1970s onium salts have primarily been used as photoinitiators for cationic polymerization. Such salts include diaryliodonium salts (referred to as iodonium salts, this will be the focus of this work) and triarylsulfonium salts. Iodonium salts, which consist of an organic iodonium component (Ar_2I^+) and a counter anion (MtX_n^-) act as photoinitiators by generating super acids upon undergoing photolysis.[3] Depicted in Figure 5.1, the mechanism by which iodonium salts undergo photolysis involves heterolytic and or homolytic cleavage of the C-I bond. Radical cations, cations, and super acids are generated, the latter of which initiates cationic polymerization.[78] Photochemical properties such as absorption of light, quantum yield, photolysis rate, photosensitivity, and thermal stability are determined by the iodonium cation. The counter anion controls the Brønsted acid strength, reactivity of cation, polymerization rate, and conversion. Weakly nucleophilic anions such as SbF_6^-,AsF_6^-, PF_6^-, and BF_4^- give rise to higher polymerization rates and lower termination rates in cationic polymerization. The decrease in termination allows this system to be viewed as a type of living polymerization. More nucleophilic anions will have a stronger ion-pair effect which leads to the quenching of the acid and therefore decreases the rate of cationic polymerization.[3]

This chapter was previously published as D. P. Gary, D. NGO, A. Bui, J. A. Pojman, Charge transfer complexes as dual thermal/photo initiators for free-radical frontal polymerization**,** J. Polym. Sci. 2022, 1. Reprinted by permission of Wiley.

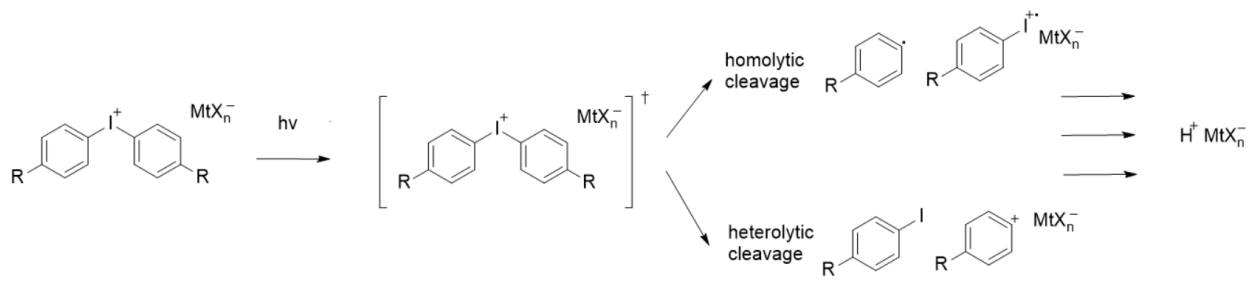

Figure 5.1. The general mechanism for photolysis of an iodonium salt.[3, 78]

Iodonium salts primarily absorb below 300 nm so efforts to extend absorption have been explored.[3] Xiano et al. used N-vinylcarbozole as a photosensitizer and additive alongside diphenyliodonium hexafluorophosphate to perform cationic ring-opening polymerization of epoxy and free-radical polymerization of methacrylates using a 392 nm LED lamp. In this system, a series of redox reactions between N-vinylcarbazole and iodonium generate the necessary species to initiate both cationic and free-radical polymerization.[79] Other studies exploring the oxidation potential of iodonium salts include Cu(II) complexes and silanes in combination with iodonium salts.[68]

The oxidation potential of iodonium salts has been extended into frontal polymerization. In 2004, Mariani and co-workers combined an iodonium salt with a peroxide thermal initiator to generate UV-Induced cationic frontal polymerization of epoxy.[33] Shown in Figure 5.2, UV light leads to cationic polymerization through the generation of super acids via photolysis of the iodonium salt. The heat generated from the cationic polymerization then cleaves the thermal initiator which generates free radicals. These free radicals are oxidized by iodonium salts to generate cations which then initiate cationic frontal polymerization and by extension additional heat is generated. The process then repeats.[3, 80] Work on free-radical induced cationic frontal polymerization was later extended by the Liska[20], Sangermano[81], and Pojman[35] research groups.

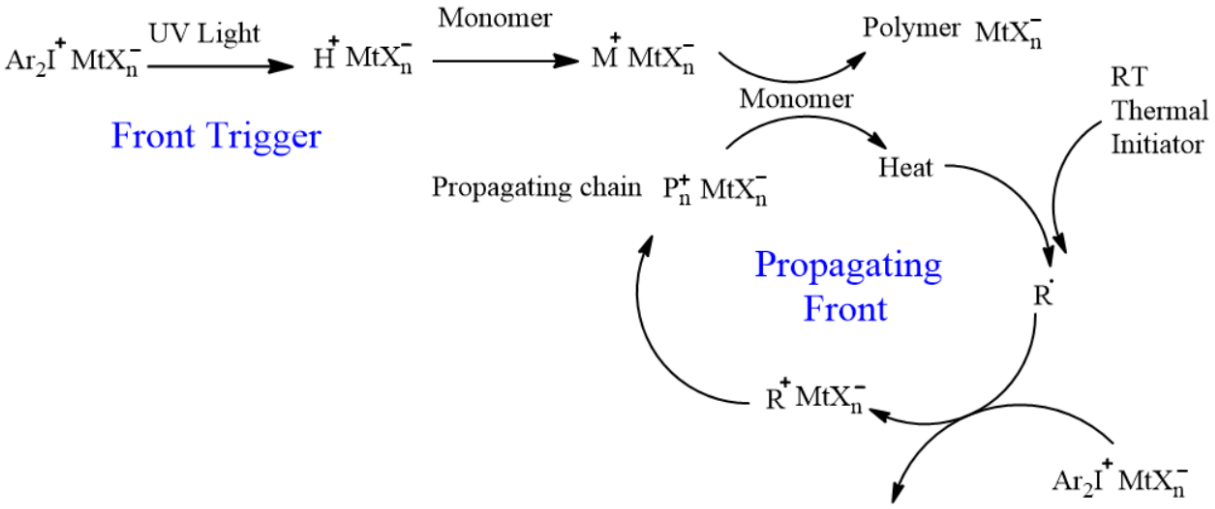

Figure 5.2. General mechanism scheme for free-radical induced cationic frontal polymerization.

5.2. Introduction to Charge Transfer Complexes

Photopolymerization is a rapid process that uses less energy than thermal curing but is limited when it comes to the curing of thick and/or filled materials.[1, 2, 82] Frontal polymerization (FP) is a process that can combine the in-depth cure and curing of highly filled systems[45, 83] offered by bulk polymerization with the high speed of photopolymerization.[16] Dual-cure initiators that can serve as both photo and thermal initiators for polymerization are of interest in the search for more energy-efficient methods of polymerization.[63, 84-86]

Charge transfer complexes (CTCs) are a potential replacement for peroxide-based initiators and have been shown to act as dual thermal and photoinitiators.[2, 85, 87-89] Charge transfer complexes (CTCs) are formed through the association of an electron donor with an electron acceptor. This interaction allows absorption of light in the visible range, which differs from the shorter absorption wavelengths of other photoinitiators such as iodonium salts. The absorption of longer wavelengths of light and the lack of peroxide and metals make CTCs an attractive alternative to traditional initiators.[82, 90] A CTC is in equilibrium with its components, and this equilibrium is affected by both electronic and steric factors.[82] Various studies[91-93] have shown that charge

transfer complexes can be used as thermal initiators, photoinitiators, and redox initiators for free-radical polymerization.

As previously discussed, the oxidation potential of iodonium salts makes them suitable electron donors. CTCs based on iodonium salts (the electron acceptor) and amines (the electron donor) can act as both thermal and photoinitiators for free-radical and cationic polymerization. Garra et al. showed that CTCs based on iodonium salts and amines can be used as photoinitiators in a light-activated redox initiation system.[94] Polymerization in shadow areas is made possible through this combination of photoionization with redox initiation. A later study demonstrated that it is possible to cure extremely thick samples using iodonium/amine-based charge transfer complexes as photoinitiators, but cure speed and conversion decrease with depth.[95] The synthesis of filled materials also remains a challenge. Electron spin resonance studies by Garra et al.[94, 96] demonstrated the formation of aryl radicals from CTCs based on iodonium salts and amines. Such studies explore the initiation potential of CTCs and give insight into the mechanism. Figure 5.3 shows the general reaction of CTC radical generation.

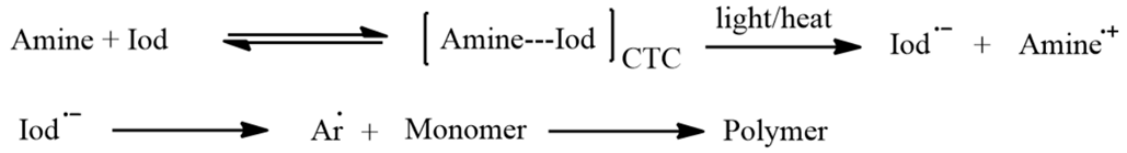

Figure 5.3. General reaction scheme for CTC radical generation.

A study by Wang et al. demonstrated the steric and electronic effects of the amine on the formation of a charge-transfer complex using an iodonium salt.[88] Wang and coworkers later demonstrated the potential of phosphine, indole, and sulfonium-based CTCs.[85, 89, 97] Thus far, composite synthesis utilizing the dual-cure nature of charge transfer complexes has been limited to a combination of surface photocuring followed by thermal curing.[98] The dual initiating ability of CTCs is advantageous; however, the requirement of photocuring followed by bulk curing to

manufacture composites remains a challenge. Current curing for such systems involves multiple passes for photocuring and several minutes or longer of bulk curing.[85, 88, 89, 97]

This research explored the use of charge transfer complexes as dual thermal and photoinitiators for free-radical frontal polymerization. Combinations of various iodonium salts and amines were used to study their effects on front velocity. The electronic and steric effects of the CTC components were explored. The effect of the mole ratio between the amine and iodonium salt on front velocity is also shown.

5.3. Materials and Methods

Trimethylolpropane triacrylate (TMPTA) was purchased from Allnex (Alpharetta, GA). N,N-dimethyl-p-toluidine (DMPT), bis(4-tert-butylphenyl)iodonium triflate (IOC-T), and bis(4-fluorophenyl)iodonium triflate (IOC-FT) were purchased from Sigma-Aldrich. Bis(4-tert-butylphenyl)iodonium hexafluorophosphate (IOC-P) and bis[4-(tert-butyl)phenyl]iodonium tetra(nonafluoro-tert-butoxy)aluminate (IOC-A) were purchased from TCI America (Portland, OR). p-(octyloxyphenyl)phenyliodonium hexafluoroantimonate (IOC-8) was purchased from Ambeed (Arlington Heights, Il). N-phenylglycine (NPG) and N,N-dimethylaniline (DMA) were purchased from Alfa Aesar (Ward Hill, MA). The chemical structures of the monomers and initiators are displayed in Figure 5.4.

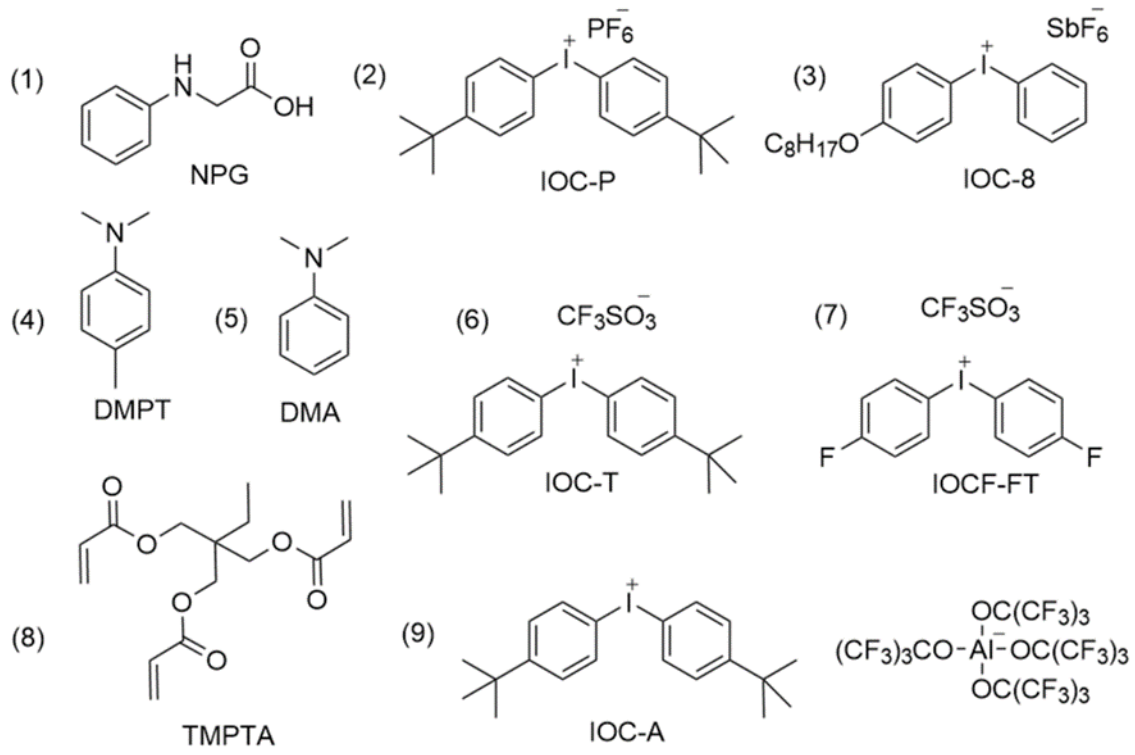

Figure 5.4. Chemical structures. Starting from the top row (from left to right): (1) N-phenylglycine (NPG), (2) bis(4-tert-butylphenyl)iodonium hexafluorophosphate (IOC-P), (3) p-(octyloxyphenyl)phenyliodonium hexafluoroantimonate (IOC-8), (4) dimethyl-p-toluidine (DMPT), (5) N,N-dimethylaniline (DMA), (6) bis(4-tert-butylphenyl)iodonium triflate (IOC-T), (7) bis(4-fluorophenyl)iodonium triflate (IOC-FT), (8) trimethylolpropane triacrylate (TMPTA), and (9) bis[4-(tert-butyl)phenyl]iodonium tetra(nonafluoro-tert-butoxy)aluminate (IOC-A).

Two different amines were mixed with IOC-8 in different ratios to study how the ratio of the amine to iodonium salt effects front velocity. N,N-dimethyl-p-toluidine (DMPT) and N,N-dimethylaniline (DMA) were used as the electron-donating amines. p-(octyloxyphenyl)phenyliodonium hexafluoroantimonate (IOC-8) was used as the electron acceptor. The solubility of NPG is limited to 0.031 molal in the formulation, so fronts were only studied using a CTC consisting of NPG and IOC-8 in a 1:1 mole ratio. To prepare the charge transfer complexes, 2 parts per hundred resin (phr) of IOC-8 was dissolved in TMPTA via sonication (30 minutes). Parts per hundred resin indicates the mass of material added per one-hundred grams of resin. This amount of iodonium salt is equivalent to a concentration of 0.031 moles per kg. Various amounts of the amine donor were then added to form a CTC with a certain

mole ratio of iodonium salt to amine. The resulting solutions were mixed and loaded into borosilicate glass tubes (16 x 150 mm). All fronts were initiated with either a soldering iron or a 395 nm LED gooseneck lamp from Prime LED CO LTD. with an intensity of 22 mW/cm^2. A video camera was used to monitor the front propagation, and the velocity was calculated by taking the slope of the position vs. time plot. Each test tube was labeled with an adhesive measuring tape to record the position of the front. All experiments were performed in triplicate.

To demonstrate the photoinitiation capabilities, the front of at least one replicate of each system was started by the LED lamp. A K-type thermocouple was used in one of the trials involving the 3:1 DMA:IOC-8 and 3:1 DMPT:IOC-8 CTC formulations to measure the front temperature of these systems. The thermocouple was placed in the center of the test tube at approximately half the depth of the solution. The general set-up and an example of FP initiated by a CTC is shown in Figure 5.5.

To study the effect of the iodonium salt, a constant amount of iodonium salt was mixed with DMPT in a 5:1 mole ratio. IOC-8, IOC-P, IOC-A, IOC-T, and IOC-FT were all tested as iodonium salts. Two different amounts of iodonium salt (1 phr or 2 phr) were added due to the limited solubility of IOC-FT. Because the iodonium salts were kept at a constant mass, the front velocities were converted into front velocity/molal of iodonium salt to elucidate the effect of changing the iodonium salt on the intrinsic reactivity of the system. As shown in equation [5.1], This conversion is done by dividing the front velocity by the molality of the given iodonium salt. The resulting units are cm/min*kg/mol.

$$\frac{Front\ velocity\ (cm/min}{molality\ (\frac{mol\ of\ iod}{kg\ of\ TMPTA})} = \frac{cm}{min} * \frac{Kg\ of\ TMPTA}{Mol\ of\ Iod} = cm/min * kg/mol \quad [5.1]$$

To study the pot life, one sample of each formulation was wrapped in aluminum foil to prevent light penetration, and another sample was exposed to the ambient light of the lab. The formulations were checked at least every few days to determine if gelation occurred.

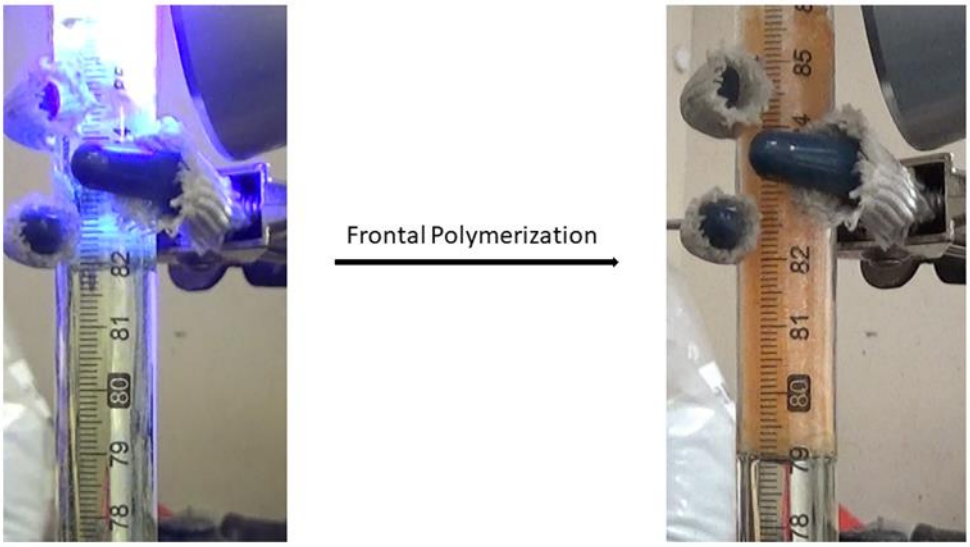

Figure 5.5. Experimental Set-up with borosilicate glass test tube and 395 nm LED lamp. The free-radical frontal polymerization of TMPTA through a charge transfer complex results in a colored crosslinked material. The front velocity was recorded as a function of position (cm) versus time (minutes).

5.4. Mole ratio study

Figure 5.6 shows the plot of front velocity vs. the mole ratio of DMPT to IOC-8. A front could not be obtained with IOC-8 alone, and the front was quenched in the formulation with the 1:4 mole ratio. This shows that the formation of the CTC is necessary for frontal polymerization. The front velocity initially increased as more amine was added and then reached a maximum velocity after the 2:1 mole ratio was reached. The minimum mole ratio detected for a self-sustaining front was 1:2 DMPT to IOC-8. Photopolymerization kinetic studies by Ghosh and co-workers showed that the polymerization rate reaches a maximum at a 2:1 mole ratio of electron donor to electron acceptor.[91, 92] Their studies involved CTCs based on morpholine and sulfur dioxide/bromine as electron donors. The researchers concluded that the full complexation of the

electron donor and acceptor occurred at this ratio.[91, 92] Front velocity is a function of the polymerization rate, so the trends are comparable. In addition, morpholine has two available electron donor groups, one for each electron acceptor. In this work, the iodonium salts and amines each have one accepting and donating group, respectively.

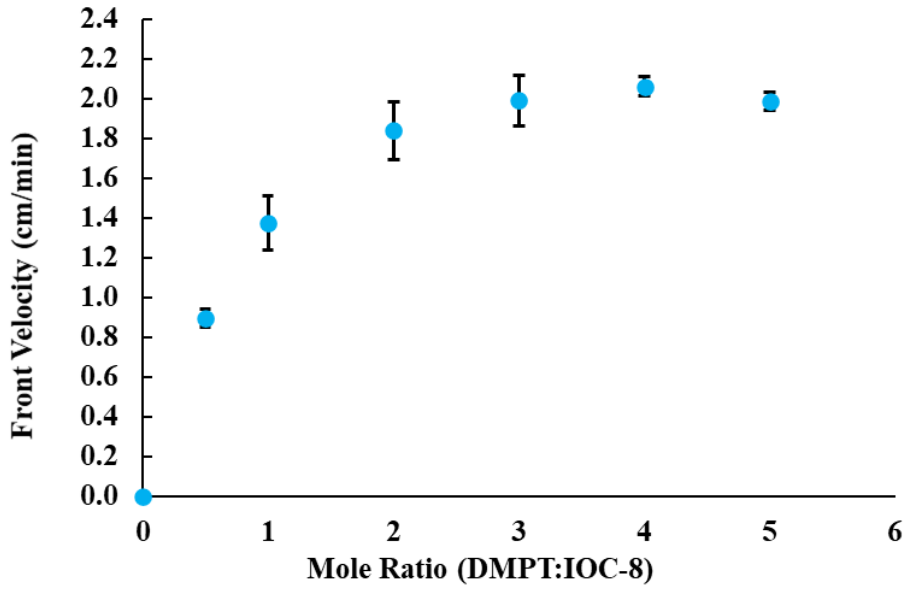

Figure 5.6. Effect of mole ratio (DMPT: IOC-8) on front velocity. The IOC-8 concentration was kept constant (0.031 molal)

As shown in Figure 5.7, the effect of the mole ratio of DMA to IOC-8 was studied in the same fashion as with DMPT. First, a 1:1 mole ratio system was tested; however, a self-sustaining front could not be initiated. Next, a 1.5:1 mole ratio was attempted, and a front could not be sustained. Finally, a 2:1 mole ratio was attempted, and an average front velocity of 1.1 cm/min was obtained. This maximum velocity is significantly lower than the 2.0 cm/min for the 2:1 mole ratio formulation containing DMPT and IOC-8. The lower maximum velocity and the higher mole ratio of amine to iodonium salt required to reach a maximum constant velocity using DMA in comparison to DMPT indicate that the system is less reactive. The lower reactivity can be attributed to DMPT being a better electron donor than DMA because of the electron-donating

methyl group in the para position. Front temperatures of 226 ˚C and 232 ˚C were recorded for the 3:1 DMPT:IOC-8 and 3:1 DMA:IOC-8 CTCs, respectively. These values are typical for frontal polymerization.

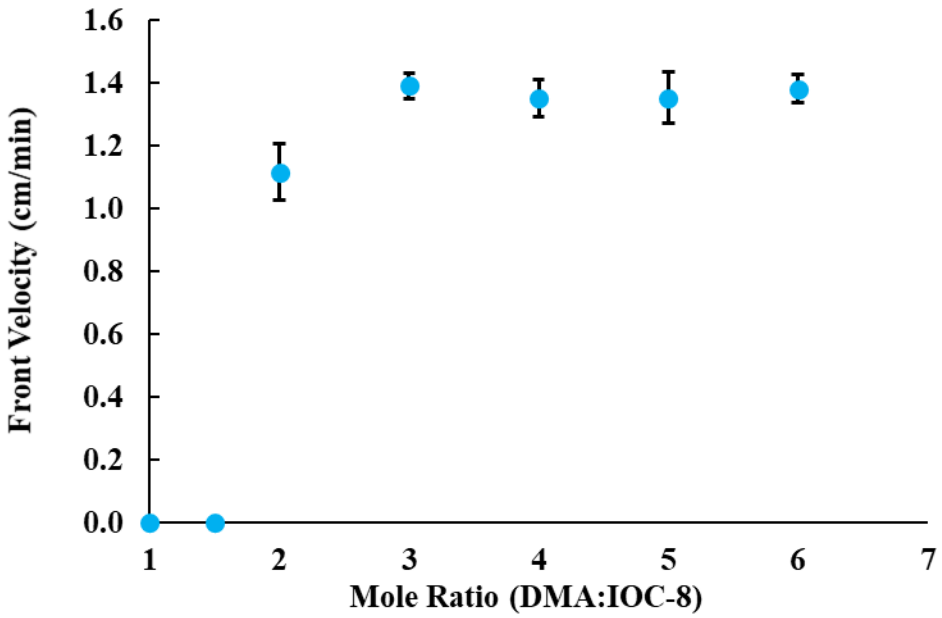

Figure 5.7. The effect of mole ratio (DMA:IOC-8) on front velocity. The concentration of IOC-8 was kept constant (0.031 molal)

It can be concluded that maximum conversion of the amine and iodonium salt to the CTC is reached at a 2:1 ratio for the DMPT:IOC-8 system and a 3:1 ratio for the DMA:IOC-8 system. The CTC formed between DMPT and IOC-8 has a higher equilibrium constant compared to the one formed between DMA and IOC-8, and additional DMA is needed to reach maximum complexation. Upon reaching complete complexation, the velocity remained constant despite the addition of more amine.

A CTC made from a 1:1 mole ratio of NPG:IOC-8 was also prepared, and its front velocity is compared to that of the 1:1 mole ratio of DMPT:IOC-8 in Figure 5.8. A mole ratio study with NPG was not done because in combination with IOC-8, the NGP was insoluble at concentrations beyond 0.0301 molal.

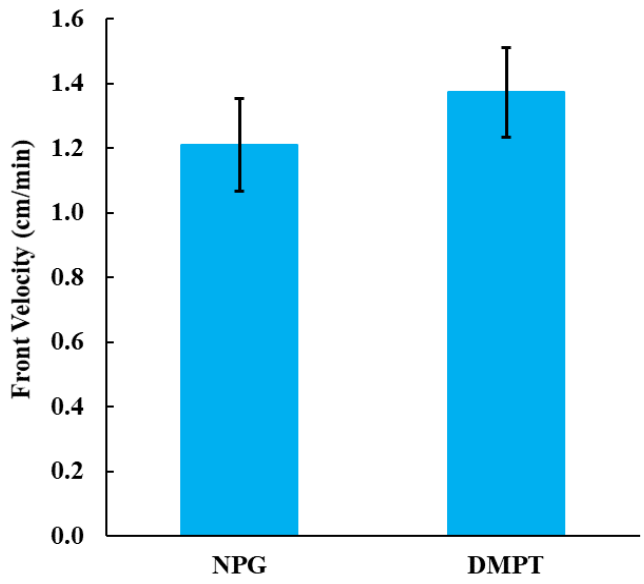

Figure 5.8. Comparison of front velocity between NPG and DMPT CTC. Each CTC contains 2 phr of IOC-8 (0.031 molal).

The results of this study, shown in Figure 5, reveal that no significant difference in front velocity was found between fronts initiated by either NPG or DMPT based CTCs. The two formulations contained equal molar amounts of the amine (NPG or DMPT) and IOC-8, which suggests that the two CTCs have similar reactivity with regards to initiating polymerization.

5.5. Structure and counterion effects of iodonium salt on front velocity

Figures 5.9 and 5.10 show the front velocity for systems with the same mass of iodonium salt combined with DMPT in a 5:1 DMPT to IOC mole ratio. Figure 5.9 demonstrates that the formulations with IOC-P and IOC-8 gave the highest front velocities while the formulation with the IOC-A gave the lowest. Figure 5.10 shows that the IOC-8, IOC-FT, and IOC-P systems have similar front velocities while those with IOC-T are significantly lower.

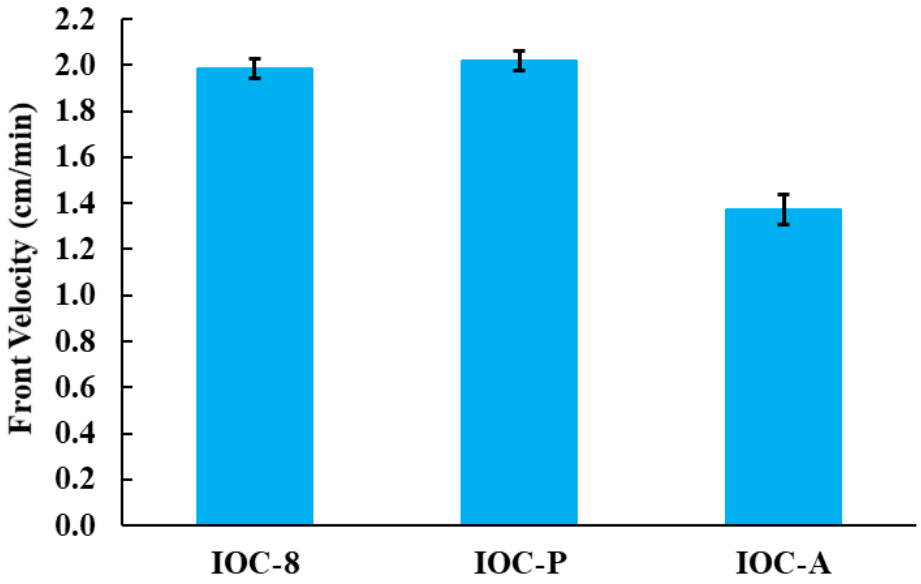

Figure 5.9. Front velocity for CTCs composed of various iodonium salts (2 phr) mixed with DMPT in a 5:1 mole ratio.

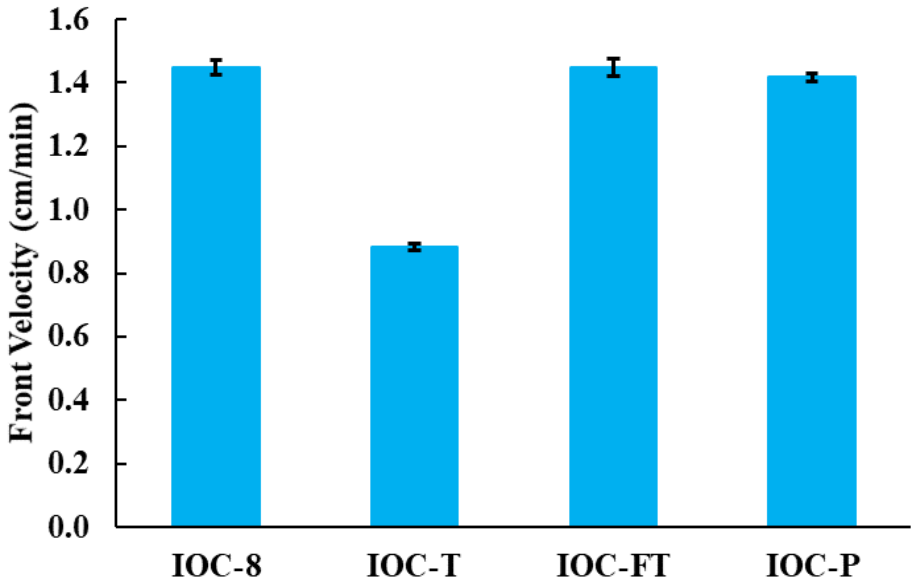

Figure 5.10. Front velocity data for CTCs composed of various iodonium salts (1 phr) mixed with DMPT in a 5:1 mole ratio.

On a mass basis, it appears that IOC-8 and IOC-P are more efficient as the electron acceptor in comparison to IOC-A and the triflate iodonium salts. However, the intrinsic reactivity of the iodonium salts in the CTCs must be judged based on concentration. The data for Figures 5.11 and 5.12 were obtained by dividing the front velocity data in Figures 5.9 and 5.10 by the molality

of the given iodonium salt. Figures 5.11 and 5.12 show these systems with a plot of front velocity per molal of iodonium salt. Based on intrinsic reactivity, the CTC with IOC-A gave the highest front velocities. The only difference between IOC-P and IOC-A is the counterion.

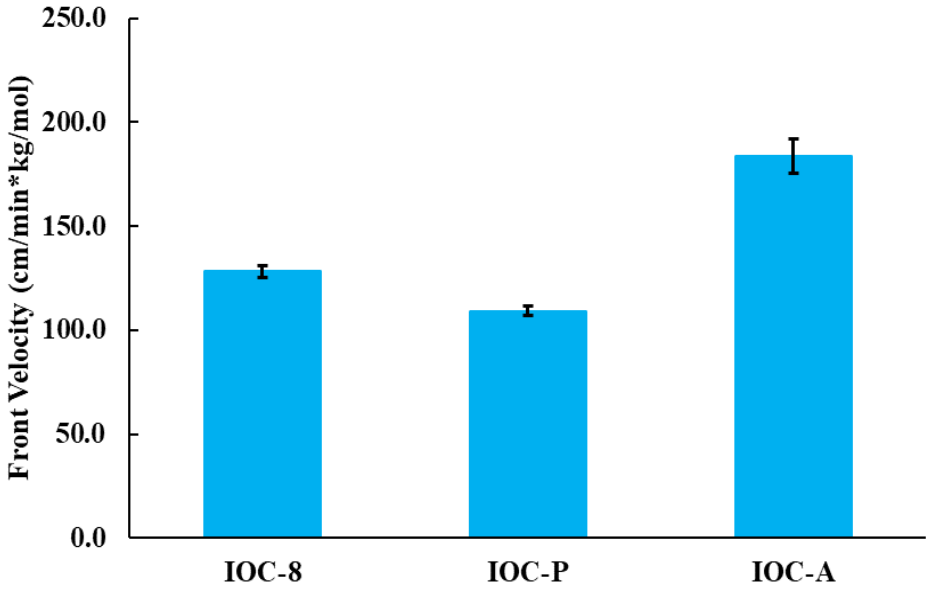

Figure 5.11. Data showing the front velocity per molal of iodonium salt for CTCs composed of various iodonium salts (2 phr) mixed with DMPT in a 5:1 mole ratio.

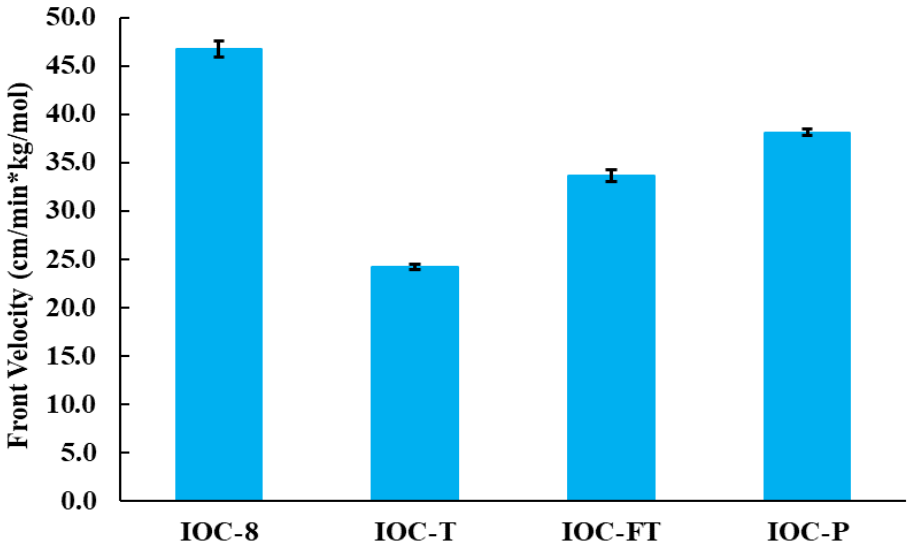

Figure 5.12. Data showing the front velocity per molal of iodonium salt for CTCs composed of various iodonium salts (1 phr) mixed with DMPT in a 5:1 mole ratio

Klikovits showed that IOC-A is a more highly reactive photoacid generator in comparison to other iodonium salts.[99] Based on previous work by Krossing et al., it was proposed that the low nucleophilicity of the aluminate ion prevents it from recombining with the propagating cation.[100] Further work by Knaack et al. found that radical-induced cationic fronts initiated using IOC-A gave higher front velocities in comparison to those initiated by IOC-8.[101]The system in this study is based on free radicals so this does not explain the observed result. Counter anions with lower nucleophilicity are less tightly bound to the cation, in this case, the iodonium salt.[82] The PF_6^- and SbF_6^- anions of IOC-P and IOC-8, respectively, are more nucleophilic and more tightly bound to the iodonium when compared to the aluminate counter anion. Because the iodonium salt of IOC-A is less tightly bound to the counter anion, it is easier for it to interact with an electron donor such as DMPT to form a charge transfer complex.

The reason for the difference in front velocity between IOC-8 and IOC-P is more difficult to elucidate because both counter anions are different along with the structure of the iodonium salt. Nevertheless, the higher nucleophilicity of PF_6^- relative to SbF_6^- is at least partly responsible since the ion pair in IOC-P will be more tightly bound relative to IOC-8. It is also possible that the presence of the two tert-butyl groups in IOC-P are increasing steric effects and further hindering CTC formation.

Figure 5.12 demonstrates that IOC-8 is more reactive than the triflate containing iodonium salts. The lower reactivity of the triflate salts is likely due to the stronger binding of the triflate to the iodonium salt. Triflate is more nucleophilic in comparison to PF_6^- and SbF_6^- and therefore will be more tightly bound to the iodonium salt.[82] The higher reactivity of IOC-FT in comparison to IOC-T can be explained by the presence of fluorine groups on the latter. IOC-FT is a better electron acceptor due to the enhanced electron-withdrawing of fluorine relative to the

tert-butyl groups. Garra et al. found similar results through UV-Vis spectroscopy and computational simulations of CTCs formed using IOC-T, IOC-FT, and IOC-P.[95] The increased steric hindrance because of the two tert-butyl groups may also hinder CTC formation between IOC-T and DMPT.

5.6. Pot-life study

In addition to the higher reactivity of DMPT, there was no apparent change in viscosity or gelation for the 1:2 and 1:1 mole ratio sample left unwrapped in glass vials for two months; gelation started after two months. Samples wrapped in foil and not exposed to light have yet to show any apparent changes in viscosity after 5 months.

5.7. Conclusions

The first use of charge transfer complexes as initiators for free-radical frontal polymerization was demonstrated. CTCs were prepared by mixing various iodonium salts and amines in the bulk resin. Different iodonium salts and amines were used to study their structural and electronic effects on front velocity. A study on the effect of the mole ratio of amine to iodonium salt was done using DMPT, DMA, and IOC-8. Both front velocity and velocity per molal of iodonium salt were plotted to show both the practical applications of CTCs as initiators for fronts as well as the intrinsic reactivity.

It was found that CTCs using DMPT as the electron donor gave higher front velocities in comparison to those with DMA-based CTCs. This demonstrated that stronger electron-donating amines are more favorable towards CTC formation. Optimal ratios of amine and iodonium salt were also found: 2:1 for DMPT:IOC-8 and 3:1 for DMA:IOC-8. Upon reaching these ratios, the front velocity reaches a maximum velocity despite the addition of more amine. It was concluded

that the front velocity reaches a maximum upon maximum complexation of the amine and iodonium salt.

The studies involving changing the counter anion of the iodonium salt reveal that a combination of steric effect and nucleophilicity affects the front velocity. Both triflate-based CTCs gave lower front velocity than CTCs with IOC-8 and IOC-P. The lower velocities can be attributed to the triflate binding more tightly to the iodonium in comparison to the less nucleophilic SBF_6^- and PF_6^- anions. The difference in front velocities per molal between the two triflate iodonium salts revealed that the addition of electron-withdrawing groups on the iodonium salt increases front velocity by enhancing the CTC reactivity.IOC-A and DMPT form the most reactive CTCs, however, CTCs composed of IOC-8 and DMPT is the most useful in terms of costs, maximizing the front velocity and solubility.

CHAPTER 6. SUMMARY AND CONCLUSIONS

Frontal polymerization shows promise in the development of cure-on-demand materials such as composites, coatings, and adhesives. This work explored the practical applications and fundamental chemistry of frontal polymerization through the study of fillers, the use of FP to develop cure-on-demand coatings and demonstrating the usage of charge transfer complexes as dual photo/thermal initiators for free-radical frontal polymerization. Chapter 1 of this work gives a good overview of frontal polymerization and its potential applications.

The thermal and chemical effects of fillers were explored in Chapter 2. It was demonstrated that fillers with a high thermal diffusivity such as milled carbon fiber can increase front velocity relative to fillers with a lower thermal diffusivity. In contrast to thermal effects, chemical effects were also considered. Certain clay mineral fillers such as bentonite and acid-activated clays were shown to inhibit free-radical frontal polymerization via radical scavenging by Lewis acid sites.

Chapters 3 and 4 presented the development of a cure-on-demand formulation for potential application as a non-skid coating for maritime usage. The coating was cured through frontal polymerization upon constant irradiation with an infrared heater. A base formulation consisting of an epoxy acrylate oligomer and reactive acrylate diluents was developed. Various parameters such as coating thickness, resin composition, filler loading, and distance between the heater and substrate were studied. Fumed silica was added to suppress buoyancy-driven convection while milled carbon fiber was added to prevent cracking. Lastly, 16 grit aluminum oxide was added to give a non-skid texture. The coating underwent rheological characterization and several common ASTM test methods including impact testing, chemical testing, corrosion

testing, coefficient of friction, and mandrel bending. The current formulation has a cure-to-service time of minutes and demonstrates acceptable physical properties for potential use on maritime vessels.

The first study involving charge transfer complexes as initiators for frontal polymerization is demonstrated in Chapter 5. The fundamental chemistry of charge transfer complexes was explored such as the mole ratio of the electron donor to the electron acceptor, an amine, an iodonium salt in this case. It was found that the front velocity reaches a maximum upon reaching a certain mole ratio of amine to iodonium salt. The electronic effects of the amine and iodonium salts on front velocity were also studied. The results demonstrated that the formulations can be tuned by changing the electron donor or acceptor, which will impact the front velocity.

APPENDIX. COPYRIGHT PERMISSIONS

JOHN WILEY AND SONS LICENSE
TERMS AND CONDITIONS

Jan 12, 2022

This Agreement between Daniel Gary ("You") and John Wiley and Sons ("John Wiley and Sons") consists of your license details and the terms and conditions provided by John Wiley and Sons and Copyright Clearance Center.

License Number

5226101291159

License date

Jan 11, 2022

Licensed Content Publisher

John Wiley and Sons

Licensed Content Publication

Journal of Polymer Science

Licensed Content Title

Thermal transport and chemical effects of fillers on free-radical frontal polymerization

Licensed Content Author

Daniel Gary, John A. Pojman, Corey Weber, Catherine Morejon-Garcia, et al

Licensed Content Date

Jul 19, 2020

Licensed Content Volume

58

Licensed Content Issue

16

Licensed Content Pages

11

Type of use

Dissertation/Thesis

Requestor type

Author of this Wiley article

Format

Print and electronic

Portion

Full article

Will you be translating?

No

Title

KINETICS, CHARACTERIZATION, AND APPLICATIONS IN THE DEVELOPMENT OF NOVEL NEXT-GENERATION CURE-ON DEMAND POLYMERIC MATERIALS THROUGH FRONTAL POLYMERIZATION

Institution name

Louisiana State University

Expected presentation date

Feb 2022

Order reference number

1993

Requestor Location

Daniel Gary
275 West Roosevelt St. APT 1230

BATON ROUGE, LA 70802
United States
Attn: LSU

Publisher Tax ID

EU826007151

Total

0.00 USD

Terms and Conditions

TERMS AND CONDITIONS

This copyrighted material is owned by or exclusively licensed to John Wiley & Sons, Inc. or one of its group companies (each a"Wiley Company") or handled on behalf of a society with which a Wiley Company has exclusive publishing rights in relation to a particular work (collectively "WILEY"). By clicking "accept" in connection with completing this licensing transaction, you agree that the following terms and conditions apply to this transaction (along with the billing and payment terms and conditions established by the Copyright Clearance Center Inc., ("CCC's Billing and Payment terms and conditions"), at the time that you opened your RightsLink account (these are available at any time at http://myaccount.copyright.com).

Terms and Conditions

- The materials you have requested permission to reproduce or reuse (the "Wiley Materials") are protected by copyright.

- You are hereby granted a personal, non-exclusive, non-sub licensable (on a stand-alone basis), non-transferable, worldwide, limited license to reproduce the Wiley Materials for the purpose specified in the licensing process. This license, **and any CONTENT (PDF or image file) purchased as part of your order,** is for a one-time use only and limited to any maximum distribution number specified in the license. The first instance of republication or reuse granted by this license must be completed within two years of the date of the grant of this license (although copies prepared before the end date may be

distributed thereafter). The Wiley Materials shall not be used in any other manner or for any other purpose, beyond what is granted in the license. Permission is granted subject to an appropriate acknowledgement given to the author, title of the material/book/journal and the publisher. You shall also duplicate the copyright notice that appears in the Wiley publication in your use of the Wiley Material. Permission is also granted on the understanding that nowhere in the text is a previously published source acknowledged for all or part of this Wiley Material. Any third party content is expressly excluded from this permission.

- With respect to the Wiley Materials, all rights are reserved. Except as expressly granted by the terms of the license, no part of the Wiley Materials may be copied, modified, adapted (except for minor reformatting required by the new Publication), translated, reproduced, transferred or distributed, in any form or by any means, and no derivative works may be made based on the Wiley Materials without the prior permission of the respective copyright owner.**For STM Signatory Publishers clearing permission under the terms of the STM Permissions Guidelines only, the terms of the license are extended to include subsequent editions and for editions in other languages, provided such editions are for the work as a whole in situ and does not involve the separate exploitation of the permitted figures or extracts,** You may not alter, remove or suppress in any manner any copyright, trademark or other notices displayed by the Wiley Materials. You may not license, rent, sell, loan, lease, pledge, offer as security, transfer or assign the Wiley Materials on a stand-alone basis, or any of the rights granted to you hereunder to any other person.

- The Wiley Materials and all of the intellectual property rights therein shall at all times remain the exclusive property of John Wiley & Sons Inc, the Wiley Companies, or their respective licensors, and your interest therein is only that of having possession of and the right to reproduce the Wiley Materials pursuant to Section 2 herein during the continuance of this Agreement. You agree that you own no right, title or interest in or to the Wiley Materials or any of the intellectual property rights therein. You shall have no rights hereunder other than the license as provided for above in Section 2. No right, license or interest to any trademark, trade name, service mark or other branding ("Marks") of WILEY or its licensors is granted hereunder, and you agree that you shall not assert any such right, license or interest with respect thereto

- NEITHER WILEY NOR ITS LICENSORS MAKES ANY WARRANTY OR REPRESENTATION OF ANY KIND TO YOU OR ANY THIRD PARTY, EXPRESS, IMPLIED OR STATUTORY, WITH RESPECT TO THE MATERIALS OR THE ACCURACY OF ANY INFORMATION CONTAINED IN THE MATERIALS, INCLUDING, WITHOUT LIMITATION, ANY IMPLIED WARRANTY OF MERCHANTABILITY, ACCURACY, SATISFACTORY QUALITY, FITNESS FOR A PARTICULAR PURPOSE, USABILITY, INTEGRATION OR NON-INFRINGEMENT AND ALL SUCH WARRANTIES ARE HEREBY EXCLUDED BY WILEY AND ITS LICENSORS AND WAIVED BY YOU.

- WILEY shall have the right to terminate this Agreement immediately upon breach of this Agreement by you.

- You shall indemnify, defend and hold harmless WILEY, its Licensors and their respective directors, officers, agents and employees, from and against any actual or threatened claims, demands, causes of action or proceedings arising from any breach of this Agreement by you.

- IN NO EVENT SHALL WILEY OR ITS LICENSORS BE LIABLE TO YOU OR ANY OTHER PARTY OR ANY OTHER PERSON OR ENTITY FOR ANY SPECIAL, CONSEQUENTIAL, INCIDENTAL, INDIRECT, EXEMPLARY OR PUNITIVE DAMAGES, HOWEVER CAUSED, ARISING OUT OF OR IN CONNECTION WITH THE DOWNLOADING, PROVISIONING, VIEWING OR USE OF THE MATERIALS REGARDLESS OF THE FORM OF ACTION, WHETHER FOR BREACH OF CONTRACT, BREACH OF WARRANTY, TORT, NEGLIGENCE, INFRINGEMENT OR OTHERWISE (INCLUDING, WITHOUT LIMITATION, DAMAGES BASED ON LOSS OF PROFITS, DATA, FILES, USE, BUSINESS OPPORTUNITY OR CLAIMS OF THIRD PARTIES), AND WHETHER OR NOT THE PARTY HAS BEEN ADVISED OF THE POSSIBILITY OF SUCH DAMAGES. THIS LIMITATION SHALL APPLY NOTWITHSTANDING ANY FAILURE OF ESSENTIAL PURPOSE OF ANY LIMITED REMEDY PROVIDED HEREIN.

- Should any provision of this Agreement be held by a court of competent jurisdiction to be illegal, invalid, or unenforceable, that provision shall be deemed amended to achieve as nearly as possible the same economic effect as the original provision, and the legality, validity and enforceability of the remaining provisions of this Agreement shall not be affected or impaired thereby.

- The failure of either party to enforce any term or condition of this Agreement shall not constitute a waiver of either party's right to enforce each and every term and condition of this Agreement. No breach under this agreement shall be deemed waived or excused by either party unless such waiver or consent is in writing signed by the party granting such waiver or consent. The waiver by or consent of a party to a breach of any provision of this Agreement shall not operate or be construed as a waiver of or consent to any other or subsequent breach by such other party.

- This Agreement may not be assigned (including by operation of law or otherwise) by you without WILEY's prior written consent.

- Any fee required for this permission shall be non-refundable after thirty (30) days from receipt by the CCC.

- These terms and conditions together with CCC's Billing and Payment terms and conditions (which are incorporated herein) form the entire agreement between you and WILEY concerning this licensing transaction and (in the absence of fraud) supersedes all prior agreements and representations of the parties, oral or written. This Agreement may not be amended except in writing signed by both parties. This Agreement shall be binding upon and inure to the benefit of the parties' successors, legal representatives, and authorized assigns.

- In the event of any conflict between your obligations established by these terms and conditions and those established by CCC's Billing and Payment terms and conditions, these terms and conditions shall prevail.

- WILEY expressly reserves all rights not specifically granted in the combination of (i) the license details provided by you and accepted in the course of this licensing transaction, (ii) these terms and conditions and (iii) CCC's Billing and Payment terms and conditions.

- This Agreement will be void if the Type of Use, Format, Circulation, or Requestor Type was misrepresented during the licensing process.

- This Agreement shall be governed by and construed in accordance with the laws of the State of New York, USA, without regards to such state's conflict of law rules. Any legal action, suit or proceeding arising out of or relating to these Terms and Conditions or the breach thereof shall be instituted in a court of competent jurisdiction in New York County in the State of New York in the United States of America and each party hereby consents and submits to the personal jurisdiction of such court, waives any objection to venue in such court and consents to service of process by registered or certified mail, return receipt requested, at the last known address of such party.

WILEY OPEN ACCESS TERMS AND CONDITIONS

Wiley Publishes Open Access Articles in fully Open Access Journals and in Subscription journals offering Online Open. Although most of the fully Open Access journals publish open access articles under the terms of the Creative Commons Attribution (CC BY) License only, the subscription journals and a few of the Open Access Journals offer a choice of Creative Commons Licenses. The license type is clearly identified on the article.

The Creative Commons Attribution License

The Creative Commons Attribution License (CC-BY) allows users to copy, distribute and transmit an article, adapt the article and make commercial use of the article. The CC-BY license permits commercial and non-

Creative Commons Attribution Non-Commercial License

The Creative Commons Attribution Non-Commercial (CC-BY-NC)License permits use, distribution and reproduction in any medium, provided the original work is properly cited and is not used for commercial purposes.(see below)

Creative Commons Attribution-Non-Commercial-NoDerivs License

The Creative Commons Attribution Non-Commercial-NoDerivs License (CC-BY-NC-ND) permits use, distribution and reproduction in any medium, provided the original work is properly cited, is not used for commercial purposes and no modifications or adaptations are made. (see below)

Use by commercial "for-profit" organizations

Use of Wiley Open Access articles for commercial, promotional, or marketing purposes requires further explicit permission from Wiley and will be subject to a fee.

Further details can be found on Wiley Online Library http://olabout.wiley.com/WileyCDA/Section/id-410895.html

Other Terms and Conditions:

v1.10 Last updated September 2015

Questions? customercare@copyright.com or +1-855-239-3415 (toll free in the US) or +1-978-646-2777.

Mar 04, 2022

This Agreement between Daniel Gary ("You") and John Wiley and Sons ("John Wiley and Sons") consists of your license details and the terms and conditions provided by John Wiley and Sons and Copyright Clearance Center.

License Number

5261510607544

License date

Mar 03, 2022

Licensed Content Publisher

John Wiley and Sons

Licensed Content Publication

Journal of Polymer Science

Licensed Content Title

Charge transfer complexes as dual thermal/photo initiators for free-radical frontal polymerization

Licensed Content Author

Daniel P. Gary, Douglas Ngo, Amber Bui, et al

Licensed Content Date

Feb 22, 2022

Licensed Content Volume

0

Licensed Content Issue

0

Licensed Content Pages

7

Type of use

Dissertation/Thesis

Requestor type

Author of this Wiley article

Format

Print and electronic

Portion

Full article

Will you be translating?

No

Title

KINETICS, CHARACTERIZATION, AND APPLICATIONS IN THE DEVELOPMENT OF NOVEL NEXT-GENERATION CURE-ON DEMAND POLYMERIC MATERIALS THROUGH FRONTAL POLYMERIZATION

Institution name

Louisiana State University

Expected presentation date

Feb 2022

Order reference number

1993

Requestor Location

Daniel Gary
275 West Roosevelt St. APT 1230

BATON ROUGE, LA 70802
United States
Attn: LSU

Publisher Tax ID

EU826007151

Total

0.00 USD

Terms and Conditions

TERMS AND CONDITIONS

This copyrighted material is owned by or exclusively licensed to John Wiley & Sons, Inc. or one of its group companies (each a"Wiley Company") or handled on behalf of a society with which a Wiley

Company has exclusive publishing rights in relation to a particular work (collectively "WILEY"). By clicking "accept" in connection with completing this licensing transaction, you agree that the following terms and conditions apply to this transaction (along with the billing and payment terms and conditions established by the Copyright Clearance Center Inc., ("CCC's Billing and Payment terms and conditions"), at the time that you opened your RightsLink account (these are available at any time at http://myaccount.copyright.com).

Terms and Conditions

- The materials you have requested permission to reproduce or reuse (the "Wiley Materials") are protected by copyright.
- You are hereby granted a personal, non-exclusive, non-sub licensable (on a stand-alone basis), non-transferable, worldwide, limited license to reproduce the Wiley Materials for the purpose specified in the licensing process. This license, **and any CONTENT (PDF or image file) purchased as part of your order,** is for a one-time use only and limited to any maximum distribution number specified in the license. The first instance of republication or reuse granted by this license must be completed within two years of the date of the grant of this license (although copies prepared before the end date may be distributed thereafter). The Wiley Materials shall not be used in any other manner or for any other purpose, beyond what is granted in the license. Permission is granted subject to an appropriate acknowledgement given to the author, title of the material/book/journal and the publisher. You shall also duplicate the copyright notice that appears in the Wiley publication in your use of the Wiley Material. Permission is also granted on the understanding that nowhere in the text is a previously published source acknowledged for all or part of this Wiley Material. Any third party content is expressly excluded from this permission.
- With respect to the Wiley Materials, all rights are reserved. Except as expressly granted by the terms of the license, no part of the Wiley Materials may be copied, modified, adapted (except for minor reformatting required by the new Publication), translated, reproduced, transferred or distributed, in any form or by any means, and no derivative works may be made based on the Wiley Materials without the prior permission of the respective copyright owner.**For STM Signatory Publishers clearing permission under the terms of the STM Permissions Guidelines only, the terms of the license are extended to include subsequent editions and for editions in other languages, provided such editions are for the work as a whole in situ and does not involve the separate exploitation of the permitted figures or extracts,** You may not alter, remove or suppress in any manner any copyright, trademark or other notices displayed by the Wiley Materials. You may not license, rent, sell, loan, lease, pledge, offer as security, transfer or assign the Wiley Materials on a stand-alone basis, or any of the rights granted to you hereunder to any other person.
- The Wiley Materials and all of the intellectual property rights therein shall at all times remain the exclusive property of John Wiley & Sons Inc, the Wiley Companies, or their respective licensors, and your interest therein is only that of having possession of and the right to reproduce the Wiley Materials pursuant to Section 2 herein during the continuance of this Agreement. You agree that you own no right, title or interest in or to the Wiley Materials or any

of the intellectual property rights therein. You shall have no rights hereunder other than the license as provided for above in Section 2. No right, license or interest to any trademark, trade name, service mark or other branding ("Marks") of WILEY or its licensors is granted hereunder, and you agree that you shall not assert any such right, license or interest with respect thereto

- NEITHER WILEY NOR ITS LICENSORS MAKES ANY WARRANTY OR REPRESENTATION OF ANY KIND TO YOU OR ANY THIRD PARTY, EXPRESS, IMPLIED OR STATUTORY, WITH RESPECT TO THE MATERIALS OR THE ACCURACY OF ANY INFORMATION CONTAINED IN THE MATERIALS, INCLUDING, WITHOUT LIMITATION, ANY IMPLIED WARRANTY OF MERCHANTABILITY, ACCURACY, SATISFACTORY QUALITY, FITNESS FOR A PARTICULAR PURPOSE, USABILITY, INTEGRATION OR NON-INFRINGEMENT AND ALL SUCH WARRANTIES ARE HEREBY EXCLUDED BY WILEY AND ITS LICENSORS AND WAIVED BY YOU.
- WILEY shall have the right to terminate this Agreement immediately upon breach of this Agreement by you.
- You shall indemnify, defend and hold harmless WILEY, its Licensors and their respective directors, officers, agents and employees, from and against any actual or threatened claims, demands, causes of action or proceedings arising from any breach of this Agreement by you.
- IN NO EVENT SHALL WILEY OR ITS LICENSORS BE LIABLE TO YOU OR ANY OTHER PARTY OR ANY OTHER PERSON OR ENTITY FOR ANY SPECIAL, CONSEQUENTIAL, INCIDENTAL, INDIRECT, EXEMPLARY OR PUNITIVE DAMAGES, HOWEVER CAUSED, ARISING OUT OF OR IN CONNECTION WITH THE DOWNLOADING, PROVISIONING, VIEWING OR USE OF THE MATERIALS REGARDLESS OF THE FORM OF ACTION, WHETHER FOR BREACH OF CONTRACT, BREACH OF WARRANTY, TORT, NEGLIGENCE, INFRINGEMENT OR OTHERWISE (INCLUDING, WITHOUT LIMITATION, DAMAGES BASED ON LOSS OF PROFITS, DATA, FILES, USE, BUSINESS OPPORTUNITY OR CLAIMS OF THIRD PARTIES), AND WHETHER OR NOT THE PARTY HAS BEEN ADVISED OF THE POSSIBILITY OF SUCH DAMAGES. THIS LIMITATION SHALL APPLY NOTWITHSTANDING ANY FAILURE OF ESSENTIAL PURPOSE OF ANY LIMITED REMEDY PROVIDED HEREIN.
- Should any provision of this Agreement be held by a court of competent jurisdiction to be illegal, invalid, or unenforceable, that provision shall be deemed amended to achieve as nearly as possible the same economic effect as the original provision, and the legality, validity and enforceability of the remaining provisions of this Agreement shall not be affected or impaired thereby.
- The failure of either party to enforce any term or condition of this Agreement shall not constitute a waiver of either party's right to enforce each and every term and condition of this Agreement. No breach under this agreement shall be deemed waived or excused by either party unless such waiver or consent is in writing signed by the party granting such waiver or consent. The waiver by or consent of a party to a breach of any provision of this Agreement shall not operate or be construed as a waiver of or consent to any other or subsequent breach by such other party.
- This Agreement may not be assigned (including by operation of law or otherwise) by you without WILEY's prior written consent.

- Any fee required for this permission shall be non-refundable after thirty (30) days from receipt by the CCC.
- These terms and conditions together with CCC's Billing and Payment terms and conditions (which are incorporated herein) form the entire agreement between you and WILEY concerning this licensing transaction and (in the absence of fraud) supersedes all prior agreements and representations of the parties, oral or written. This Agreement may not be amended except in writing signed by both parties. This Agreement shall be binding upon and inure to the benefit of the parties' successors, legal representatives, and authorized assigns.
- In the event of any conflict between your obligations established by these terms and conditions and those established by CCC's Billing and Payment terms and conditions, these terms and conditions shall prevail.
- WILEY expressly reserves all rights not specifically granted in the combination of (i) the license details provided by you and accepted in the course of this licensing transaction, (ii) these terms and conditions and (iii) CCC's Billing and Payment terms and conditions.
- This Agreement will be void if the Type of Use, Format, Circulation, or Requestor Type was misrepresented during the licensing process.
- This Agreement shall be governed by and construed in accordance with the laws of the State of New York, USA, without regards to such state's conflict of law rules. Any legal action, suit or proceeding arising out of or relating to these Terms and Conditions or the breach thereof shall be instituted in a court of competent jurisdiction in New York County in the State of New York in the United States of America and each party hereby consents and submits to the personal jurisdiction of such court, waives any objection to venue in such court and consents to service of process by registered or certified mail, return receipt requested, at the last known address of such party.

WILEY OPEN ACCESS TERMS AND CONDITIONS

Wiley Publishes Open Access Articles in fully Open Access Journals and in Subscription journals offering Online Open. Although most of the fully Open Access journals publish open access articles under the terms of the Creative Commons Attribution (CC BY) License only, the subscription journals and a few of the Open Access Journals offer a choice of Creative Commons Licenses. The license type is clearly identified on the article.

The Creative Commons Attribution License

The Creative Commons Attribution License (CC-BY) allows users to copy, distribute and transmit an article, adapt the article and make commercial use of the article. The CC-BY license permits commercial and non-

Creative Commons Attribution Non-Commercial License

The Creative Commons Attribution Non-Commercial (CC-BY-NC)License permits use, distribution and reproduction in any medium, provided the original work is properly cited and is not used for commercial purposes.(see below)

Creative Commons Attribution-Non-Commercial-NoDerivs License

The Creative Commons Attribution Non-Commercial-NoDerivs License (CC-BY-NC-ND) permits use, distribution and reproduction in any medium, provided the original work is properly cited, is not used for commercial purposes and no modifications or adaptations are made. (see below)

Use by commercial "for-profit" organizations

Use of Wiley Open Access articles for commercial, promotional, or marketing purposes requires further explicit permission from Wiley and will be subject to a fee.

Further details can be found on Wiley Online Library http://olabout.wiley.com/WileyCDA/Section/id-410895.html

Other Terms and Conditions:

v1.10 Last updated September 2015

Questions? customercare@copyright.com or +1-855-239-3415 (toll free in the US) or +1-978-646-2777.

REFERENCES

1) Javadi, A.; Mehr, H. S.; Sobani, M.; Soucek, M. D. "Cure-on-Command Technology: A Review of the Current State of the Art," *Prog. Org. Coat.* **2016**, *100*, 2-31.

2) Garra, P.; Dietlin, C.; Morlet-Savary, F.; Dumur, F.; Gigmes, D.; Fouassier, J.-P.; Lalevee, J. "Photopolymerization Processes of Thick Films and in Shadow Areas: A Review for the Access to Composites," *Polym. Chem.* **2017**, *8*, 7088-7101.

3) Malik, M. S.; Schlogl, S.; Wolfahrt, M.; Sangermano, M. "Review on UV-Induced Cationic Frontal Polymerization of Epoxy Monomers," *Polym.* **2020**, *12*, 2146.

4) Pojman, J. A.; Ilyashenko, V. M.; Khan, A. M. "Free-Radical Frontal Polymerization: Self-Propagating Thermal Reaction Waves," *J. Chem. Soc., Faraday Trans.* **1996**, *92*, 2825-2837.

5) Chechilo, N. M.; Khvilivitskii, R. J.; Enikolopyan, N. S. "On the Phenomenon of Polymerization Reaction Spreading," *Dokl. Akad. Nauk SSSR* **1972**, *204*, 1180-1181.

6) Chechilo, N. M.; Enikolopyan, N. S. "Structure of the Polymerization Wave Front and Propagation Mechanism of the Polymerization Reaction," *Dokl. Phys. Chem.* **1974**, *214*, 174-176.

7) Chechilo, N. M.; Enikolopyan, N. S. "Effect of the Concentration and Nature of Initiators on the Propagation Process in Polymerization," *Dokl. Phys. Chem.* **1975**, *221*, 392-394.

8) Chechilo, N. M.; Enikolopyan, N. S. "Effect of Pressure and Initial Temperature of the Reaction Mixture During Propagation of a Polymerization Reaction," *Dokl. Phys. Chem.* **1976**, *230*, 840-843.

9) Pojman, J. A. "Traveling Fronts of Methacrylic Acid Polymerization," *J. Am. Chem. Soc.* **1991**, *113*, 6284-6286.

10) Pojman, J. A.; Craven, R.; Khan, A.; West, W. "Convective Instabilities in Traveling Fronts of Addition Polymerization," *J. Phys. Chem.* **1992**, *96*, 7466-7472.

11) Pojman, J. A.; Nagy, I. P.; Salter, C. "Traveling Fronts of Addition Polymerization with a Solid Monomer," *J. Am. Chem. Soc.* **1993**, *115*, 11044-11045.

12) Pojman, J. A.; Willis, J.; Fortenberry, D.; Ilyashenko, V.; Khan, A. "Factors Affecting Propagating Fronts of Addition Polymerization: Velocity, Front Curvature, Temperature Profile, Conversion and Molecular Weight Distribution," *J. Polym. Sci. Part A: Polym Chem.* **1995**, *33*, 643-652.

13) Pojman, J. A.; Curtis, G.; Ilyashenko, V. M. "Frontal Polymerization in Solution," *J. Am. Chem. Soc.* **1996**, *118*, 3783-3784.

14) Khan, A. M.; Pojman, J. A. "The Use of Frontal Polymerization in Polymer Synthesis," *Trends Polym. Sci. (Cambridge, U.K.)* **1996**, *4,* 253-257.

15) Pojman, J. A.; West, W. W.; Simmons, J. "Propagating Fronts of Polymerization in the Physical Chemistry Laboratory," *J. Chem. Ed.* **1997**, *74,* 727-730.

16) Pojman, J. A. Frontal Polymerization: in *Polymer Science: A Comprehensive Reference*; Matyjaszewski, K. Möller, M., Ed.; Elsevier BV: Amsterdam, 2012; pp 957–980.

17) Odian, G. *Principles of Polymerization, 4th Ed.*; Wiley: New York, 2004.

18) Masere, J.; Chekanov, Y.; Warren, J. R.; Stewart, F.; Al-Kaysi, R.; Rasmussen, J. K.; Pojman, J. A. "Gas-Free Initiators for High-Temperature Polymerization," *J. Poly. Sci. Part A. Polym. Chem.* **2000**, *38,* 3984-3990.

19) Mariani, A.; NUVoli, D.; Alzari, V.; Pini, M. "Phosphonium-Based Ionic Liquids as a New Class of Radical Initiators and Their Use in Gas-Free Frontal Polymerization," *Macromolecules* **2008**, *41,* 5191-5196.

20) Bomze, D.; Knaack, P.; Liska, R. "Successful Radical Induced Cationic Frontal Polymerization of Epoxy-Based Monomers by C-C Labile Compounds," *Polym. Chem.* **2015**, *6,* 8161-8167.

21) Bomze, D.; Knaack, P.; Koch, T.; Jin, H.; Liska, R. "Radical Induced Cationic Frontal Polymerization as a Versatile Tool for Epoxy Curing and Composite Production," *J. Polym. Sci. Part A: Polym Chem.* **2016**, *54,* 3751-3759.

22) Pojman, J. "Frontal Polymerization. Polymer Science: A Comprehensive Reference," **2012**.

23) Bowden, G.; Garbey, M.; Ilyashenko, V. M.; Pojman, J. A.; Solovyov, S.; Taik, A.; Volpert, V. "The Effect of Convection on a Propagating Front with a Solid Product: Comparison of Theory and Experiments," *J. Phys. Chem. B* **1997**, *101,* 678-686.

24) McCaughey, B.; Pojman, J. A.; Simmons, C.; Volpert, V. A. "The Effect of Convection on a Propagating Front with a Liquid Product: Comparison of Theory and Experiments," *Chaos* **1998**, *8,* 520-529.

25) Pojman, J. A.; Willis, J. R.; Khan , A. M.; West, W. W. "The True Molecular Weight Distributions of Acrylate Polymers Formed in Propagating Fronts," *J. Polym. Sci. Part A: Polym Chem.* **1996**, *34,* 991-995.

26) Mota-Morales, J. D.; Gutierrez, M. C.; Sanchez, I. C.; Luna-Barcenas, G.; del Monte, F. "Frontal Polymerizations Carried out in Deep-Eutectic Mixtures Providing Both the Monomers and the Polymerization Medium," *Chem. Comm.* **2011**, *47,* 5328-5330.

27) Mota-Morales, J. D.; Gutierrez, M. C.; Ferrer, M. L.; Jimenez, R.; Santiago, P.; Sanchez, I. C.; Terrones, M.; Del Monte, F.; Luna-Barcenas, G. "Synthesis of Macroporous Poly(Acrylic Acid)-Carbon Nanotube Composites by Frontal Polymerization in Deep-Eutectic Solvents," *J. Mater. Chem. A,* **2013**, *1,* 3970-3976.

28) Mota-Morales, J. D.; Gutiérrez, M. C.; Ferrer, M. L.; Sanchez, I. C.; Elizalde-Peña, E. A.; Pojman, J. A.; Monte, F. D.; Luna-Bárcenas, G. "Deep Eutectic Solvents as Both Active Fillers and Monomers for Frontal Polymerization," *J. Polym. Sci. Part A: Polym. Chem.* **2013**, *51,* 1767–1773.

29) Fazende, K. F.; Phachansitthi, M.; Mota-Morales, J. D.; Pojman, J. A. "Frontal Polymerization of Deep Eutectic Solvents Composed of Acrylic and Methacrylic Acids," *J. Polym. Sci. A Polym. Chem.* **2017**, *55,* 4046-4050.

30) Washington, R. P.; Steinbock, O. "Frontal Polymerization Synthesis of Temperature-Sensitive Hydrogels," *J. Am. Chem. Soc.* **2001**, *123,* 7933-7934.

31) Mariani, A.; Fiori, S.; Chekanov, Y.; Pojman, J. A. "Frontal Ring-Opening Metathesis Polymerization of Dicyclopentadiene," *Macromolecules* **2001**, *34,* 6539-6541.

32) NUVoli, D.; Alzari, V.; Pojman, J.; Sanna, V.; Ruiu, A.; Sanna, D.; Malucelli, G.; Mariani, A. "Synthesis and Characterization of Functionally Gradient Materials Obtained by Frontal Polymerization," *ACS Appl. Mater. Interfaces* **2015**, *7,* 3600−3606.

33) Mariani, A.; Bidali, S.; Fiori, S.; Sangermano, M.; Malucelli, G.; Bongiovanni, R.; Priola, A. "UV-Ignited Frontal Polymerization of an Epoxy Resin," *J. Poly. Sci. Part A. Polym. Chem.* **2004**, *42,* 2066-2072.

34) Scognamillo, S.; Bounds, C.; Luger, M.; Mariani, A.; Pojman, J. A. "Frontal Cationic Curing of Epoxy Resins," *J. Polym. Sci. Part A: Polym. Chem.* **2010**, *48,* 2000-2005.

35) Groce, B. R.; Gary, D. P.; Cantrell, J. K.; Pojman, J. A. "Front Velocity Dependence on Vinyl Ether and Initiator Concentration in Radical-Induced Cationic Frontal Polymerization of Epoxies," *J. Polym. Sci.* **2021**, *59,* 1678-1685.

36) Xin, Y.; Xiao, S.; Pang, Y.; Zou, Y. "Nir-Sensitized Cationic Frontal Polymerization of Vinyl Ether and Epoxy Monomers," *Prog. Org. Coat.* **2021**, *153,* 106149.

37) Zhang, R.; Qiu, Z.; Qiu, H.; Zhang, X. "Frontal Polymerization of Superabsorbent Nanocomposites Based on Montmorillonite and Polyacrylic Acid with Enhanced Soil Properties," *J. Appl. Polym. Sci.* **2014**, *131,* n/a-n/a.

38) Feng, Q.; Chen, X.; Zhao, Y.-q.; Hu, S.-s.; Xia, Z.-w.; Yan, Q.-Z. "Preparation of Poly(N-Isopropylacrylamide)/Montmorillonite Composite Hydrogel by Frontal Polymerization," *Colloid Polym Sci.* **2017**, *295,* 883-890.

39) Robertson, I. D.; Yourdkhani, M.; Centellas, P. J.; Aw, J. E.; Ivanoff, D. G.; Goli, E.; Lloyd, E. M.; Dean, L. M.; Sottos, N. R.; Geubelle, P. H.; Moore, J. S.; White, S. R. "Rapid Energy-Efficient Manufacturing of Polymers and Composites Via Frontal Polymerization," *Nature* **2018**, *557*, 223-227.

40) Sangermano, M.; Antonazzo, I.; Sisca, L.; Carello, M. "Photoinduced Cationic Frontal Polymerization of Epoxy–Carbon Fibre Composites," *Polym Int.* **2019**, *68*, 1662-1665.

41) Holt, T.; Fazende, K.; Jee, E.; Wu, Q.; Pojman, J. A. "Cure-on-Demand Wood Adhesive Based on the Frontal Polymerization of Acrylates," *J. Appl. Polym. Sci.* **2016**, *133*, 44064.

42) Bansal, K.; Pojman, J. A.; Webster, D.; Quadir, M. "Frontal Polymerization of a Thin Film on a Wood Substrate," *ACS Macro Lett.* **2020**, *9*, 169-173.

43) Pojman, J. A.; Viner, V.; Binici, B.; Lavergne, S.; Winsper, M.; Golovaty, D.; Gross, L. "Snell's Law of Refraction Observed in Thermal Frontal Polymerization," *Chaos* **2007**, *17*, 033125.

44) Viner, V.; Viner, G. "Effect of Filler Choice on a Binary Frontal Polymerization System," *J. Phys. Chem. B* **2011**, *115*, 6862-6867.

45) Nason, C.; Pojman, J. A.; Hoyle, C. "The Effect of a Trithiol and Inorganic Fillers on the Photo- Induced Thermal Frontal Polymerization of a Triacrylate," *J. Polym. Sci. Part A Polym. Chem.* **2008**, *46*, 8091-8096.

46) Novozhilov, B. V. "The Rate of Propagation of the Front of an Exothermic Reaction in a Condensed Phase," *Dokl. Akad. Nauk SSSR* **1961**, *141*, 151-153.

47) Solomon, D. H.; Rosser, M. J. "Reactions Catalyzed by Minerals. Part I. Polymerization of Styrene," *J. Appl. Polym. Sci.* **1965**, *9*, 1261-1271.

48) Solomon, D. H.; Swift, J. D. "Reactions Catalyzed by Minerals. Part Ii. Chain Termination in Free-Radical Polymerizations," *J. Appl. Polym. Sci.* **1967**, *11*, 2567-2575.

49) Solomon, D. "Clay Minerals as Electron Acceptors and/or Electron Donors in Organic Reactions," *Clays Clay Miner.* **1968**, *16*, 31-39.

50) Theng, B. K. G. *Clay Mineral Catalysis of Organic Reactions*; Chapman and Hall/CRC: Milton, 2018.

51) Solomon, D. H.; Loft, B. C. "Reactions Catalyzed by Minerals. Part Iii. The Mechanism of Spontaneous Interlamellar Polymerizations in Aluminosilicates," *J. Appl. Polym. Sci.* **1968**, *12*, 1253-1262.

52) Wang, Q.; Zhou, Z.; Song, L.; Xu, H.; Wang, L. "Nanoscopic Confinement Effects on Ethylene Polymerization by Intercalated Silicate with Metallocene Catalyst," *J. Polym. Sci. Part A: Polym. Chem.* **2004**, *42*, 38-43.

53) Komadel, P. "Acid Activated Clays: Materials in Continuous Demand," *Appl. Clay Sci.* **2016**, *131*, 84-99.

54) Zweifel, H. *Plastics Additves Handbook*; Hanser Gardner: Cincinnati, 2001.

55) Gailhanou, H.; Blanc, P.; Rogez, J.; Mikaelian, G.; Kawaji, H.; Olives, J.; Amouric, M.; Denoyel, R.; Bourrelly, S.; Montouillout, V.; Vieillard, P.; Fialips, C. I.; Michau, N.; Gaucher, E. C. "Thermodynamic Properties of Illite, Smectite and Beidellite by Calorimetric Methods: Enthalpies of Formation, Heat Capacities, Entropies and Gibbs Free Energies of Formation," *Geochimica et Cosmochimica Acta* **2012**, *89*, 279-301.

56) Plötze, M.; Schärli, U.; Koch, A.; Weber, H., Thermophysical Properties of Bentonite, *International Meeting-Clays in Natural & Engineered Barriers for Radioactive Waste Confinement, France*, **2007**, 579-580.

57) "Fumed Silica and Fumed Alumina in Coatings Applications," *Cabot Corporation* **2008**.

58) Liu, D.; Yuan, P.; Liu, H.; Cai, J.; Qin, Z.; Tan, D.; Zhou, Q.; He, H.; Zhu, J. "Influence of Heating on the Solid Acidity of Montmorillonite: A Combined Study by Drift and Hammett Indicators," *Appl. Clay Sci.* **2011**, *52*, 358-363.

59) Goldfeder, P. M.; Volpert, V. A.; Ilyashenko, V. M.; Khan, A. M.; Pojman, J. A.; Solovyov, S. E. "Mathematical Modeling of Free-Radical Polymerization Fronts," *J. Phys. Chem. B* **1997**, *101*, 3474-3482.

60) Noè, C.; Iannucci, L.; Malburet, S.; Graillot, A.; Sangermano, M.; Grassini, S. "New UV-Curable Anticorrosion Coatings from Vegetable Oils," *Macromol. Mater. Eng.* **2021**, *306*, 2100029.

61) Thanamongkollit, N.; Miller, K. R.; Soucek, M. D. "Synthesis of UV-Curable Tung Oil and UV-Curable Tung Oil Based Alkyd," *Prog. Org. Coat.* **2012**, *73*, 425-434.

62) Chittavanich, P.; Miller, K.; Soucek, M. D. "A Photo-Curing Study of a Pigmented UV-Curable Alkyd," *Prog. Org. Coat.* **2012**, *73*, 392-400.

63) Sangermano, M.; Cerrone, M.; Colucci, G.; Roppolo, I.; Acosta Ortiz, R. "Preparation and Characterization of Hybrid Thiol-Ene/Epoxy UV–Thermal Dual-Cured Systems," *Polym. Int.* **2010**, *59*, 1046-1051.

64) Chen, C.; Li, B.; Wang, C.; Iwasaki, S.; Kanari, M.; Lu, D. UV and Thermal Cure Epoxy Adhesives: in *Paint and Coatings Industry*; Ed. **2018**.

65) Crivello, J. V. "Redox Initiated Cationic Polymerization," *J. Polym. Sci. Part A: Polym Chem.* **2009**, *47*, 1825-1835.

66) Salz, U.; Zimmermann, J.; Salzer, T. "Self-Curing, Self-Etching Adhesive Cement Systems," *J. Adhes. Dent.* **2005**, *7*, 7-17.

67) Moszner, N.; Salz, U. "Recent Developments of New Components for Dental Adhesives and Composites," *Macromol. Mater. Eng.* **2007**, *292*, 245-271.

68) Garra, P.; Dietlin, C.; Morlet-Savary, F.; Dumur, F.; Gigmes, D.; Fouassier, J.-P.; Lalevée, J. "Redox Two-Component Initiated Free Radical and Cationic Polymerizations: Concepts, Reactions and Applications," *Prog. Polym. Sci.* **2019**, *94*, 33-56.

69) Viner, V. G.; Viner, G. "Effect of Acrylate Choice on Binary Frontal Polymerization," *PMSE* **2013**.

70) Bynum, S.; Tullier, M.; Morejon-Garcia, C.; Guidry, J.; Runnoe, E.; Pojman, J. A. "The Effect of Acrylate Functionality on Frontal Polymerization Velocity and Temperature," *J. Poly. Sci: Part A: Pol. Chem.* **2019**, *57*, 982-988.

71) Zhou, H.; Liu, H.-Y.; Fu, K.; Yuan, H.; Du, X.; Mai, Y.-W. "Numerical Simulation of Failure of Composite Coatings Due to Thermal and Hygroscopic Stresses," *Coatings* **2019**, *9*, 243.

72) Jones, D. A. *Principles and Prevnetion of Corrosion*; Prentice-Hall, Inc.: Upper Aaddle River, NJ, 1996.

73) Sørensen, P. A.; Kiil, S.; Dam-Johansen, K.; Weinell, C. E. "Anticorrosive Coatings: A Review," *J. Coat. Technol. Res.* **2009**, *6*, 135-176.

74) Lyon, S. B.; Bingham, R.; Mills, D. J. "Advances in Corrosion Protection by Organic Coatings: What We Know and What We Would Like to Know," *Prog. Org. Coat.* **2017**, *102*, 2-7.

75) Qualified Products Database. https://qpldocs.dla.mil/search/parts.aspx?qpl=1532&param=QPL-24667&type=256 (accessed 09/01/2021, 2021).

76) Marrion, A. *The Chemistry and Physics of Coatings*; 2004.

77) Gloeckner, P. *Radiation Curing*; Vincentz Network: Hannover Germany, 2008.

78) Dadashi-Silab, S.; Doran, S.; Yagci, Y. "Photoinduced Electron Transfer Reactions for Macromolecular Syntheses," *Chem. Rev* **2016**, *116*, 10212-10275.

79) Xiao, P.; Lalevée, J.; Zhao, J.; Stenzel, M. H. "N-Vinylcarbazole as Versatile Photoinaddimer of Photopolymerization under Household UV Led Bulb (392 Nm)," *Macromol. Rapid Commun.* **2015**, *36,* 1675-1680.

80) Turani, M.; Baggio, A.; Casalegno, V.; Salvo, M.; Sangermano, M. "An Epoxy Adhesive Crosslinked through Radical-Induced Cationic Frontal Polymerization," *Macromol. Mater. Eng.* **2021**, *306,* 2100495.

81) Klikovits, N.; Liska, R.; D'Anna, A.; Sangermano, M. "Successful UV-Induced RICFP of Epoxy-Composites," *Macromol. Chem. Phys.* **2017**, *218,* 1700313.

82) Garra, P.; Fouassier, J. P.; Lakhdar, S.; Yagci, Y.; Lalevée, J. "Visible Light Photoinitiating Systems by Charge Transfer Complexes: Photochemistry without Dyes," *Prog. Polym. Sci.* **2020**, *107,* 101277.

83) Gary, D. P.; Bynum, S.; Thompson, B. D.; Groce, B. R.; Sagona, A.; Hoffman, I. M.; Morejon-Garcia, C.; Weber, C.; Pojman, J. A. "Thermal Transport and Chemical Effects of Fillers on Free-Radical Frontal Polymerization," *J. Polym. Sci.* **2020**, *58,* 2267-2277.

84) Crivello, J. V.; Bulut, U. "Dual Photo- and Thermally Initiated Cationic Polymerization of Epoxy Monomers," *J. Polym. Sci. Part A: Polym. Chem.* **2006**, *44,* 6750-6764.

85) Wang, D.; Garra, P.; Lakhdar, S.; Graff, B.; Fouassier, J. P.; Mokbel, H.; Abdallah, M.; Lalevée, J. "Charge Transfer Complexes as Dual Thermal and Photochemical Polymerization Initiators for 3d Printing and Composites Synthesis," *ACS Appl. Polym. Mater.* **2019**, *1,* 561-570.

86) Wang, D.; Garra, P.; Fouassier, J. P.; Lalevée, J. "Silane/Iodonium Salt as Redox/Thermal/Photoinitiating Systems in Radical and Cationic Polymerizations for Laser Write and Composites," *Polym. Chem.* **2020**, *11,* 857-866.

87) Garra, P.; Morlet-Savary, F.; Dietlin, C.; Fouassier, J. P.; Lalevée, J. "On-Demand Visible Light Activated Amine/Benzoyl Peroxide Redox Initiating Systems: A Unique Tool to Overcome the Shadow Areas in Photopolymerization Processes," *Macromolecules* **2016**, *49,* 9371-9381.

88) Wang, D.; Arar, A.; Garra, P.; Graff, B.; Lalevée, J. "Charge Transfer Complexes Based on Various Amines as Dual Thermal and Photochemical Polymerization Initiators: A Powerful Tool for the Access to Composites," *J. Polym. Sci.* **2020**, *58,* 811-823.

89) Wang, D.; Garra, P.; Fouassier, J. P.; Graff, B.; Yagci, Y.; Lalevée, J. "Indole-Based Charge Transfer Complexes as Versatile Dual Thermal and Photochemical Polymerization Initiators for 3d Printing and Composites," *Polym. Chem.* **2019**, *10,* 4991-5000.

90) Goetz, K. P.; Vermeulen, D.; Payne, M. E.; Kloc, C.; McNeil, L. E.; Jurchescu, O. D. "Charge-Transfer Complexes: New Perspectives on an Old Class of Compounds," *J. Mater. Chem. C* **2014**, *2*, 3065-3076.

91) Ghosh, P.; Pal, G. "Photopolymerization of Methyl Methacrylate Using Morpholine–Bromine Charge Transfer Complex as the Photoinitiator," *Eur. Polym. J.* **1998**, *34*, 677-682.

92) Ghosh, P.; Pal, G. "Photopolymerization of Methyl Methacrylate Using a Morpholine–Sulfur Dioxide Charge-Transfer Complex as the Photoinitiator," *J. Polym. Sci. Part A: Polym Chem.* **1998**, *36*, 1973-1979.

93) Garra, P.; Morlet-Savary, F.; Dietlin, C.; Fouassier, J.-P.; Lalevée, J. "Charge-Transfer Complexes as New Inhibitors/Photoinitiators for on-Demand Amine/Peroxide Redox Polymerization," *ACS Omega* **2018**, *3*, 6827-6832.

94) Garra, P.; Morlet-Savary, F.; Dietlin, C.; Fouassier, J. P.; Lalevée, J. "On-Demand Visible Light Activated Amine/Benzoyl Peroxide Redox Initiating Systems: A Unique Tool to Overcome the Shadow Areas in Photopolymerization Processes," *Macromolecules* **2016**.

95) Garra, P.; Graff, B.; Morlet-Savary, F.; Dietlin, C.; Becht, J.-M.; Fouassier, J.-P.; Lalevée, J. "Charge Transfer Complexes as Pan-Scaled Photoinitiating Systems: From 50 Mm 3d Printed Polymers at 405 Nm to Extremely Deep Photopolymerization (31 Cm)," *Macromolecules* **2017**, *51*, 57-70.

96) Garra, P.; Caron, A.; Al Mousawi, A.; Graff, B.; Morlet-Savary, F.; Dietlin, C.; Yagci, Y.; Fouassier, J.-P.; Lalevée, J. "Photochemical, Thermal Free Radical, and Cationic Polymerizations Promoted by Charge Transfer Complexes: Simple Strategy for the Fabrication of Thick Composites," *Macromolecules* **2018**, *51*, 7872-7880.

97) Wang, D.; Kaya, K.; Garra, P.; Fouassier, J.-P.; Graff, B.; Yagci, Y.; Lalevée, J. "Sulfonium Salt Based Charge Transfer Complexes as Dual Thermal and Photochemical Polymerization Initiators for Composites and 3d Printing," *Polym. Chem.* **2019**, *10*, 4690-4698.

98) Wang, D.; Garra, P.; Lakhdar, S.; Graff, B.; Fouassier, J. P.; Mokbel, H.; Abdallah, M.; Lalevée, J. "Charge Transfer Complexes as Dual Thermal and Photochemical Polymerization Initiators for 3d Printing and Composites Synthesis," *ACS Applied Polymer Materials* **2019**, *1*, 561-570.

99) Klikovits, N.; Knaack, P.; Bomze, D.; Krossing, I.; Liska, R. "Novel Photoacid Generators for Cationic Photopolymerization," *Polym. Chem.* **2017**, *8*, 4414-4421.

100) Krossing, I. "The Facile Preparation of Weakly Coordinating Anions: Structure and Characterisation of Silverpolyfluoroalkoxyaluminates $Agal(Or_f)_4$, Calculation of the Alkoxide Ion Affinity," *Chem. Eur. J.* **2001**, *7*, 490-502.

101) Knaack, P.; Klikovits, N.; Tran, A. D.; Bomze, D.; Liska, R. "Radical Induced Cationic Frontal Polymerization in Thin Layers," *J. Polym. Sci. Part A: Polym Chem.* **2019**, *57*, 1155-1159.

VITA

Daniel Paul Gary was born and raised in Sulphur, Louisiana, and earned his bachelor's degree in Chemistry from McNeese State University in May 2017. Daniel Pursued his Ph.D. in Chemistry at Louisiana State University in the Fall of 2017 and joined Dr. John Pojman's Lab in the Summer of 2018. During his stay at LSU, Daniel's research focus was on the chemistry and application of cure-on-demand materials through frontal polymerization. Daniel's work has resulted in three coauthor publications, one first-author publication, and a provisional patent with two more publications in the works. He will start his career with Axalta Coatings Systems in High Point North Carolina as a UV Coatings Scientist in May 2022.